Tracking Cell Fate with Synthetic Memory and Pulse Detecting Transcriptional Circuits

Tracking Cell Fate with Synthetic Memory and Pulse Detecting Transcriptional Circuits

A dissertation presented

by

Mara Christine Inniss

to

The Division of Medical Sciences

in partial fulfillment of the requirements

for the degree of

Doctor of Philosophy

in the subject of

Biological and Biomedical Sciences

Harvard University

Cambridge, Massachusetts

April 2014

Dissertation advisor: Pamela A. Silver Mara Christine Inniss

Tracking Cell Fate with Synthetic Memory and Pulse Detecting Transcriptional Circuits

ABSTRACT

Synthetic biology aims to engineer biological systems to meet new challenges and teach us more about natural biological systems. These pursuits range from the building of relatively simple transcriptional circuits, to engineering the metabolism of an organism, to reconstructing entire genomes. While we are still emerging from the foundational stages of this new field, we are already using engineered cells to discover underlying biological mechanisms, develop new therapeutics, and produce natural products. In this dissertation, we discuss the application of synthetic biology principles to the development of memory and pulse-detecting genetic circuits. In Chapter 2, we use novel transcriptional positive-feedback based memory devices integrated in human cells to study heterogeneous responses to cellular stresses. We built doxycycline, hypoxia, and DNA damage sensing versions of the device, demonstrating its modularity. In Chapter 3, we discuss further applications of the memory device in the study of long-term responses to hypoxia, gamma radiation, and inflammation. Finally, in Chapter 4 we describe work leading to the future construction of a pulse-detecting genetic circuit integrated in the *E. coli* genome. The work presented here illustrates the general applicability of synthetic biology in the study of biological phenomena and brings us one step closer to achieving a more exquisite understanding and control of natural systems.

Acknowledgements

It is hard to believe I have finally reached the point where I am about to defend my dissertation, and I would never have made it this far without the support of so many people. I knew that choosing to come to Boston for graduate school would provide me with amazing scientific opportunities but I could never have predicted I would meet so many awesome people. I have to thank Pamela Silver for accepting me into her lab and supporting me through my time at Harvard. She has inspired me to reach higher and never underestimate what I can do. She put together an environment that really pushed me to learn to be self-reliant while still recognizing when I needed to reach out to others for help.

Aside from scientific development, the Silver lab is where I formed some of the most lasting friendships of my graduate career. The bobcats, Devin Burrill, Patrick Boyle, Christina Agapakis, Qingqing Wang, Jake Wintermute, Bill Senapedis, Karmella Haynes, Danny Ducat, and I were always ready to keep things fun and keep each other from letting the tough parts of science get us down. While all these people have moved on, I was not left alone in the lab. Steph Hays, Tyler Ford, Cameron Myhrvold, Gairik Sachdeva, Jordan Kerns, Jonathan Kotula, and Mike Certo and the rest of the Silver lab now put up with the occasional rants of this old graduate student. I owe so much of what I accomplished to my fellow BBS student, Silver lab member, collaborator and friend Devin Burrill. She took me in during recruitment weekend, introduced me to my future graduate lab, and let me team up with her to work on what became Chapter 2 of my thesis. Without her, I have no idea where I would have ended up in Harvard, but I find it difficult to imagine it would be better than the zany, creative atmosphere of the Silver lab.

I would also like to thank my dissertation advisory committee: Keith Joung, Galit Lahav, Peter Sorger, and Bill Kaelin. Throughout the years I spent here, they provided guidance, advice, and input on the various projects I explored. They made sure I stayed on track and got to where I am today. I would also like to thank my defense committee for agreeing to be there for this final step: Stirling Churchman, Ron Weiss, Ahmad Khalil, and Keith Joung.

My family have supported me long before I got to Harvard and I'm sure they will support me long after. Even though my parents, Bonnie and Brian, and brother, Geoffrey, are far away, they kept me grounded. When things got too stressful, they provided an escape from the academic science bubble and reminded me that everything would work out just fine. Even though I've moved around a lot over the years, I know my home is always with them in Montreal. Thanks to my parents for getting me subscriptions to all the kid's science magazines when I was growing up, and not getting too annoyed when I used all your spices for "chemistry" experiments. Thanks to my brother for putting up with me, letting me watch you play video games, and making sure I didn't turn into too big of a nerd.

Last, but certainly not least, I want to thank Mark Logan for being there for me through the last stages of my degree. Everyday I think about how lucky I am to have met you and I'm glad I didn't have to do this without you.

Table of Contents

[1] Equal contribution
[2] Equal contribution

List of Figures

List of Tables

Attributions

All work described in this thesis was performed by myself with the following exceptions:

The experiments in Chapter 2 were designed and carried out equally with Devin R. Burrill, and Patrick M. Boyle and Pamela A. Silver provided guidance and took part in the writing of the manuscript. Microarray experiments presented in Chapters 2 and 3 were performed by the Dana Farber Microarray Core Facility.

Design of the experiments in Chapter 3 was done by myself. Assembly of constructs described in Chapters 3 was performed by Caroline Kim and Nicolas Hafner under my supervision. Exposure of DNA damage memory device to γ-radiation was performed by myself and qRT-PCR was performed by Caroline Kim. Testing of the inflammation memory device was performed by Nicolas Hafner.

Experiments described in Chapter 4 were designed by Jeffrey Way and myself. Assembly of constructs was performed by Leigh Matano, Caroline Kim, and Lauren Kennedy, under my supervision. Inducible wild-type cI and lambda memory strains described in Chapter 4 were produced by S. Jordan Kerns and Jonathan Kotula.

Copyright Information

[1] Equal contribution
[2] Equal contribution

Chapter 1

Introduction

Introduction to synthetic circuits[1]

Synthetic biology encompasses a vast range of pursuits including building novel transcriptional circuits(Gardner, Cantor, and Collins 2000; Ajo-Franklin et al. 2007), engineering metabolism on a large-scale(Wang et al. 2009), and creating a minimal cell(Gardner, Cantor, and Collins 2000; Forster and Church 2006; Ajo-Franklin et al. 2007). Early projects were mostly limited to building small genetic circuits consisting of only a few parts(Gardner, Cantor, and Collins 2000; Basu et al. 2005; Ajo-Franklin et al. 2007; Wang et al. 2009), however current work has extended our range to large multi-gene devices(Xie et al. 2011) and even entire chromosomes and genomes(Gibson et al. 2010; Annaluru et al. 2014) The history of the field of synthetic biology has been described in great detail elsewhere(Cameron, Bashor, and Collins 2014; Way et al. 2014).

While some of the first synthetic circuits were built from a small number of parts, they exhibited complex behavior including oscillations and pattern formation(Basu et al. 2005). Cellular memory circuits were also among these early synthetic devices(Gardner, Cantor, and Collins 2000). Cellular memory refers to the cell's ability to convert a transient signal or stimulus into a sustained response. Biological phenomena that rely on natural memory circuits include the lambda phage switch, cellular differentiation, and cell division(Ptashne 2004; Burrill and Silver 2010). Synthetic memory circuits can either require active cellular processes to maintain their state (volatile memory) or not (non-volatile memory). Volatile memory circuits include transcription-based devices, while non-volatile memory circuits can be based on recombination. An important feature of volatile memory circuits is they are bistable – they tend to exist in one of two states and stochastic switching between the stable states

[1] Portions of this Chapter are reproduced with permission of the Elsevier from the following published work:
Inniss MC, Silver PA. 2013. Building synthetic memory. Curr Biol 23:R812–6.

should be rare(Ferrell 2002). Additionally, the change in state of both volatile and non-volatile memory circuits can be reversible or irreversible (Figure 1.1A).

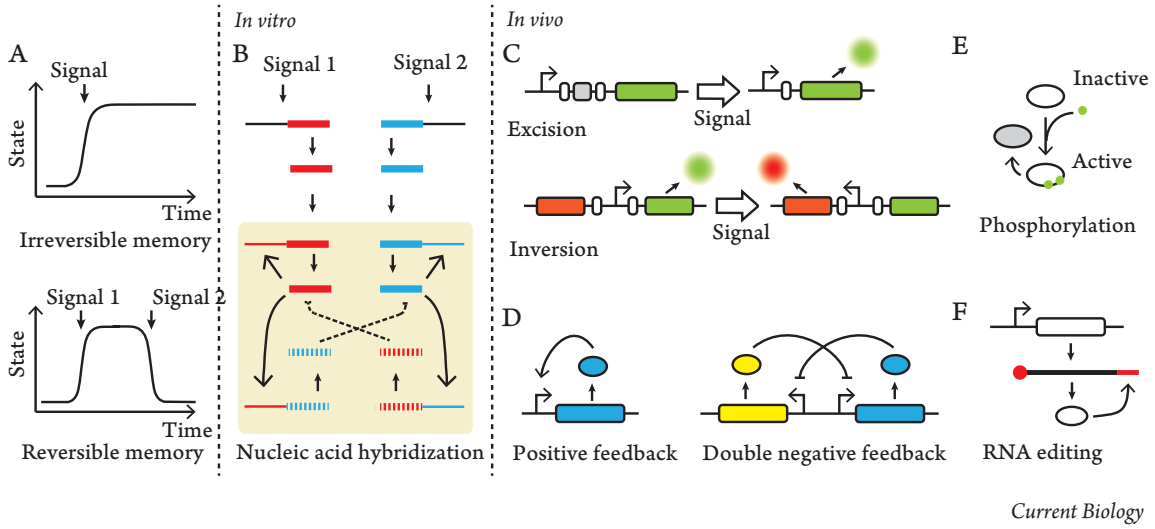

Figure 1.1. Cellular memory circuits can be built in many ways. (A) The change in state of synthetic memory circuits can be either reversible or irreversible. (B) *In vitro* memory circuits rely on hybridization of nucleic acids. Interlocking negative and positive feedback loops form the bistable core (in box) of such devices. Once activated, each positive feedback loop produces an oligonucleotide that promotes its own production as well as an inhibitory oligonucleotide to the opposing positive feedback loop. (C-F) In vivo memory circuits are built using diverse strategies. (C) Recombination-based memory circuits can be based on excision or inversion of DNA sequences. (D) Both positive and double negative transcriptional feedback loops can be used to engineer cellular memory. Novel memory circuits based on (E) protein phosphorylation and (F) RNA editing have also been proposed.

Synthetic memory circuits can be engineered using a variety of biological mechanisms including nucleic acid hybridization, DNA recombination, chromatin modification, transcription, and post-

transcriptional phenomena. Here we will explore the current state of engineered memory circuits and their applications. We will then discuss the future of these devices in medicine and industry.

In vitro memory circuits

Synthetic genetic circuits can be constructed *in vitro*. These circuits consist solely of DNA, capable of performing calculations or logic functions via hybridization(Qian, Winfree, and Bruck 2011), or more complex mixtures of DNA and purified enzymes that can carry out transcription and translation(Kim, White, and Winfree 2006; Padirac, Fujii, and Rondelez 2012). The advantage of building synthetic circuits *in vitro* is the high level of control over the environment in which the device will function (Hockenberry and Jewett 2012). This control results in increased predictability and allows careful unpacking and analysis of the specific interactions between circuit components. This detailed understanding should allow better predictions and interpretations of device behavior when it is introduced into the more complex worlds of the cell and multicellular organisms.

In particular, there have been several recent examples of *in vitro* toggle switches and memory devices based on hybridization of oligonucleotides. One such circuit was built by engineering two mutually repressive DNA-hybridization based transcriptional switches(Kim, White, and Winfree 2006). The circuit consists of DNA oligonucleotides, and two enzymes: T7 RNA polymerase and RNase H. The presence of activating single stranded (ss) DNA, complementary to each switch, allows T7 RNA polymerase to transcribe inhibitory RNAs to the opposing switches while RNase H degrades the inhibitory RNAs. By careful balancing of production and degradation rates, bistable behavior is observed: depending on the initial amounts of the opposing activating ssDNAs production of one inhibitory RNA will completely suppress production of the other. Importantly, these results agree very

closely with model predictions. While this system is bistable, it is not switchable; the circuit output depends entirely on the initial state of the system(Kim, White, and Winfree 2006).

While reversibility is not necessary for a synthetic memory device, it may prove a useful feature. Recently, an *in vitro* switchable memory circuit was engineered consisting of DNA oligonucleotides, DNA polymerase, an endonuclease, and an exonuclease(Padirac, Fujii, and Rondelez 2012). The bistable core of the circuit consists of four templates: two positive feedback loops, and two mutually repressive feedback loops. There are two additional templates that produce two activating oligonucleotides in response to external signals. In this case, these signals are the addition of additional complementary oligonucleotides. Each of the newly produced oligonucleotides interacts with the templates in the bistable core to promote their own production and repress production of the other. Thus, by adding the appropriate external stimulus, the circuit can be switched from one state to the other (Figure 1.1B).

While, in principle, these *in vitro* memory circuits could be modified to function in cells, these strategies for engineering bistability remain unexplored *in vivo*. However, these studies have produced extremely detailed mechanistic understanding that will benefit future efforts to transfer these devices into the cellular environment.

Writing cellular memory into DNA

Heritable memory encoded at the DNA level has been used in biological studies for many years(Stern and Fraser 2001). Developmental biologists use recombinase systems such as Cre:loxP to permanently mark cells of a given lineage, and to knock-out genes in specific cell types or at desired times(Nagy 2000; Srinivas et al. 2001). To accomplish this, transgenic animals are created carrying circuits in which a

reporter gene is interrupted by a transcriptional terminator flanked by loxP sites(Srinivas et al. 2001), or by replacing a gene of interest with a loxP flanked version(Nagy 2000). Cre recombinase expression is then put under the control of a tissue-specific or inducible promoter. Differentiation into a specific tissue or addition of an exogenous inducer results in expression of recombinase, which excises the DNA between the loxP sites creating either a functional reporter gene or knocking-out the gene of interest respectively. As a recombination event results in a change at the DNA sequence level, the change is irreversible and transmits memory of the stimulus heritably and permanently(Figure 1.1C).

By using invertases instead of standard recombinases, more complex multi-state memory circuits can be designed(Ham et al. 2008; Bonnet, Subsoontorn, and Endy 2012; Siuti, Yazbek, and T.K. Lu 2013)(Figure 1.1C) . For instance, a double inversion recombination switch was built in *E. coli* by constructing a plasmid with two overlapping inversion modules(Ham et al. 2008). A separate plasmid carried the two inducible invertase genes. The state of this device can be probed by using a carefully chosen set of primers. The presence or absence of certain amplicons not only indicates whether each inducer has been added, but also the order in which they were introduced. More recently, memory circuits have been integrated with logic gates by flanking combinations of terminators, promoters, or reporter genes by two different pairs of recombinase target sites(Bonnet et al. 2013; Siuti, Yazbek, and T.K. Lu 2013). Depending on the arrangement of these elements, all input logic gates (AND, OR, NOR, AND NAND) can be created. Additionally, multiple inversion-based memory circuits can be linked to build a genetic counter capable of indicating the number of pulses of inducer experienced by the cell(Friedland et al. 2009). As with the systems used in lineage tracing experiments(Nagy 2000; Srinivas et al. 2001), activation of these devices is irreversible.

Recently a rewritable recombination based memory device was demonstrated in *E. coli*. This recombinase addressable data (RAD) module consists of a promoter flanked by phage attachment sites, attB and attP, situated between two fluorescent protein genes(Bonnet, Subsoontorn, and Endy 2012). The device is "set" by expression of an integrase (Int), flipping the promoter and converting attB and attP sites to attL and attR sites, and reset by coexpression of Int and an excisionase (Xis), restoring the attB and attP sites. Depending on the orientation of the promoter, one of the two fluorescent proteins is produced. The state of the device is stable over many generations and can be switched back and forth reliably many times. A reversible memory circuit enables the design of a combinatorial genetic counter(Subsoontorn and Endy 2012). In contrast to a counter built from irreversible memory circuits – using N modules for N counts – a combinatorial counter with N modules can count to 2^N(Subsoontorn and Endy 2012).

Transmitting memory through transcriptional networks

The vast majority of synthetic genetic circuits implemented *in vivo* rely on the successful engineering of transcriptional regulation. One of the best-understood transcriptional regulation systems, lambda phage, is an example of a natural memory circuit(Ptashne 2004). As such, several synthetic memory circuits are transcription-based(Gardner, Cantor, and Collins 2000; Kramer et al. 2004; Ajo-Franklin et al. 2007; Lou et al. 2010; Burrill and Silver 2011; Burrill et al. 2012). There are two main gene network topologies that can demonstrate sustained memory behavior; double negative feedback loops, and a positive feedback loop(Ferrell 2002)(Figure 1.1D). Both of these strategies have been explored in different contexts and each has advantages and disadvantages. While the former is a much simpler circuit with

fewer components to engineer, the latter, by virtue of its increased complexity, provides more options for modification and tuning.

An early example of a synthetic genetic circuit was an engineered toggle switch in *E. coli*(Gardner, Cantor, and Collins 2000). Inspired by the natural lambda phage immunity region(Ptashne 2004), which has previously been shown to function in a novel context(Toman et al. 1985) and more recently used to build an antibiotic detecting memory device in gut bacteria(Kotula et al. 2014), a double-negative feedback circuit was constructed consisting of two repressors driven by constitutive promoters. Each repressor can repress synthesis of the other, therefore, when one repressor is expressed, the other is repressed, thus creating two stable states. Importantly, it is possible to selectively inactivate each repressor by the addition of a specific small molecule, permitting the device to switch states. Careful tuning of promoter strength based on the choice of repressor created toggle switches that demonstrated bistability and long-term memory. Later, similar synthetic switches were shown to function in mammalian cells demonstrating the modularity of the design(Kramer et al. 2004; Deans, Cantor, and Collins 2007). Recently, a toggle switch was combined with genetic logic circuits to create a switch that can be switched on and off by repeated addition of a single trigger molecule(Lou et al. 2010).

While several autoregulatory circuits were built having some degree of bistability(Becskei, Séraphin, and Serrano 2001; Isaacs et al. 2003; Kramer and Fussenegger 2005), the first positive feedback loop that predictably and reliably transmitted memory for many cell divisions was built in *Saccharomyces cerevisiae*(Ajo-Franklin et al. 2007). To create this device, the activities of several transcription factors under the control of a galactose inducible promoter were characterized and a computational model of the circuit was used to predict which of these would form a functional memory

circuit. Indeed, the model correctly predicted which of the transcription factors would succeed and which would fail. This memory device was later shown to be modular; when the galactose inducible promoter was replaced with the promoter for a DNA repair response gene, the circuit maintained its activity albeit while responding to DNA damage instead of galactose(Burrill and Silver 2011). This reengineered circuit was able to identify a subpopulation of cells that maintained a differential response to DNA damage for many generations post-exposure. As with the toggle switch, the modularity of the positive feedback based memory device extends to its transferability to a different organism. A similar device designed to either respond to doxycycline, ultraviolet radiation, or hypoxia was built in human cells and was successfully used to isolate a subpopulation of cells that responded differentially to these stimuli(Burrill et al. 2012).

Memory after transcription

While cellular memory circuits have been engineered that operate at the DNA sequence level as well as through regulation of transcription, post-transcriptional processes have yet to be explored. Natural systems exhibit bistability and even memory dependent on processes such as phosphorylation(Gunawardena 2005) and post-transcriptional modification of RNA(Salz and Erickson 2010). Recent efforts to model these systems open the possibility of harnessing them in engineered circuits.

The phosphorylation state of proteins with multiple phosphorylation sites has been shown to be switch-like or bistable(Gunawardena 2005). For example, multi-site phosphorylation is thought to contribute to the bistability of the MAP kinase cascade(Hadač, Schreiber, and Přibyl 2013). Other models predict that scaffolding is also a significant contributor to bistable phosphorylation

cascades(Chan et al. 2012). Now, synthetic phosphorylation based circuits can be built to test these predictions, adding protein phosphorylation to the selection of tools available for engineering cellular memory(Figure 1.1E). This will allow synthetic biologists to build novel circuits that can respond on much quicker timescales than transcriptional or recombination based circuits.

As another point of post-transcriptional regulation, translation level and thus protein level, can be controlled through RNA modifications. Recently, construction of a positive feedback loop dependent on control of mRNA polyadenylation has been proposed(Aslam and Shouval 2012)(Figure 1.1F). Transcripts with more polyadenylation are more likely to be translated compared to those without(Gallie 1991; Wilusz, Wormington, and Peltz 2001). By encoding expression of a polyadenylating enzyme on a transcript carrying its cognate polyadenylation signal, a positive feedback loop can be created(Aslam and Shouval 2012). This circuit has the potential to be bistable, making it a candidate for becoming the basis of a cellular memory device. These diverse methods of creating cellular memory will provide a powerful toolkit for building future synthetic circuits.

Pulse detection and generation

While numerous strategies for building a memory device have been discussed, these circuits are triggered whether or not the stimulus has ended. This ability to distinguish between subsequent events is necessary for one of the more complex applications of memory devices: counting(Bonnet, Subsoontorn, and Endy 2012; Subsoontorn and Endy 2012). In order to avoid advancing a counter prematurely, the synthetic circuit must be able to distinguish between a pulse of stimulus and a sustained stimulus (a single long pulse). Pulse detecting circuits are usually triggered by either the rising or falling edge (beginning or ending) of a pulse of stimulus. A rising edge detector can also be characterized as a pulse

generator as it produces a burst of output in response to inducer regardless of continued induction. This temporal behavior can be achieved through an incoherent feedforward loop; one component of a cascade represses an earlier component(Kaplan et al. 2008). Many natural examples exist(Kuttykrishnan et al. 2010; Nir Yosef 2011) and, indeed, examples of this type of circuit have been engineered(Basu et al. 2004). However, a falling edge detector has yet to be built.

Learning through building

Synthetic biologists have envisioned what may be possible once we can reliably and predictably reengineer biology. While building novel genetic circuits both *in vitro* and *in vivo* has been a pursuit of synthetic biologists for several years, most of these have yet to find utility in real world applications. Nevertheless, these early efforts have proven useful both as research tools and in gaining a better understanding of natural biological mechanisms(Figure 1.2A). Synthetic memory circuits have been used to explore what is needed to engineer bistability. In particular, transcription-based circuits have been extensively modeled(Rodrigo and Jaramillo 2007; Ghim and Almaas 2009; Widder, Macía, and Solé 2009; Rodrigo et al. 2010) and many examples have been built in diverse contexts(Gardner, Cantor, and Collins 2000; Kramer et al. 2004; Ajo-Franklin et al. 2007; Lou et al. 2010; Burrill and Silver 2011; Burrill et al. 2012). The knowledge gained through these pursuits will allow synthetic biologists to better understand natural and novel transcriptional networks. In addition, memory circuits have been used to study biological questions that would be otherwise intractable. As described earlier, recombination based memory circuits have been used extensively to trace developmental lineages of cells (Stern and Fraser 2001). These circuits also allow conditional gene knock-outs, making it possible

to study the effects of gene loss in certain cell types and at specific times during development(Nagy 2000).

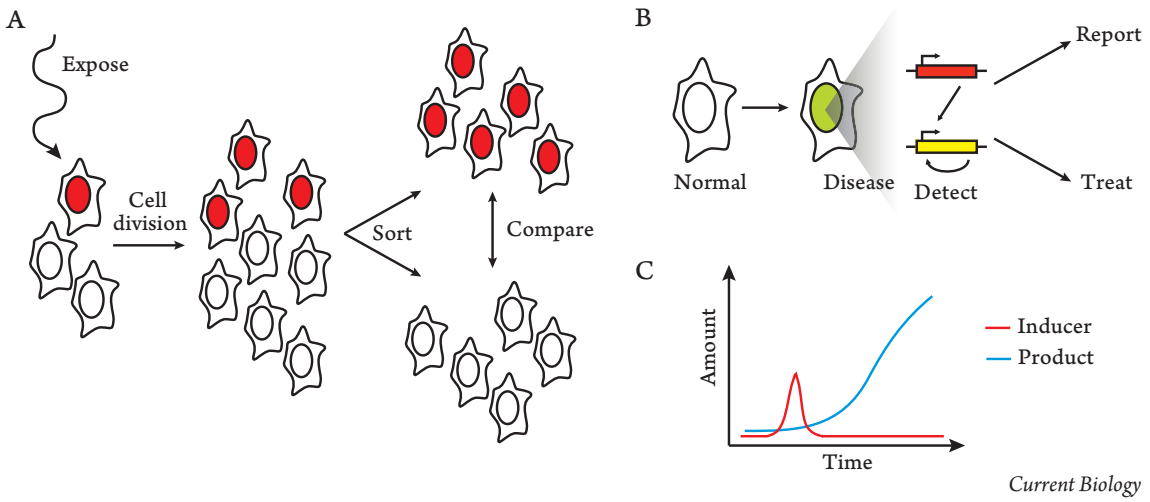

Figure 1.2. Engineered cellular memory circuits can be used to study biology and may be used to diagnosis and treat disease, as well as solve unmet industrial needs. (A) Memory circuits can be used to study heterogeneously responding cell populations. (B) When a cell changes from a healthy to a disease state, memory circuits can detect and report this change or treat the underlying condition. (C) Memory circuits will allow long-term expression by transient addition of inducer.

Synthetic memory circuits based on transcriptional positive feedback loops have been used to study the long-term effects of transient stimuli in *S. cerevisiae* and human cells(Burrill and Silver 2011; Burrill et al. 2012). *S. cerevisiae* carrying the DNA damage responsive memory circuit were exposed to genotoxic doses of EMS or hydroxyurea. Due to the nature of the bistable circuit, cells only switch to the memory state if they respond above a certain threshold allowing isolation of a more strongly responsive subpopulation. This subpopulation was shown to have a higher rate of mitochondrial activity and iron

uptake and this phenotype persisted for many generations post-exposure(Burrill and Silver 2011). Similarly, a DNA damage responsive memory device in human cells was also used to isolate a subpopulation of strongly responding cells. Gene expression in these memory cells differed from the non-memory population for many days post-exposure to UV radiation(Burrill et al. 2012). Thus, using synthetic memory circuits, we can mark and influence biologically relevant subpopulations of cells.

The future of engineered cellular memory

While synthetic memory devices have been useful in learning more about biology and the function of genetic networks, we expect that in the future, these circuits will find new applications in fields such as medicine or industrial biotechnology(Figure 1.2B-C). Other types of synthetic circuits and engineered cells are already being explored as potential next-generation therapies in the treatment of diseases such as diabetes, metabolic syndrome, and cancer(Burrill, Boyle, and Silver 2011; Ruder, T. Lu, and Collins 2011; Weber and Fussenegger 2011; Ye et al. 2013). The ability to induce a sustained response to a transient stimulus will enable new forms of treatment and diagnosis as well as meet unsolved industrial challenges(Ruder, T. Lu, and Collins 2011).

Current medical treatment relies on diagnosis of a disease before an appropriate treatment can be administered and, often, a patient will have to take repeated doses of a drug over the course of treatment(Folcher and Fussenegger 2012; Wieland and Fussenegger 2012). A synthetic memory circuit could be engineered to detect a biological signal of disease and start producing either an easily detectable reporter or a therapeutic(Figure 1.2B). Transcriptional positive feedback loops have already been shown to be modular and thus can be coupled to different biological signaling pathways to detect transient changes in the biology of the cell(Burrill and Silver 2011). Alternatively the device can be engineered to

respond to an extracellular stimulus, such as radiation or hypoxia. These devices will allow a physician to know whether a certain stimulus or condition has occurred even if it is no longer present. While the output of the memory device can be a reporter that can easily be detected such as a fluorophore, beta-galactosidase, or secreted alkaline phosphatase, in the future, the output of these devices may be a therapeutic(Ausländer and Fussenegger 2012). This will automate both the detection and treatment of disease, decreasing the time between the start of the condition and the first dose of therapy(Figure 1.2B).

Cellular memory devices will also be useful in an industrial setting. One barrier to cost-effective production of chemical products is the cost of constantly inducing the culture(Siuti, Yazbek, and T.K. Lu 2013). A synthetic memory device would convert transient induction of a large culture into permanent expression of the exogenous biosynthetic pathways of interest, significantly reducing the cost of production(Siuti, Yazbek, and T.K. Lu 2013)(Figure 1.2C). In addition, one can imagine designing a synthetic memory circuit to be activated at a certain cell density or other internal condition eliminating the need for an external inducer.

Conclusions

Engineering synthetic memory circuits has already taught us about designing bistability and building genetic circuits both *in vitro* and *in vivo*, and helped answer diverse biological questions. However, there remain unmet needs that will enable new applications. Namely, more diverse and well characterized parts – e.g. transcription factors, recombinases, and inducible promoters – as well as more predictive models describing the interactions of these parts. As we apply this deepened understanding and incorporate new tools such as phosphorylation and RNA modification, more complex systems will be

designed and implemented making these devices an important part of next generation medical treatments and bioindustry.

In this dissertation, we will discuss the use of synthetic biology approaches for tracking cell fate and detecting pulsed stimuli. In Chapter 2, the engineering of transcriptional memory devices that can sense and respond to doxycycline, hypoxia, and DNA damage is described. We show that using a positive feedback loop, we can create a device capable of transmitting memory of exposure to a given stimulus through cell division. Additionally, this device can be used to segment a heterogeneously responding population of cells and allows isolation of a differentially responding subpopulation. In Chapter 3, we explore further applications of the memory device described earlier. These include further study of a long-term response to transient hypoxia, memory of exposure to γ-radiation, and development of an inflammation-responsive memory device. Finally, in Chapter 4, the design of a pulse-detecting genetic circuit and characterization of its components is discussed. Such a circuit would allow the assembly of far more complex circuits such as an event counter.

I have also included reprints of the papers I wrote as a graduate student as Appendices. Appendix D is a research paper describing the development of the mammalian transcriptional memory devices. Appendix E is the publication coming from the Harvard 2010 iGEM team introducing plants as a chassis for synthetic biology in the iGEM competition. Lastly, Appendix F is a review of the current state of building synthetic memory circuits.

References

Ajo-Franklin CM, Drubin DA, Eskin JA, Gee EPS, Landgraf D, Phillips I, Silver PA. 2007. Rational design of memory in eukaryotic cells. Genes Dev 21:2271–2276.

Annaluru N, Muller H, Mitchell LA, Ramalingam S, Stracquadanio G, Richardson SM, Dymond JS,

Kuang Z, Scheifele LZ, Cooper EM, et al. 2014. Total Synthesis of a Functional Designer Eukaryotic Chromosome. Science 344:55–58.

Aslam N, Shouval HZ. 2012. Regulation of cytoplasmic polyadenylation can generate a bistable switch. BMC Syst Biol 6:12.

Ausländer S, Fussenegger M. 2012. From gene switches to mammalian designer cells: present and future prospects. Trends Biotechnol.

Basu S, Gerchman Y, Collins CH, Arnold FH, Weiss R. 2005. A synthetic multicellular system for programmed pattern formation. Nature 434:1130–1134.

Basu S, Mehreja R, Thiberge S, Chen M-T, Weiss R. 2004. Spatiotemporal control of gene expression with pulse-generating networks. Proc Natl Acad Sci USA 101:6355–6360.

Becskei A, Séraphin B, Serrano L. 2001. Positive feedback in eukaryotic gene networks: cell differentiation by graded to binary response conversion. EMBO J 20:2528–2535.

Bonnet J, Subsoontorn P, Endy D. 2012. Rewritable digital data storage in live cells via engineered control of recombination directionality. Proc Natl Acad Sci USA.

Bonnet J, Yin P, Ortiz ME, Subsoontorn P, Endy D. 2013. Amplifying genetic logic gates. Science 340:599–603.

Burrill DR, Boyle PM, Silver PA. 2011. A New Approach to an Old Problem: Synthetic Biology Tools for Human Disease and Metabolism. Cold Spring Harb Symp Quant Biol.

Burrill DR, Inniss MC, Boyle PM, Silver PA. 2012. Synthetic memory circuits for tracking human cell fate. Genes Dev 26:1486–1497.

Burrill DR, Silver PA. 2010. Making cellular memories. Cell 140:13–18.

Burrill DR, Silver PA. 2011. Synthetic circuit identifies subpopulations with sustained memory of DNA damage. Genes Dev 25:434–439.

Cameron DE, Bashor CJ, Collins JJ. 2014. A brief history of synthetic biology. Nature reviews Microbiology.

Chan C, Liu X, Wang L, Bardwell L, Nie Q, Enciso G. 2012. Protein scaffolds can enhance the bistability of multisite phosphorylation systems. PLoS Comput Biol 8:e1002551.

Deans TL, Cantor CR, Collins JJ. 2007. A tunable genetic switch based on RNAi and repressor proteins for regulating gene expression in mammalian cells. Cell 130:363–372.

Ferrell JE. 2002. Self-perpetuating states in signal transduction: positive feedback, double-negative feedback and bistability. Curr Opin Cell Biol 14:140–148.

Folcher M, Fussenegger M. 2012. Synthetic biology advancing clinical applications. Current opinion in chemical biology 16:345–354.

Forster AC, Church GM. 2006. Towards synthesis of a minimal cell. Mol Syst Biol 2:45.

Friedland AE, Lu TK, Wang X, Shi D, Church G, Collins JJ. 2009. Synthetic gene networks that count. Science 324:1199–1202.

Gallie DR. 1991. The cap and poly(A) tail function synergistically to regulate mRNA translational efficiency. Genes & Development 5:2108–2116.

Gardner TS, Cantor CR, Collins JJ. 2000. Construction of a genetic toggle switch in Escherichia coli. Nature 403:339–342.

Ghim C-M, Almaas E. 2009. Two-component genetic switch as a synthetic module with tunable stability. Phys. Rev. Lett. 103:028101.

Gibson DG, Glass JI, Lartigue C, Noskov VN, Chuang R-Y, Algire MA, Benders GA, Montague MG, Ma L, Moodie MM, et al. 2010. Creation of a bacterial cell controlled by a chemically synthesized genome. Science 329:52–56.

Gunawardena J. 2005. Multisite protein phosphorylation makes a good threshold but can be a poor switch. Proc Natl Acad Sci USA 102:14617–14622.

Hadač O, Schreiber I, Přibyl M. 2013. On the origin of bistability in the Stage 2 of the Huang-Ferrell model of the MAPK signaling. J Chem Phys 138:065102.

Ham TS, Lee SK, Keasling JD, Arkin AP. 2008. Design and construction of a double inversion recombination switch for heritable sequential genetic memory. PLoS ONE 3:e2815.

Hockenberry AJ, Jewett MC. 2012. Synthetic in vitro circuits. Current opinion in chemical biology 16:253–259.

Isaacs FJ, Hasty J, Cantor CR, Collins JJ. 2003. Prediction and measurement of an autoregulatory genetic module. Proc Natl Acad Sci USA 100:7714–7719.

Kaplan S, Bren A, Dekel E, Alon U. 2008. The incoherent feed-forward loop can generate non-monotonic input functions for genes. Mol Syst Biol 4:203.

Kim J, White KS, Winfree E. 2006. Construction of an in vitro bistable circuit from synthetic transcriptional switches. Mol Syst Biol 2:68.

Kotula JW, Kerns SJ, Shaket LA, Siraj L, Collins JJ, Way JC, Silver PA. 2014. Programmable bacteria detect and record an environmental signal in the mammalian gut. Proc Natl Acad Sci USA.

Kramer BP, Fussenegger M. 2005. Hysteresis in a synthetic mammalian gene network. Proc Natl Acad

Sci USA 102:9517–9522.

Kramer BP, Viretta AU, Daoud-El-Baba M, Aubel D, Weber W, Fussenegger M. 2004. An engineered epigenetic transgene switch in mammalian cells. Nat Biotechnol 22:867–870.

Kuttykrishnan S, Sabina J, Langton LL, Johnston M, Brent MR. 2010. A quantitative model of glucose signaling in yeast reveals an incoherent feed forward loop leading to a specific, transient pulse of transcription. Proc Natl Acad Sci USA 107:16743–16748.

Lou C, Liu X, Ni M, Huang Y, Huang Q, Huang L, Jiang L, Lu D, Wang M, Liu C, et al. 2010. Synthesizing a novel genetic sequential logic circuit: a push-on push-off switch. Mol Syst Biol 6:350.

Nagy A. 2000. Cre recombinase: The universal reagent for genome tailoring. genesis 26:99–109.

Nir Yosef AR. 2011. Impulse control: Temporal dynamics in gene transcription. Cell 144:886.

Padirac A, Fujii T, Rondelez Y. 2012. Bottom-up construction of in vitro switchable memories. Proc Natl Acad Sci USA 109:E3212–20.

Ptashne M. 2004. A Genetic Switch. Cold Spring Harbor Laboratory Pr.

Qian L, Winfree E, Bruck J. 2011. Neural network computation with DNA strand displacement cascades. Nature 475:368–372.

Rodrigo G, Carrera J, Elena SF, Jaramillo A. 2010. Robust dynamical pattern formation from a multifunctional minimal genetic circuit. BMC Syst Biol 4:48.

Rodrigo G, Jaramillo A. 2007. Computational design of digital and memory biological devices. Syst Synth Biol 1:183–195.

Ruder WC, Lu T, Collins JJ. 2011. Synthetic biology moving into the clinic. Science 333:1248–1252.

Salz HK, Erickson JW. 2010. Sex determination in Drosophila: The view from the top. Fly (Austin) 4:60–70.

Siuti P, Yazbek J, Lu TK. 2013. Synthetic circuits integrating logic and memory in living cells. Nat Biotechnol.

Srinivas S, Watanabe T, Lin C-S, William CM, Tanabe Y, Jessell TM, Costantini F. 2001. BMC Developmental Biology | Full text | Cre reporter strains produced by targeted insertion of EYFP and ECFP into the ROSA26 locus. BMC Dev Biol 1:4.

Stern CD, Fraser SE. 2001. Tracing the lineage of tracing cell lineages. Nat. Cell Biol. 3:E216–E218.

Subsoontorn P, Endy D. 2012. Design and Analysis of Genetically Encoded Counters. Procedia Computer Science 11:43–54.

Toman Z, Dambly-Chaudière C, Tenenbaum L, Radman M. 1985. A system for detection of genetic and epigenetic alterations in Escherichia coli induced by DNA-damaging agents. J Mol Biol 186:97–105.

Wang HH, Isaacs FJ, Carr PA, Sun ZZ, Xu G, Forest CR, Church GM. 2009. Programming cells by multiplex genome engineering and accelerated evolution. Nature 460:894–898.

Way JC, Collins JJ, Keasling JD, Silver PA. 2014. Integrating Biological Redesign: Where Synthetic Biology Came From and Where It Needs to Go. Cell 157:151–161.

Weber W, Fussenegger M. 2011. Emerging biomedical applications of synthetic biology. Nat Rev Genet:1–15.

Widder S, Macía J, Solé R. 2009. Monomeric bistability and the role of autoloops in gene regulation. PLoS ONE 4:e5399.

Wieland M, Fussenegger M. 2012. Engineering molecular circuits using synthetic biology in mammalian cells. Annu. Rev. Chem. Biomol. Eng. 3:209–234.

Wilusz CJ, Wormington M, Peltz SW. 2001. The cap-to-tail guide to mRNA turnover. Nat Rev Mol Cell Biol 2:237–246.

Xie Z, Wroblewska L, Prochazka L, Weiss R, Benenson Y. 2011. Multi-Input RNAi-Based Logic Circuit for Identification of Specific Cancer Cells. Science 333:1307–1311.

Ye H, Charpin-El Hamri G, Zwicky K, Christen M, Folcher M, Fussenegger M. 2013. Pharmaceutically controlled designer circuit for the treatment of the metabolic syndrome. Proc Natl Acad Sci USA 110:141–146.

Chapter 2

Synthetic memory circuits for tracking human cell fate

Abstract[1]

A variety of biological phenomena, from disease progression to stem cell differentiation, are typified by a prolonged cellular response to a transient environmental cue. While biologically relevant, heterogeneity in these long-term responses is difficult to assess at the population level, necessitating the development of biological tools to track cell fate within subpopulations. Here we present a novel synthetic biology approach for identifying and tracking mammalian cell subpopulations. We constructed three genomically-integrated circuits that employ bistable auto-regulatory transcriptional feedback to retain memory of exposure to brief stimuli. These 'memory devices' are used to isolate and track the progeny of cells that responded differentially to doxycycline, DNA damaging agents, or hypoxia. Following ultra-violet radiation or hypoxic exposure, strongly responding cells activate the memory device and exhibit changes in gene expression, growth rates, and viability for multiple generations after the initial stimulus. Taken together, these results indicate that a heritable memory of DNA damage and hypoxia exists in subpopulations that differ in long-term cell behavior.

[1] Portions of this chapter were reproduced with permission from Cold Spring Harbor Laboratory Press:
Burrill DR, Inniss MC, Boyle PM, Silver PA. 2012. Synthetic memory circuits for tracking human cell fate. Genes Dev 26:1486–1497.

Introduction

Biological heterogeneity exists in most cell populations; even isogenic populations exhibit some natural cell-to-cell variability in parameters including gene expression and cell morphology (Bishop et al. 2006). Heterogeneity can result from factors such as noise in gene expression and signal transduction, epigenetic modifications, and cell age (Avery 2006; Bishop et al. 2006). A consequence of this diversity is that not all cells within a population will respond identically to a given stimulus. Biological systems can take advantage of such heterogeneity to produce specific cell types (e.g. differentiation) or optimize fitness in fluctuating environments (e.g. immunity) (Acar, Mettetal, and van Oudenaarden 2008). Conversely, heterogeneity can leave some cell subpopulations more sensitive to drug treatment (e.g. chemotherapy) or disease states (e.g. metastasis) (Murray-Zmijewski, Slee, and X. Lu 2008). Distinct cell fates can be heritably-encoded using multiple gene-regulatory strategies, including epigenetic marks, stable cytoplasmic factors, and transcriptional auto-regulatory circuits (Burrill and Silver 2011). Thus, biological diversity can produce cell subpopulations harboring different memories of an experienced stimulus.

By the very nature of its heterogeneity, memory of a biological decision is difficult to study. Population-scale data can obscure subpopulations (Bishop et al. 2006), and single-cell level experiments remain expensive, technically difficult, and hard to scale (Spiller et al. 2010). Studies of biological memory require a technique for tracking a cellular decision through cell division. Recombinase systems are commonly used to confer memory by leaving a permanent genomic mark, however, DNA rearrangement and recombinase expression can have off-target effects that negatively affect genomic fidelity (Forni et al. 2006). Furthermore, tunable, reversible DNA recombinase-based memory has only recently been demonstrated in bacteria (Bonnet 2012) and has yet to be developed in eukaryotic cells.

One solution is the application of synthetic, transcriptional auto-regulatory circuits to track heritable, differential responses to a stimulus. In this circuit design, a stimulus induces transcription of a trigger gene expressing a transactivator, which binds the promoter of a second gene. The second gene produces more of the same transactivator, initiating a positive feedback loop, or memory (Figure 2.1A). Memory is self-sustainable when the input exceeds the circuit's bistable threshold for feedback, allowing the circuit to switch to an alternative state that is transmitted through cell division. Examples of this in nature include the cell cycle and cell differentiation (Burrill and Silver 2010), and synthetic versions have been built in bacteria, yeast, and mammalian cells (for review, Haynes and Silver 2009; Burrill and Silver 2010). In recent work, we constructed a memory circuit in yeast that detects DNA repair, allowing for isolation of cells that initiated a repair response above the circuit's bistable threshold (Burrill and Silver 2011). Strongly responsive cells exhibited a heritable damage response that was distinct from less responsive cells for many generations.

Here we report the construction and implementation of synthetic memory circuits in human cells to track differential cellular decisions following a global stimulus. Activation of the device was linked to endogenous hypoxia and DNA damage response pathways, as these stressors elicit heterogeneous responses at the single-cell level (Bristow and Hill 2008; Murray-Zmijewski, Slee, and X. Lu 2008). A synthetic memory device that responds to low oxygen (O_2) concentrations could help to study the sustained effects of hypoxic exposure during tumor formation. Hypoxia stabilizes the HIF-1 transcription factor, which can activate or silence target genes, as well as increase genomic instability by mediating the bypass of DNA repair checkpoints (Chen et al. 2006; Bristow and Hill 2008; Denko 2008; Lee et al. 2009; Y. Lu et al. 2011). Tumors can harbor cell subpopulations that have been exposed to acute or chronic hypoxia and subsequently reoxygenated, and these tumors are associated with a more

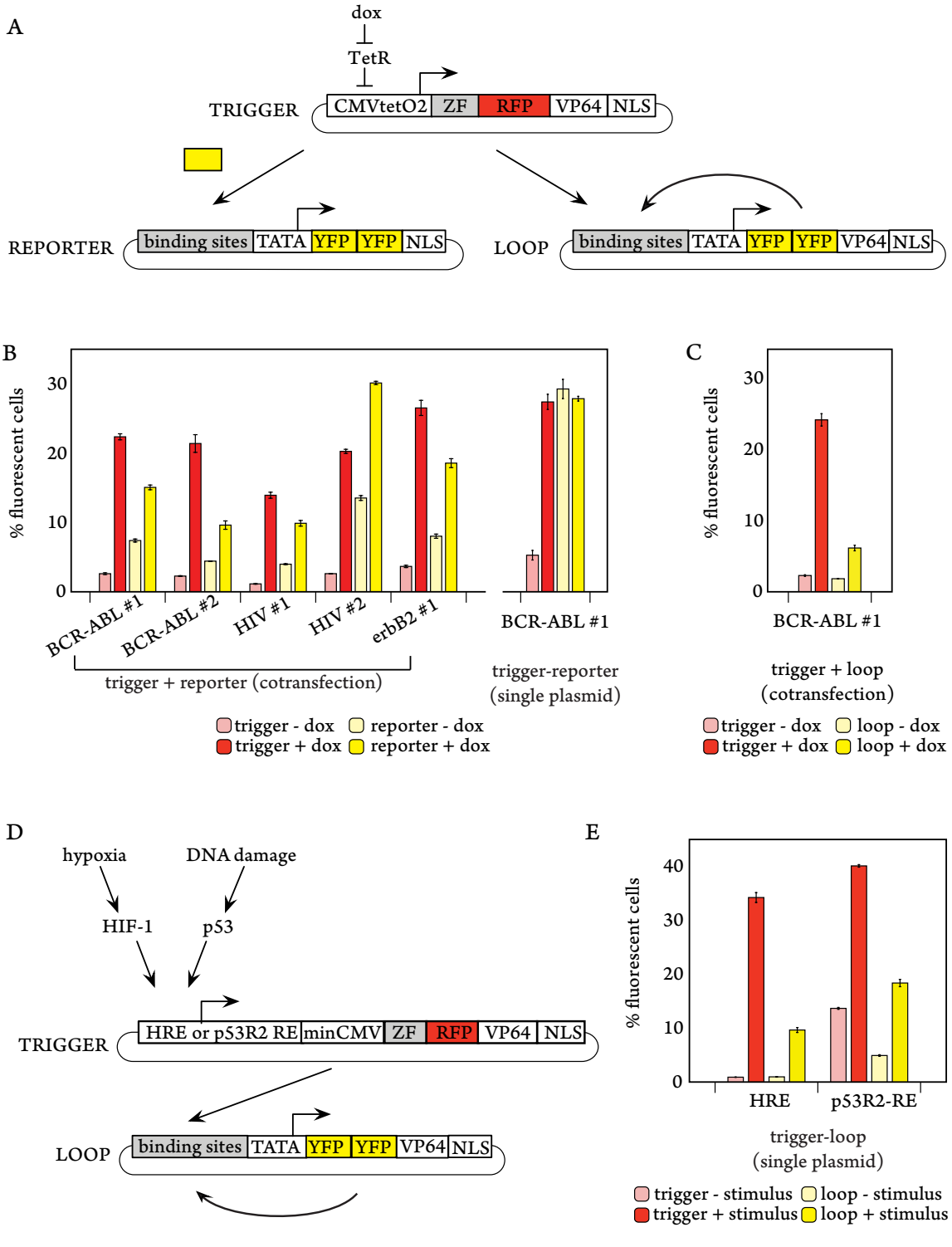

Figure 2.1. Design and testing of trigger and loop genes.

Figure 2.1 (continued). Design and testing of trigger and loop genes. (A) Schematic of dox trigger, reporter, and loop genes. (B) Synthetic ZFs (BCR-ABL #1 & 2, HIV #1 & 2, erbB2 #1) were tested as transactivators via co-transfection with corresponding reporters. BCR-ABL #1 was also tested on a single plasmid with its corresponding reporter gene. (C) BCR-ABL #1 trigger and loop were tested via co-transfection on separate plasmids. (D) BCR-ABL #1 trigger was adapted to be sensitive to DNA damage or hypoxia. (E) HRE and p53R2-RE triggers were tested via co-transfection with loop. (B, C, E) FACS determined % cells positive for trigger RFP and reporter or loop YFP. Values represent mean ± SE, n = 3.

aggressive disease(Bristow and Hill 2008). A memory device activated by HIF-1 could potentially detect, isolate, and track these subpopulations within the heterogeneous tumor microenvironment to determine their specific contributions toward tumor development and metastasis.

Like hypoxia, DNA damage also produces a complex array of biological responses at the single cell level. Linking a memory circuit to native DNA damage pathways could help identify how DNA damage responses are transmitted to subsequent generations and impact long-term cell behavior. The variable activation of the tumor suppressor p53 largely determines a single cell's response to DNA damage (Murray-Zmijewski, Slee, and X. Lu 2008). A memory device triggered at the level of a p53-induced repair factor, such as the ribonucleotide reductase p53R2, would facilitate the isolation and tracking of progeny whose ancestors underwent a repair response strong enough to activate the memory loop, versus those that did not (Tanaka et al. 2000). This could reveal how a cell's specific history of DNA damage translates into long-term biological consequences.

Collectively, our work illustrates a novel, synthetic biology approach for studying cell heterogeneity and fate. The described genomically-integrated devices facilitate the investigation of biological questions that require long-term cell division and stable inheritance of a genetic circuit. The modularity of our system is demonstrated by the construction of memory circuits that respond to diverse and relevant stimuli. Our studies reveal the existence of a heritable biological memory of DNA damage and hypoxia, providing unique insight into protracted responses to transient stimuli.

Results

Characterizing memory circuit components via transient transfection

To engineer a memory device, we first designed a set of fluorescently-labeled synthetic transcriptional activators (triggers) and their corresponding reporter genes (Figure 2.1A,). Each trigger gene consisted of a synthetic zinc finger (ZF) DNA-binding domain (Hurt et al. 2003), one copy of the red fluorescent protein (RFP) mCherry (Shaner et al. 2004), the VP64 activation domain (Beerli et al. 1998), and a nuclear localization sequence (NLS) (Kalderon et al. 1984), all under the control of a doxycycline (dox)-inducible CMV-TetOx2 promoter with a human kozak sequence. ZFs were mammalian codon-optimized versions of those previously engineered by Hurt, *et al*, to bind specifically to target DNA sequences in a BCR-ABL translocation (BCR-ABL #1, #2), the erbB2 gene (erbB2 #1), or the HIV promoter (HIV #1, #2) (Hurt et al. 2003). Each reporter gene had six tandem copies of DNA-binding sites for a given ZF upstream of a minimal promoter (composed of a TATA sequence and human kozak sequence), and its protein-coding region encoded two copies of the yellow fluorescent protein (YFP) variant Venus (Shaner, Steinbach, and Tsien 2005) tagged with an NLS (Figure 2.1A). In the presence of dox, trigger genes were expected to express RFP and a functional transactivator that should bind to its corresponding reporter binding sites, producing a YFP signal.

To evaluate functionality of our constructs in human cell culture, triggers and reporters were built on separate plasmids and transiently co-transfected in a U2OS cell line that expresses the Tet repressor (Table A.1). Following the addition of dox, trigger RFP and reporter YFP co-expression was monitored by fluorescence-activated cell sorting (FACS) (Figure 2.1B). All triggers activated transcription of their target reporters by at least 2-fold. HIV #2 reporter exhibited the most leaky expression, with over 10.0% of cells expressing YFP in the absence of dox. Trigger/reporter pairs were

specific and orthogonal to one another, as minimal YFP expression was observed when reporters alone (Figure A.1A) or mismatched trigger/reporter combinations (Figure A.1B) were transfected. Thus, all triggers were capable of producing a functional transcriptional circuit.

This set of synthetic transactivators provided the components to construct auto-regulatory loops intended to confer memory of a stimulus to a single cell and its progeny. In our proposed device, an input causes synthesis of an RFP-labeled transactivator, which activates expression of a 2xYFP-labeled transactivator (Figure 2.1A). This protein binds to its own promoter and, given certain parameters, continues to self-activate in the absence of stimulus, resulting in sustained YFP expression. For simplicity, all memory devices were built with the BCR-ABL #1 domain, although the above transient experiments suggested that all tested ZFs would provide similar results.

Since tracking long-term memory requires a stably-integrated device, a trigger-reporter circuit was assembled on a single plasmid and tested by transient transfection for circuit activation to determine whether the circuit could be integrated in one step. On a single plasmid, the dox memory device demonstrated constitutive reporter YFP expression in the absence of dox, likely due to cis-activation caused by enhancer elements in the trigger's CMV-TetOx2 promoter (Boshart et al. 1985) (Figure 2.1B). However, the dox device demonstrated inducible expression of the loop gene when the trigger and loop were co-transfected on separate plasmids (Figure 2.1C).

We next aimed to construct memory circuits capable of recording exposure to dox, hypoxia, or DNA damage. The hypoxia-inducible promoter we used was based on one previously engineered by Shibata, *et al*, and is composed of five copies of HIF-1 binding sites, known as hypoxia-responsive elements (HREs), ligated to a minimal human CMV promoter (Shibata, Giaccia, and Brown 2000). This promoter is activated when a cell triggers the HIF-1 pathway in response to hypoxia (Figure 2.1D).

A DNA damage-inducible promoter (p53R2-RE) was generated by linking four copies of the p53 binding site in p53R2 (Ohno et al. 2008) to a minimal human CMV promoter (Shibata, Giaccia, and Brown 2000). This promoter is activated when a cell executes a p53R2-mediated repair response (Figure 2.1D).

Unlike the dox device, the HRE and p53R2-RE triggers do not contain strong enhancer elements and can be assembled as a single construct with the loop gene. When the hypoxia and DNA damage devices were transfected as a single plasmid and exposed to the hypoxia mimic cobalt chloride or the DNA damaging-agent neocarzinostatin (NCS), respectively, RFP and YFP were co-expressed in a significant percentage of cells above basal levels (Figure 2.1E). These observations were similar whether or not the circuits were built on one plasmid (Figure A.1C). Thus, we determined that while a dox memory stable cell line would require two integrations, only one was necessary to produce DNA damage and hypoxia memory cell lines. To test the capacity of the loop element to retain memory of dox, hypoxia, or DNA damage exposure, we proceeded to genomically integrate the circuits.

An integrated dox memory device

The dox trigger and loop were randomly integrated as separate genes to create the cell line MD10/TetOx2 (Table A.2). Dox exposure resulted in trigger RFP and loop YFP expression in 99.8% and 42.7% of cells, respectively, as determined by FACS (Figure 2.2A) and fluorescence microscopy (Figure 2.2B). Upon the removal of dox, trigger RFP turned off in most cells within 1 d, while loop YFP achieved a bimodal distribution, such that two distinct memory and non-memory subpopulations co-existed (Figure A.2). YFP expression persisted in a large percentage of cells for at least 3 d (~ 4

generations), suggesting heritable memory loop activity (Figure 2.2B). These traits were not specific to MD10/TetOx2, as multiple alternative clones were analyzed and demonstrated similar behavior (Figure A.3).

Sustainable memory behavior within a subpopulation of dividing cells was further revealed in time-lapse fluorescence microscopy of cells recovering from dox exposure (Figure 2.2C, File A.1). Distribution of YFP intensity in the memory subpopulation was constant over time, suggesting persistent protein production (Figure 2.3A). Furthermore, spontaneous loop activation in the absence of dox was not observed when MD10/TetOx2 was cultured for 9 d (~ 10 generations), indicating that any loop activity was due solely to dox exposure (Figure 2.3B). To rule out a difference in RFP and YFP protein degradation rates as causal of the observed memory behavior, cells were exposed to dox to activate fluorophore expression, and cycloheximide was then added to inhibit protein biosynthesis. RFP and YFP degradation rates were determined to be approximately equivalent: 10.6 versus 11.5 arbitrary intensity units/h, respectively (Figure A.4). Thus, loop YFP protein persisted by positive feedback and not by protein stability. We concluded that MD10/TetOx2 was capable of recording dox exposure and transmitting memory of this response to progeny.

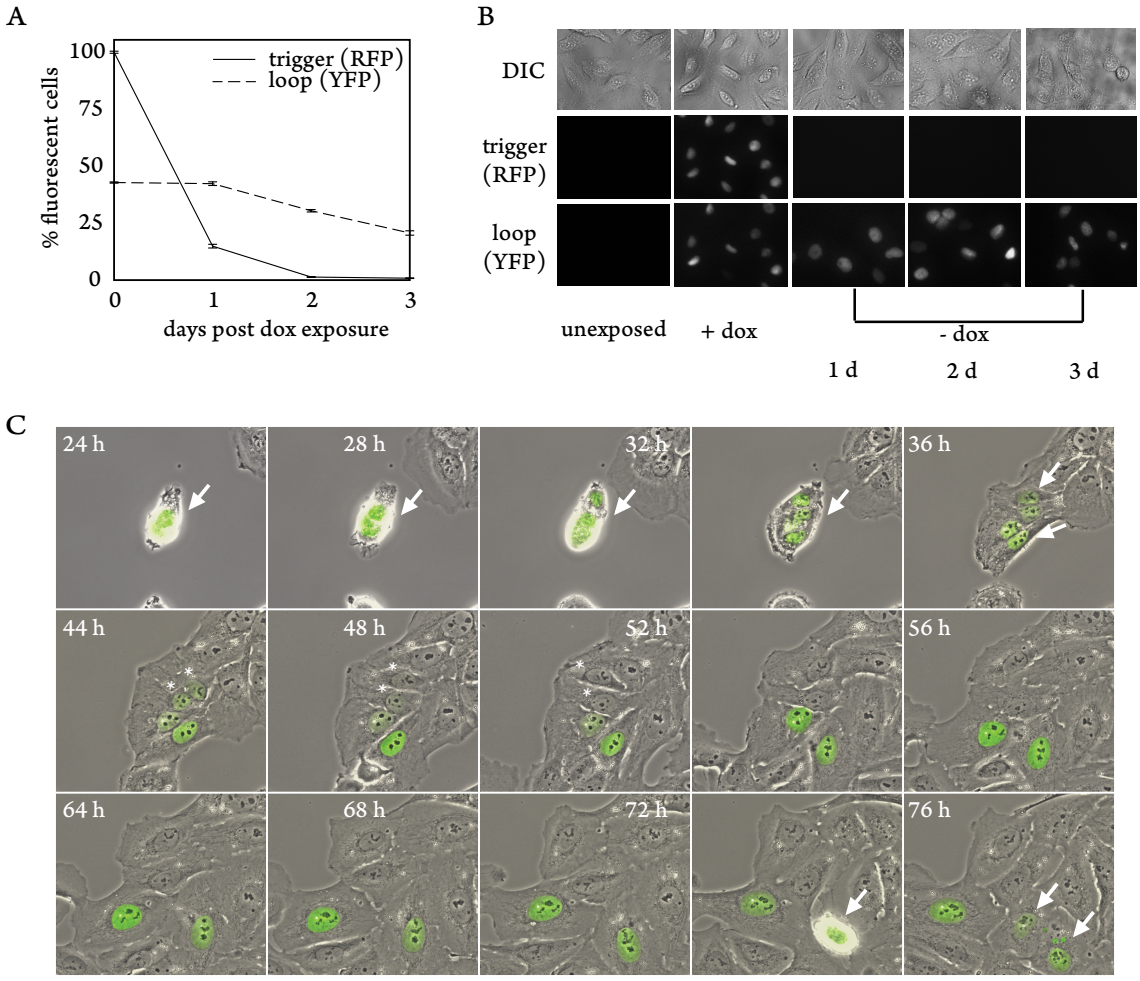

Figure 2.2. MD10/TetOx2 transmits memory of dox exposure. Memory behavior was analyzed by (A) FACS and (B) fluorescence microscopy. FACS determined % cells positive for trigger RFP and loop YFP. Values represent mean ± SE, n = 3. (C) Fluorescence microscopy montage of MD10/TetOx2 post-dox exposure. Phase, RFP and YFP channels were overlaid. Arrows: dividing memory cells. Asterisks: cells where the circuit does not remain active after division.

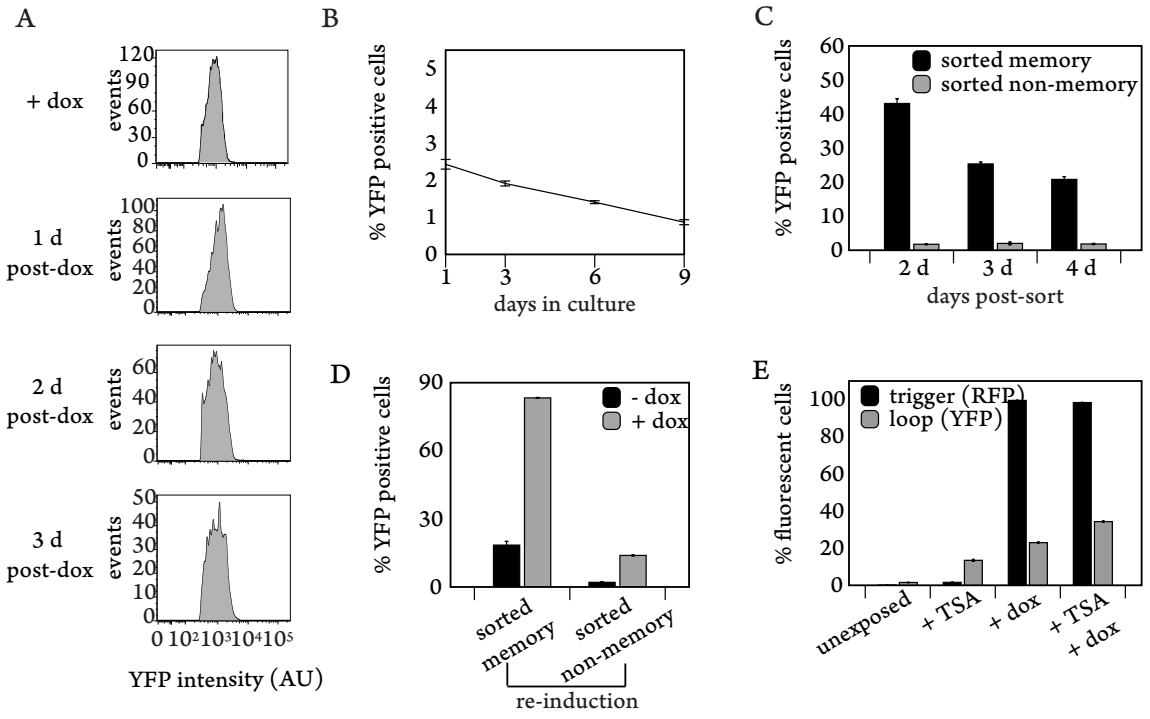

Figure 2.3. Further characterization of MD10/TetOx2. (A) FACS plots of YFP intensity of memory loop cells only, versus event rate over time. (B) Unexposed cells were tracked via FACS to determine rate of spontaneous loop activation. (C) Memory and non-memory cells were sorted 2 d post-dox exposure and tracked by FACS to determine % cells positive for loop YFP. (D) Sorted memory and non-memory cells were re-induced 3 d post-sort with dox, and FACS determined % cells positive for loop YFP. (E) Cells were exposed to dox, TSA, or TSA+dox to identify epigenetic silencing of the device. FACS determined % cells positive for trigger RFP and loop YFP. (A-E) Values represent mean ± SE, n = 3.

To investigate the independent behavior of memory and non-memory cells, cell sorting based on YFP expression was used to physically separate and expand the two cell populations for biological analysis. Over a period of 3 d, sorted memory cells behaved similarly to unsorted memory cells, in that

the percentage that maintained loop expression decreased over time (Figure 2.3C). Sorted memory cells were re-exposed 3 d post-sort to dox, at which time about 20.2% were still expressing the loop, but only 83.3% reactivated the loop (Figure 2.3D). Furthermore, sorted non-memory cells largely failed to re-induce the loop (Figure 2.3D). These observations suggested that epigenetic silencing might play a role in permanently deactivating the memory loop. To test this theory, trichostatin A (TSA) – a histone deacetylase inhibitor – was applied to unsorted MD10/TetOx2 cells before dox exposure to reverse gene silencing. While the number of cells expressing the trigger did not change, 12.5% more cells activated the memory loop if first exposed to TSA (Figure 2.3E), indicating that decreased loop activity over time could be due to epigenetic silencing. This may also explain why only 42.7% of cells initially activated the loop. Every selected MD10/TetOx2 clone exhibited this behavior, suggesting that the loop became silenced during the selection process. Despite this effect, however, this cell line exhibits persistent inducible memory loop expression in a significant percentage of cells, allowing for tracking of the cellular response to dox through cell division.

An integrated hypoxia memory device

To track memory of hypoxia through cell division, the stable cell line MD15/HRE was constructed via random genomic integration of the HRE trigger and loop as a single plasmid. While $CoCl_2$ induced a hypoxic response in transient experiments, it was not appropriate for long-term cell tracking due to its deleterious effect on cell viability and possible non-specific activity as a hypoxia mimic. Alternatively, an anaerobic chamber caused less cell death and created an anoxic environment in which MD15/HRE could be easily characterized since the HRE promoter is maximally active under anoxic conditions (Shibata, Giaccia, and Brown 2000). As fluorophores require O_2 to fold properly, any trigger or loop

protein produced during anoxia was not fluorescent, necessitating a recovery period before analysis. After 1 d of anoxic exposure and 1 d of recovery, the trigger was expressed in 21.5% of cells at a low intensity, since the anoxic response had likely subsided by that time, and the loop was activated in 10.8% of cells, as determined by FACS (Figure 2.4A) and fluorescence microscopy (Figure 2.4B). Loop-expressing cells were expected to have activated the trigger's anoxia-inducible promoter above the bistable threshold required for loop expression. A scatter plot of single cell RFP versus YFP intensities post-dox exposure shows that higher RFP expression corresponds to higher YFP expression, as measured by FACS (Figure A.5A). Thus, loop expression results from stronger trigger activation in response to anoxia.

During the first 2 d post-exposure, we observed a decrease in the memory subpopulation as a fraction of the total population (Figure 2.4A). We hypothesized that memory cells, having activated a stronger response to anoxia, were likely more susceptible to growth defects and being diluted out of the population. This made it difficult to observe, by FACS, whether memory of anoxia indeed persisted through cell division within a subpopulation of cells (Figure A.6). By microscopy, however, we determined that memory was maintained in small clonal populations. When memory cells were isolated from their non-memory counterparts via cell sorting and observed by fluorescence microscopy, a significant proportion of sorted memory cells expressed the loop for at least 6 d (~ 5 generations) post-sort and grew in clusters, indicating active maintenance of memory through cell division (Figure 2.4B).

To determine the contribution of epigenetic silencing to the decrease in memory population, sorted non-memory cells were re-induced 6 d post-sort. Only 3.3% and 2.5% of sorted non-memory cells reactivated the trigger and loop, respectively (Figure 2.4C). In addition, when TSA was applied to unsorted MD15/HRE cells prior to anoxic exposure, 8.8% and 13.5% more cells activated the trigger

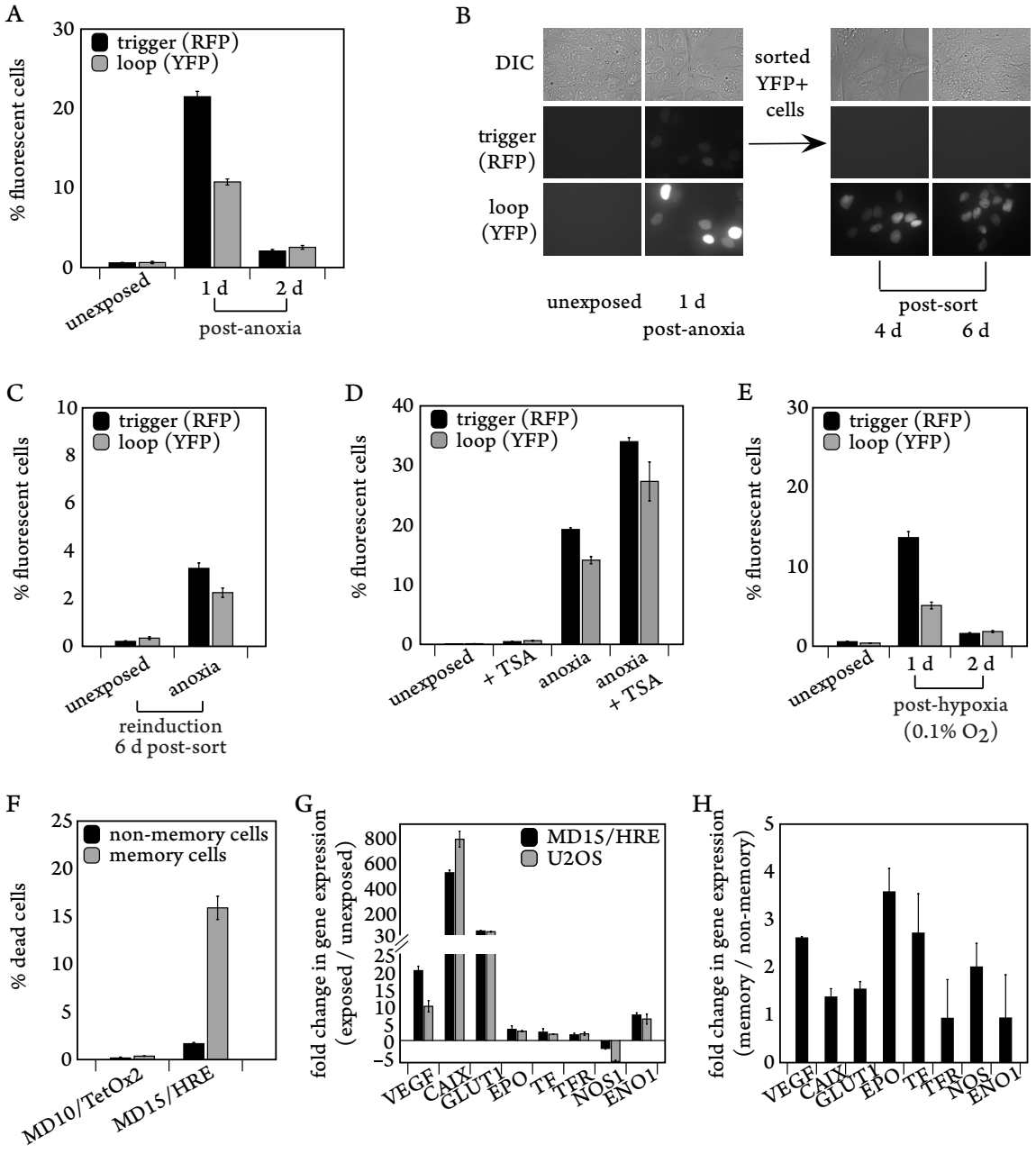

Figure 2.4. MD15/HRE device identifies a subpopulation with unique memory of low O_2 exposure.

Figure 2.4 (continued). MD15/HRE device identifies a subpopulation with unique memory of low O_2 exposure. (A) Cells were exposed to anoxia, and tracked by FACS for 2 d. (B) Cells were exposed to anoxia and recovered for 1d. Memory cells (YFP+) were sorted and followed by microscopy for 6 d. (C) Cells were exposed to anoxia and recovered for 1d. Non-memory cells were sorted and re-exposed to anoxia 6 d post-sort. (D) Cells were exposed to dox, TSA, or TSA+anoxia to identify epigenetic silencing of the device. (E) Cells were exposed to hypoxia and tracked by FACS for 2 d. (A,C,D,E). FACS determined % cells positive for trigger RFP and loop YFP. Values represent mean ± SE, n = 3 (F) Cells were exposed to hypoxia and recovered for 1 d. MD10/TetOx2 was exposed to dox and recovered for 1 d. Cell death was measured in memory versus non-memory cells by FACS. Values represent mean ± SE, n = 3. (G) MD15/HRE and U2OS cells were exposed to hypoxia, and HIF target gene expression was measured. Values represent mean fold expression change over unexposed cells ± SE, n = 3. (H) Cells were exposed to hypoxia and recovered for 1 d. Memory and non-memory cells were sorted, and HIF target gene expression was measured in each subpopulation. Values represent mean fold expression change in memory versus non-memory cells ± SE, n = 2.

and loop, respectively (Figure 2.4D), indicating that epigenetic silencing was occurring in this cell line. We also noted that the slower growth of memory cells contributed to a decrease in the percentage of loop-expressing cells. When equal numbers of sorted memory and non-memory cells were plated 1 d post-exposure, memory cells exhibited a growth defect, reaching confluency 1 d later than non-memory cells (Figure A.7A). This phenotype was not caused by synthetic gene expression, as no growth difference was observed between sorted MD10/TetOx2 memory and non-memory cells (Figure A.7B). In sum, epigenetic silencing and slow growth likely caused the observed decline in memory cells when memory and non-memory cells were co-cultured.

To interrogate the biological relevance of the subpopulations captured by the circuit, hypoxia (0.1% O_2) was next used to activate the MD15/HRE device. While the trigger's HRE promoter is known to be less active under increasing O_2 conditions, hypoxia is commonly used to mimic a tumor microenvironment and plays a significant biological role in disease and development (Bristow and Hill 2008). As expected, hypoxia activated the device in fewer cells (13.6% trigger RFP positive and 5.1% loop YFP positive) than anoxia, presumably due to the higher O_2 concentration (Figure 2.4E, A.5B). However, in cells that were activated, similar memory behavior was observed as under anoxic conditions: unsorted memory cells were quickly diluted out (Figure 2.4E, A.6), while sorted memory cells grew in clonal populations for at least 8 d (~ 7 generations) (Figure A.8). A viability assay using the dead cell stain Sytox Blue (Invitrogen) revealed that memory cells remained less viable than non-memory cells 1 d post-hypoxic exposure: (15.9% death versus 1.68% death, respectively), as compared to MD10/TetOx2 memory and non-memory cells (Figure 2.4F). This difference in viability contributed not only to dilution of the memory population over time, but was also indicative of memory and non-memory subpopulations having distinct biological responses to hypoxia.

To investigate these responses, we first established that endogenous pathways responsive to low O_2 concentrations were similarly functional in MD15/HRE and its background strain. Both cell lines were exposed to hypoxia, and HIF target gene expression was measured by real-time PCR (Figure 2.4G) (Ke and Costa 2006). Since gene activation patterns were similar in both cell lines, we concluded that MD15/HRE responded to hypoxia with normal gene regulation. While this experiment examined hypoxic responses of the population as a whole, we next assessed whether expression of target genes was specifically up-regulated in memory cells, as compared to non-memory cells. Since memory cells had surpassed the circuit's bistable threshold for loop expression, they were expected to have responded more strongly to hypoxia. Memory and non-memory cells were sorted 1 d post-hypoxic exposure, and HIF target gene expression was compared by real-time PCR (Figure 2.4H). Indeed, we found that a subset of HIF target genes were up-regulated in memory cells. Some target genes were not up-regulated, which was likely due to the fact that exposed cells needed to recover for 1 d for fluorophores to develop, to allow for FACS analysis, during which time the initial transcriptional response to hypoxia subsided. Nevertheless, these results demonstrate that the synthetic circuit integrated in the cell line MD15/HRE is capable of sensing and tracking subpopulations that differ in their responses to hypoxia.

An integrated DNA damage memory device

To follow memory of DNA damage, the stable cell line MD12/p53R2-RE was generated via random genomic integration of the p53R2-RE trigger and loop as a single plasmid. While NCS was used as a DNA damaging agent in transient experiments, it was not amenable to long-term cell tracking due to its highly deleterious effects on cell viability. Alternatively, a brief burst of 10 J/m^2 shortwave ultraviolet radiation (UV) allowed greater cell viability (Latonen, Taya, and Laiho 2001; Sharma et al. 2010). UV

exposure resulted in trigger and loop activation in 20.2% and 8.3% of cells, respectively, as determined by FACS (Figure 2.5A), and higher trigger activation corresponded to greater loop activation (Figure A.5C); this behavior was similar between all positive selected clones (Figure A.9). Fluorescence microscopy indicated that memory persisted for at least 2 d post-exposure within a subpopulation of cells (Figure 2.5B), however, a significant decrease in the percentage of cells expressing the loop was observed during the first 2 d post-exposure.

While this characteristic precluded FACS analysis of sustained memory, fluorescence microscopy revealed that loop expression was maintained in small clonal populations when memory cells were isolated 2 d post-UV exposure (Figure 2.5B, A.6). The loop was expressed in a subpopulation of cells for at least 10 d (~ 8 generations) post-sort. This indicated that a subpopulation successfully activated the device above the bistable threshold for loop expression, permitting tracking of memory and non-memory cells. Gene dysfunction was not a contributing factor to the observed memory population decrease, as sorted non-memory cells were able to re-induce both the trigger and loop to levels comparable to their initial induction (Figure 2.5C). Furthermore, epigenetic silencing of the device did not likely affect its function over time: exposure to TSA alone caused no significant induction of the device, and pre-treatment with TSA did not increase the number of cells that responded to subsequent UV exposure (Figure 2.5D).

These results implied that the proportion of memory cells — having executed a stronger DNA damage response — decreased post-damage due to a growth defect or cell death, resulting in dilution of the population over time by the more rapidly growing or viable non-memory cells. When equal numbers of sorted memory and non-memory cells were plated and observed for 4 d by

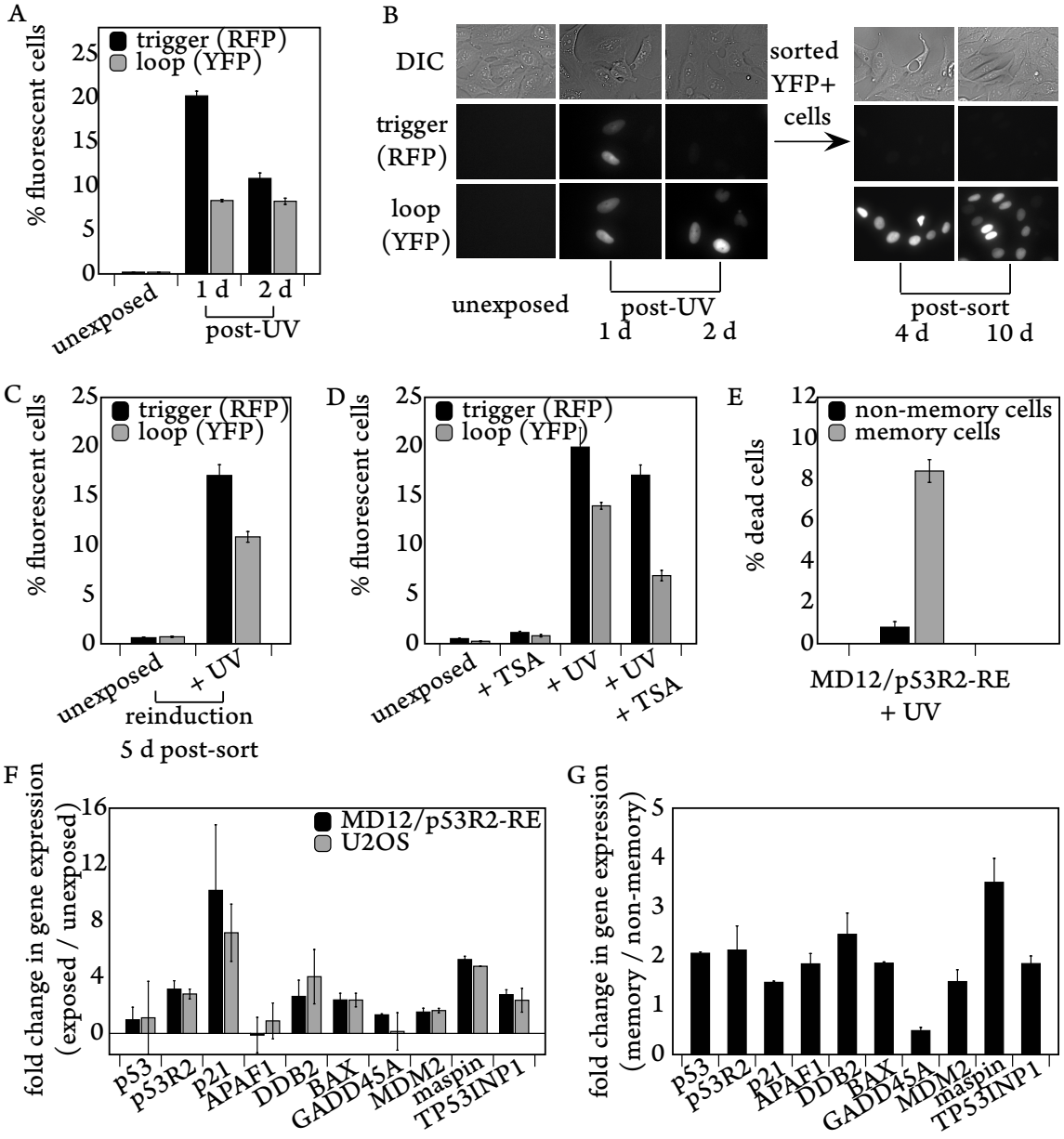

Figure 2.5. MD12/p53R2-RE device identifies a subpopulation with unique memory of DNA damage.

Figure 2.5 (continued). MD12/p53R2-RE device identifies a subpopulation with unique memory of DNA damage. (A) Cells were exposed to UV and tracked by FACS for 2 d. (B) Cells were exposed to UV and recovered for 1d. Memory cells (YFP+) were sorted and followed by microscopy for 10 d. (C) Cells were exposed to UV and recovered for 1d. Non-memory cells were sorted and re-exposed to UV 5 d post-sort. (D) Cells were exposed to dox, TSA, or TSA+UV to identify epigenetic silencing of the device. (A,C,D) FACS determined % cells positive for trigger RFP and loop YFP. Values represent mean ± SE, n = 3. (E) Cells were exposed to UV and recovered for 2 d. Cell death was measured in memory versus non-memory cells by FACS. Values represent mean ± SE, n = 3. (G) MD12/p53R2-RE and U2OS cells were exposed to UV, and p53 target gene expression was measured. Values represent mean fold expression change over unexposed cells ± SE, n = 3. (H) Cells were exposed to UV and recovered for 1 d. Memory and non-memory cells were sorted, and p53 target gene expression was measured in each subpopulation. Values represent mean fold expression change in memory versus non-memory cells ± SE, n = 2.

fluorescence microscopy, non-memory cells reached confluency 2 d sooner than memory cells (Figure A.7C). This slow growth phenotype could account for memory cells being diluted out of the population over time when memory and non-memory cells are grown together. Using the dead cell stain Sytox Blue, we also determined thatmemory cells were less viable than non-memory cells 2 d post-UV exposure: 8.4% cell death versus 0.8%, respectively (Figure 2.5E). All together, these data suggest that memory cells maintained distinct growth and viability phenotypes after UV exposure.

We next asked whether unique gene expression profiles characterized how distinct subpopulations responded initially to DNA damage. Endogenous response pathways were similarly functional in MD12/p53R2-RE and its background strain post-UV exposure, as measured by p53 target gene expression using real-time PCR (Figure 2.5F) (Brady and Attardi 2010). Furthermore, a subset of target genes was specifically up-regulated in memory cells (Figure 2.5G). Memory and non-memory subpopulations were sorted 1 d post-UV exposure, and p53 target gene expression was compared by real-time PCR. Since exposed cells required 1 d of recovery before sorting, not all target genes were up-regulated at the indicated time-point. In sum, these results verify that the synthetic circuit is capable of differentiating between subpopulations that uniquely respond to DNA damage.

To assess whether specific initial responses translated into each subpopulation maintaining distinct long-term expression profiles, we performed gene expression profiling of memory and non-memory cells multiple days after UV exposure. After 3 d of recovery from UV treatment, memory and non-memory cells were sorted. The expression signature of memory cells was distinct from their non-memory counterparts: 127 genes were up-regulated and 31 were down-regulated in memory cells (fold change ≥ 2.0, corrected P-value ≤ 0.05) (File A.2). Bioinformatics analysis identified the transcriptional pattern of oxidative stress in memory cells (Figure 2.6A): up-regulated genes were enriched for those

responsive to external stimulus (P = 1.48e-03), wounding (P = 1.56e-03), hydrogen peroxide (P = 3.41e-03), stress (P = 3.89e-03), reactive oxygen species (ROS) (P = 6.05e-03), and chemical stimulus (P = 9.29e-03). Enrichments were validated by real-time PCR (Figure A.10A). To eliminate any background effect of expression of a synthetic device, transcriptional profiling of MD10/TetOx2 sorted memory versus non-memory cells was also performed and up-regulated genes were removed from the MD12/p53R2-RE data analysis (Figure A.10B, File A.2).

While the microarray data defined a set of genes that were uniquely expressed in memory cells multiple days post-DNA damage, it does not inform upon the expression level of those genes at earlier time-points. To address this question, we tested the expression of 4 up-regulated genes - *CDNF, MXD1, SCL39A2,* and *GRK5* – 1 d after UV exposure. Interestingly, all four tested genes showed significant up-regulation in YFP+ cells, as compared to YFP- cells. Thus, these genes were expressed both 1 d and 3 d after UV exposure. This suggested UV-mediated DNA damage produced a transcriptional response that was maintained over time in memory and non-memory cells. Since differences not only in gene expression, but also viability and growth, were shown to persist for multiple days, we concluded that the MD12/p53R2-RE circuit is capable of capturing subpopulations with distinct long-term memories to DNA damage.

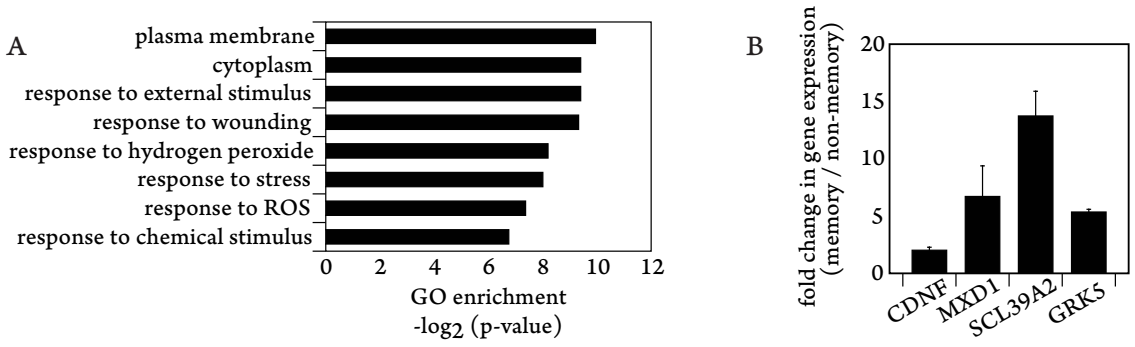

Figure 2.6. MD12/p53R2-RE device identifies a subpopulation with a unique transcriptional profile. (A) Gene ontology enrichment of genes up-regulated in memory cells 3 d post-UV exposure. (B) Cells were exposed to UV and recovered for 1 d. Memory and non-memory cells were sorted and gene expression was measured in each subpopulation. Values represent mean fold expression change in memory versus non-memory cells ± SE, n = 2.

Discussion

Building a prototype memory circuit in mammalian cells

In this study, we present the successful engineering and implementation of synthetic memory devices in human cells. The construction of a prototype, dox-inducible circuit (MD10/TetOx2) revealed behavioral qualities of an integrated, transcription-based device that could inform further applied systems. In all isolated clones, most cells activated the trigger in response to dox, and a significant fraction activated the memory loop. Moreover, a subpopulation of loop-expressing cells transmitted the memory protein to daughter cells for multiple generations. These cells likely activated the circuit above its bistable threshold. The MD10/TetOx2 circuit provides one of the first synthetic examples of what is required to create a bistable mammalian memory switch based on positive feedback.

While a significant percentage of cells maintained loop expression post-exposure, this population decreased over time. Indeed, time-lapse fluorescence microscopy revealed that some daughter cells failed to inherit memory protein from loop-expressing mother cells. As this was observed for all selected clones, the genomic integration location was unlikely to be causative. However, we hypothesize that epigenetic silencing resulted in memory loop deactivation, and stochastic noise in memory loop protein segregation during cell division might also have played a role. If a daughter cell randomly fails to receive a sufficient amount of loop protein to maintain feedback, it will switch to a non-memory state that is propagated in future progeny. This behavior has been observed for both natural and synthetic transcriptional auto-regulatory circuits (Becskei, Séraphin, and Serrano 2001; Weinberger and Shenk 2007; To and Maheshri 2010). Producing more loop protein before cell division, either by increasing the synthesis rate or reducing the rate of cell division, is expected to minimize any loss of memory over time (Ajo-Franklin et al. 2007). However, for certain uses — such as drug dosage in a clinical setting — short-term memory loop expression could be desirable. Indeed, exploring the tunability of our memory system could help define any constraints on the device's potential applications.

Integrating synthetic circuits with endogenous pathways

To demonstrate its further potential to report on biological phenomena, the MD10/TetOx2 device was reconfigured to respond to endogenous hypoxia and DNA damage response pathways. Memory cells were identified as descendents of cells that experienced HIF-1 or p53R2 activity above the circuit's bistable threshold, while non-memory cells were those that responded more weakly such that the loop was not activated. The formation and defining characteristics of these memory cells, versus their non-

memory counterparts, could vary depending on cell state, DNA damaging or hypoxic agents, length of exposure, and time of recovery. Furthermore, a given stressor likely produces many subpopulations with uniquely protracted responses. Our goal was to use the described circuits to identify how an initial response translated into sustained biological characteristics that distinguished what we defined as memory and non-memory cell subpopulations.

Interestingly, the DNA damage and hypoxia memory devices behaved quite differently from the dox memory device. MD10/TetOx2 responded to dox by activating the trigger to similar levels in all cells and the memory loop to similar levels in approximately 43% of cells (Figure A.2). In contrast, MD15/HRE and MD12/p53R2-RE responded to hypoxia and DNA damage, respectively, with largely variable activation of the trigger and loop in a smaller percentage of cells (Figure A.5). Furthermore, while memory of dox exposure was sustained in a significant number of cells, memory of hypoxia and DNA damage persisted in a small subset.

Behavioral differences were likely due to the more heterogeneous activation of hypoxia and DNA damage signaling pathways. MD10/TetOx2 induction occurs when the tet-repressor can no longer bind the trigger's promoter due to the presence of dox, resulting in strong, homogeneous trigger expression (Figure A.2). In contrast, MD12/p53R2-RE and MD15/HRE activation is dependent on signals transduced by biological pathways composed of numerous proteins, each with its own degree of biological noise affecting its behavior. Unlike the dox-inducible trigger, HIF-1 and p53 should not be uniformly activated within a population (Bristow and Hill 2008; Murray-Zmijewski, Slee, and X. Lu 2008), resulting in heterogeneous trigger and memory loop activation (Figure A.5). MD15/HRE and MD12/p53R2-RE thus permit the isolation of two distinct subpopulations post-hypoxia or damage.

The utility of the hypoxia and DNA damage memory devices to detect biologically unique populations was assessed in multiple ways. We determined in initial response to hypoxia or UV, HIF and p53 target gene expression was elevated in MD15/HRE and MD12/p53R2-RE cells that activated both the trigger and loop, as compared to cells that only activated the trigger. This result indicated that the devices work as intended: cells with a stronger response are capable of overcoming the bistable threshold of the circuit, such that the loop is expressed. We also established that a stronger response translated into long-term phenotypes, including slow growth and poor viability. Memory cells exhibited these characteristics for multiple generations past the point of exposure, as compared to their non-memory counterparts.

Finally, gene expression profiling of revealed that DNA damaged memory cells had a persistent gene expression signature that was entirely different from that of non-memory cells and was maintained over time. The memory cell expression profile was largely enriched for genes responsive to oxidative stress, as well as stress in general, including DNA-damage-inducible transcript (*DDIT3*), glutathione peroxidase 3 (*GPX3*), MAX dimerization protein 1 (*MXD1*), egl nine homolog 3 (*EGLN3*), and tumor protein p53 inducible nuclear protein 1 (*TP53INP1*). UV radiation is known to cause significant intracellular production of ROS and reactive nitrogen species, as well as alter the levels of intracellular antioxidant enzymes (Zhang et al. 1997; Birch-Machin and Swalwell 2010). Our study shows that transcriptional responses to UV-induced oxidative damage persist through multiple generations in a subpopulation of cells. It is possible that this differential maintenance of gene expression translates into differences in vulnerability to future damage or aging, and may also dictate the mechanisms by which each subpopulation protects the fate of its progeny.

Conclusions

The memory devices presented here have the potential to illuminate previously undescribed biological phenomena. The DNA damage and hypoxia memory circuits could be utilized in further analyses — such as deep-sequencing or epigenetic mapping — of differentially-responsive populations, to create a more detailed picture of how a cell's history contributes to its biological future. Differentially regulated genes in memory cells could potentially serve as targets in future work toward defining how the inherited expression profile is maintained. This approach could implicate genes that play a role in disease development. The work might also be translated to a xenograft model in mice to study the *in vivo* heterogeneous effects of DNA damage and hypoxia through the development of a solid tumor. It would be interesting to identify whether these transient stimuli produce subpopulations that are more or less prone to disease development. Given their modular nature, the circuits could potentially produce outputs other than fluorophores. For example, once a memory device is proven safe for patients, it could possibly be used in a clinical setting by modifying the loop to produce a therapeutic drug in response to a transient stimulus. The loop could also be altered to create a useful tissue engineering tool that produces morphogens or growth factors for differentiation control in tissue engineering applications. While these proposed ventures will require significant re-tooling and testing of the device, their pursuit will help advance and challenge the utility of synthetic circuits.

Our work demonstrates that complex biological problems can be investigated with an synthetic devices. To date, development of new synthetic devices has been hindered by a slow design cycle and poor device robustness, particularly in mammalian cell culture (Burrill, Boyle, and Silver 2011). Streamlining the mammalian design cycle is critical as synthetic biology strives to better integrate with complex human applications such as stem cell therapy and tissue engineering. Building more complex

mammalian devices will undoubtedly provide invaluable data for more comprehensive quantitative models, which will allow better predictions of function at the preliminary design stage and thereby reduce the number of tested iterations of a device. Synthetic devices destined for clinical applications must also demonstrate faithful performance; constructing genomically integrated devices, as with our memory devices, is an important first step. Improving mammalian cell design remains an essential task for synthetic biology, as the field continues to engage in the engineering of increasingly complex cell types.

Materials and Methods

Plasmid constructs

Escherichia coli DH5α was used for all plasmid manipulations. Bacteria were grown in LB-ampicillin media to maintain plasmids; if engineered constructs contained synthetic zinc fingers, media was supplemented with 0.02 mM zinc chloride. DNA fragments with universal cloning sites (EcoRI, NotI, XbaI, SpeI, and PstI) were generated by PCR and assembled via BioBrick DNA assembly (Phillips and Silver 2006).

A CMV-TetOx2 promoter fragment (from pcDNA5/FRT/TO©, Invitrogen) ligated in front of a human kozak sequence produced a doxycycline (dox)-inducible promoter. HRE promoter was provided by the Brown lab (Shibata, Giaccia, and Brown 2000). Response elements from human p53R2 gene (Ohno et al. 2008) were constructed as annealed oligos (Integrated DNA Technologies) and ligated in front a minimal promoter (Shibata, Giaccia, and Brown 2000) to generate p53R2-RE promoter. Human codon-optimized synthetic zinc fingers (Hurt et al. 2003) were commercially synthesized by Mr. Gene (Regensburg, Germany).

For transient transfections, triggers and reporters were cloned as NotI/SpeI fragments into the Flp-In™ T-REx™ vector in which the promoter was deleted (Invitrogen, Silver Lab). For MD10/TetOx2 (clone MD10.21), trigger and memory loop genes were cloned as separate fragments into a pcDNA3.1™ (+)-based vector (Invitrogen) in which the neomycin resistance marker was replaced with hygromycin or puromycin resistance, respectively, and the constitutive CMV promoter was deleted (Silver Lab). For MD12/p53R2-RE (clone MD12.34) and MD15/HRE (clone MD15.21), trigger and loop genes were cloned as one fragment into the puromycin-resistant pcDNA3.1™ (+)-based vector (Invitrogen, Silver Lab).

Memory device design strategy

Devices were built in two stages. First, multiple gene circuits were designed and tested via transient transfection. In these plasmid-based experiments, multiple designs were characterized to identify elements that generated the most effective circuit activation and least basal activity. Selected prototypes were then genomically-integrated to produce the final stable devices that are characterized in greater detail in this work.

Cell culture and transfection

Plain U2OS and U2OS Flp-In™ T-REx™ cells (Blacklow Lab) were grown in McCoy's 5A medium supplemented with 10% tetracycline-screened fetal bovine serum (FBS) and 1% penicillin and streptomycin; T-REx™ cells were further supplemented with 15 ug/mL blasticidin and 200 ug/mL zeocin. Cells were grown at 37˚C in a humidified CO_2 incubator.

Transient transfections were performed by plating 1.2 X 10^5 cells/well in 12-well culture dishes and transfecting with 800 ng total plasmid DNA and 2 ul Lipofectamine® 2000 (Invitrogen) in 1 ml of antibiotic-free medium (Table A.1). Media was changed 4 h post-transfection and cells were exposed 20 h later to 1 ug/mL dox (Sigma-Aldrich), 0.5 ug/mL neocarzinostatin (NCS) (Sigma-Aldrich), or 100 μM cobalt chloride ($CoCl_2$) (Sigma-Aldrich) for 24 h and analyzed by fluorescence activated cell sorting (FACS).

Stable cell lines were generated by plating 3.0 X 10^5 cells/well in 6-well culture dishes and transfecting with 2 ug plasmid DNA and 5 ul Lipofectamine® 2000 in 2 mL of antibiotic-free medium. Media was changed 4 h post-transfection and cells were exposed to selection media the following day (Table A.2). After 5 d of selection, media was changed to maintenance antibiotic concentrations (Table A.2). Clones were picked and screened for inducible expression via 1 ug/mL dox, 0.5 ug/mL NCS or 100 μM $CoCl_2$. Positive clones were expanded and maintained as stable lines.

Induction of MD12/p53R2-RE and MD15/HRE cell lines

To analyze MD12/p53R2-RE behavior, 3.0 x 10^5 cells/well were plated in 6-well plates. The following day, plates were exposed to a brief burst of 10 J/m^2 shortwave ultraviolet radiation (UV) (Lahav Lab, Harvard Systems Biology). To analyze MD15/HRE behavior, 3.0 x 10^6 cells were plated in 10 cm plates. The following day, plates were exposed to anoxia (0% O_2, ~2.0% H_2) in an anaerobic chamber (Wyss Institute for Biologically Inspired Engineering) for 1 d in CO_2-independent media (Invitrogen) or hypoxia (0.1% O_2, 5.0% CO_2) in a hypoxic chamber (Kaelin lab, Dana Farber Cancer Institute). When cells were returned to normoxia, media was replaced with appropriate maintenance media.

Flow cytometry and cell sorting

Prior to FACS analysis, cells were fixed in 4% paraformaldehyde/1x PBS solution for 10 min, resuspended in 200 uL of 1x PBS, and stored at 4˚C. Cells were later loaded in 96 well plates or 5 mL polystyrene tubes (BD Biosciences) on an LSRII (BD Biosciences) with 488-nm (DsRed) and 568-nm (Fitc) lasers (Harvard Systems Biology). 1.0 X 10^4 cells were analyzed for RFP (DsRed) and YFP (FITC) fluorescence and gated based on cell size and granularity. Unexposed cells controlled for basal fluorophore expression. Data was analyzed using FlowJo software.

To sort MD10/TetOx2 cells, 3, 6-well plates were exposed to dox, washed with 1x PBS, and moved to 3, T-150 flasks for 2 d. Cells were then trypsinized, spun at 1100 rpm for 5 min, washed with 1x PBS, spun a second time, resuspended in 3 mL of 1x PBS/1% FBS, and filtered. To sort MD12/p53R2-RE cells, 12, 6-well plates were exposed to UV and recovered for 2 d. Cells were then processed as described above, except that 4, 6-well plates of cells were pooled to produce three replicates. To sort MD15/HRE cells, 9, 10 cm plates were exposed to anoxia or hypoxia and recovered for 1 d. Cells were then processed as described above, except that 3, 10cm plates were pooled to produce three replicates.

Processed cells were run on a FACS Aria II with a 100 uM nozzle at 20 psi (Harvard Systems Biology). Excitation optics for RFP consisted of a 75 mW 594 nm laser; detection optics included a 630/22 bandpass filter. Excitation optics for YFP consisted of a 15 mW 488 nm laser; detection optics included a 520 nm longpass dichroic mirror and a 530/30 bandpass filter. For microscopy, 200,000 memory and non-memory cells were sorted. Sorted MD10/TetOx2 and sorted MD15/HRE cells were seeded in 12-well dishes; sorted MD12/p53R2-RE cells were seeded in 24-well dishes.

Fluorescence microscopy

For short-term microscopy, cells were imaged at 20x with a Nikon TE2000-E inverted fluorescence microscope equipped with a Hamamatsu ORCA-ER camera, and HcRed (RFP) and JP2 (YFP) filters (Silver Lab). Images were acquired and analyzed using Metamorph software.

For long-term imaging, 5.0 X 10^4 cells/well were seeded in a 12-well glass-bottom culture dish (MatTek) and exposed to dox for 1 d. Wells were next washed with media. Cells were allowed to recover for 1 d and then imaged every hour for 3 d using a Plan Apo 20x 0.75 NA objective lens on a Nikon TE200E motorized inverted microscope equipped with a Hamamatsu ORCA-ER cooled CCD camera, Prior Proscan II motorized stage and shutters, EXFO X-cite 120-XL fluorescence illuminator, a 37˚C, 5% CO_2 custom-built microscope enclosure incubation chamber, and mCherry (RFP) and YFP filter sets (Nikon Imaging Center, Harvard Medical School). Images were acquired and analyzed using Metamorph software.

Cycloheximide assay

MD10/TetOx2 cells were plated in 12-well dishes and exposed to dox in triplicate. After 24 h incubation, cells were exposed to 100 uM cycloheximide (CHX) (Sigma-Aldrich) for 8 h. 3 wells were fixed in 4% PFA / 1x PBS per hour and later analyzed by FACS. Same procedure was applied to regular T-REx™ cells.

Histone deacetylase inhibitor assay

MD10/TetOx2 cells were plated in 12-well dishes, MD12/p53R2-RE were plated in 6-well dishes, and MD15/HRE were plated in 10 cm plates. Cells were exposed in triplicate to 50 ng/mL trichostatin A

(TSA) (Sigma-Aldrich) for 16 h, and then washed and exposed in triplicate to dox, UV, or anoxia. 3 wells were fixed in 4% PFA / 1x PBS and later analyzed by FACS.

Sytox Blue assay

MD15/HRE cells were plated in 10 cm plates, exposed to hypoxia, and recovered for 1 d. MD10/TetOx2 cells were plated in 6-well plates, exposed to dox, and recovered for 1 d. MD12/p53R2-RE cells were plated in 6-well plates, exposed to UV, and recovered for 2 d. To analyze viability, cells were trypsinized, spun at 1100 rpm for 5 min and resuspended in 10 mL 1x PBS. 500 uL from each plate was stained with 1 uM Sytox Blue Dead Cell Stain (Invitrogen), incubated for 5 min, and analyzed by FACS using the AmCyan filter. Unexposed cells were similarly to treated to control for basal levels of cell death.

Endogenous pathway induction

MD12/p53R2-RE and MD15/HRE were plated and exposed to UV or hypoxia, respectively. Whole cell RNA was extracted using the RNeasy Mini Kit (Qiagen), and cDNA was prepared using the SuperScript III First Strand Synthesis System (Invitrogen). Unexposed cells served as controls for background expression.

Gene expression profiling

MD10/TetOx2 and MD12/p53R2-RE cells were plated in 6-well plates, exposed to dox or UV in triplicate, respectively, and allowed to recover for 3 d. Cells were then processed as described above for cell sorting. For each biological replicate, 200,000 memory and non-memory cells were sorted and RNA was extracted using the RNeasy Mini Kit (Qiagen). cDNA was prepared, biotinylated, and hybridized to

Gene 1.0 ST arrays (Affymetrix). Arrays were scanned and quantified according to standard Affymetrix protocols at the Dana Farber Microarray Core Facility (Dana Farber Cancer Institute). Datasets have been submitted to the GEO database, record XXXXXX.

Identification and analysis of differentially regulated genes

Data was annotated and normalized by RMA-analysis using Affymetrix Expression Console Software. Differential gene expression was determined using the Matlab Bioinformatics Toolbox (MathWorks). P-values were calculated using a permutation t-test of 10,000 permutations. Genes with a fold change ≥ 2 and p-value ≤ 0.05 were considered differentially expressed and analyzed for gene ontology enrichment via GoStat (http://gostat.wehi.edu.au), with Benjamini correction for multiple hypothesis testing; enrichment was considered significant with P ≤ 0.01. Differentially expressed genes were validated by real-time PCR using 0.5 ug RNA of specified cell populations. Primers amplified ~ 100 base pairs (Table A.3). Differential expression was normalized to human gene *ACTB*.

Acknowledgements and attributions

We owe special thanks to D. Drubin for initiating this project. We further thank D. Ducat, C. Agapakis, Q. Wang, J. Lohmueller, T. Armel, K. Haynes, the Lahav Lab (Harvard Systems Biology), C. Shen, W. Kaelin, J. Way, K. Joung, and J. Hurt for thoughtful contributions to this manuscript and for sharing reagents. Technical expertise was generously provided by J. Moore and A. Kressler (Harvard Systems Biology Flow Cytometry Facility); the Dana Farber Cancer Institute Microarray Core and Flow Cytometry Core; and, J. Waters and L. Piedmont (Nikon Imaging Center at Harvard Medical School). D.R.B. is supported by the National Science Foundation (NSF) Synthetic Biology Engineering Research

Center (SynBERC); M.C.I. by the Natural Sciences and Engineering Research Council of Canada; P.M.B. by the Harvard University Center for the Environment and NSF SynBERC; and, P.A.S. by the National Institutes of Health and the Wyss Institute for Biologically Inspired Engineering.

The experiments in Chapter 2 were designed and carried out equally with Devin R. Burrill, and Patrick M. Boyle and Pamela A. Silver provided guidance and took part in the writing of the manuscript. Microarray experiments presented in Chapters 2 and 3 were performed by the Dana Farber Microarray Core Facility.

References

Acar M, Mettetal JT, van Oudenaarden A. 2008. Stochastic switching as a survival strategy in fluctuating environments. Nat. Genet. 40:471–475.

Ajo-Franklin CM, Drubin DA, Eskin JA, Gee EPS, Landgraf D, Phillips I, Silver PA. 2007. Rational design of memory in eukaryotic cells. Genes Dev 21:2271–2276.

Avery SV. 2006. Microbial cell individuality and the underlying sources of heterogeneity. Nature reviews Microbiology 4:577–587.

Becskei A, Séraphin B, Serrano L. 2001. Positive feedback in eukaryotic gene networks: cell differentiation by graded to binary response conversion. EMBO J 20:2528–2535.

Beerli RR, Segal DJ, Dreier B, Barbas CF. 1998. Toward controlling gene expression at will: specific regulation of the erbB-2/HER-2 promoter by using polydactyl zinc finger proteins constructed from modular building blocks. Proc Natl Acad Sci USA 95:14628–14633.

Birch-Machin MA, Swalwell H. 2010. How mitochondria record the effects of UV exposure and oxidative stress using human skin as a model tissue. Mutagenesis 25:101–107.

Bishop AL, Rab FA, Sumner ER, Avery SV. 2006. Phenotypic heterogeneity can enhance rare-cell survival in "stress-sensitive" yeast populations. Mol Microbiol 63:507–520.

Boshart M, Weber F, Jahn G, Dorsch-Häsler K, Fleckenstein B, Schaffner W. 1985. A very strong enhancer is located upstream of an immediate early gene of human cytomegalovirus. Cell 41:521–530.

Brady CA, Attardi LD. 2010. p53 at a glance. J Cell Sci 123:2527–2532.

Bristow RG, Hill RP. 2008. Hypoxia and metabolism. Hypoxia, DNA repair and genetic instability. Nat Rev Cancer 8:180–192.

Burrill DR, Boyle PM, Silver PA. 2011. A New Approach to an Old Problem: Synthetic Biology Tools for Human Disease and Metabolism. Cold Spring Harb Symp Quant Biol.

Burrill DR, Silver PA. 2010. Making cellular memories. Cell 140:13–18.

Burrill DR, Silver PA. 2011. Synthetic circuit identifies subpopulations with sustained memory of DNA damage. Genes Dev 25:434–439.

Chen H, Yan Y, Davidson TL, Shinkai Y, Costa M. 2006. Hypoxic stress induces dimethylated histone H3 lysine 9 through histone methyltransferase G9a in mammalian cells. Cancer Res 66:9009–9016.

Denko NC. 2008. Hypoxia, HIF1 and glucose metabolism in the solid tumour. Nat Rev Cancer 8:705–713.

Forni PE, Scuoppo C, Imayoshi I, Taulli R, Dastrù W, Sala V, Betz UAK, Muzzi P, Martinuzzi D, Vercelli AE, et al. 2006. High levels of Cre expression in neuronal progenitors cause defects in brain development leading to microencephaly and hydrocephaly. J. Neurosci. 26:9593–9602.

Haynes KA, Silver PA. 2009. Eukaryotic systems broaden the scope of synthetic biology. J. Cell Biol. 187:589–596.

Hurt JA, Thibodeau SA, Hirsh AS, Pabo CO, Joung JK. 2003. Highly specific zinc finger proteins obtained by directed domain shuffling and cell-based selection. Proc Natl Acad Sci USA 100:12271–12276.

Kalderon D, Roberts BL, Richardson WD, Smith AE. 1984. A short amino acid sequence able to specify nuclear location. Cell 39:499–509.

Ke Q, Costa M. 2006. Hypoxia-Inducible Factor-1 (HIF-1). Molecular Pharmacology 70:1469–1480.

Latonen L, Taya Y, Laiho M. 2001. UV-radiation induces dose-dependent regulation of p53 response and modulates p53-HDM2 interaction in human fibroblasts. Oncogene 20:6784–6793.

Lee SH, Kim J, Kim W-H, Lee YM. 2009. Hypoxic silencing of tumor suppressor RUNX3 by histone modification in gastric cancer cells. Oncogene 28:184–194.

Lu Y, Chu A, Turker MS, Glazer PM. 2011. Hypoxia-Induced Epigenetic Regulation and Silencing of the BRCA1 Promoter. Mol Cell Biol 31:3339–3350.

Murray-Zmijewski F, Slee EA, Lu X. 2008. A complex barcode underlies the heterogeneous response of p53 to stress. Nat Rev Mol Cell Biol 9:702–712.

Ohno K, Ishihata K, Tanaka-Azuma Y, Yamada T. 2008. A genotoxicity test system based on p53R2

gene expression in human cells: Assessment of its reactivity to various classes of genotoxic chemicals. Mutation Research/Genetic Toxicology and Environmental Mutagenesis 656:27–35.

Phillips IE, Silver PA. 2006. A New Biobrick Assembly Strategy Designed for Facile Protein Engineering. [Internet]:1–6. Available from: http://hdl.handle.net/1721.1/32535

Shaner NC, Campbell RE, Steinbach PA, Giepmans BNG, Palmer AE, Tsien RY. 2004. Improved monomeric red, orange and yellow fluorescent proteins derived from Discosoma sp. red fluorescent protein. Nat Biotechnol 22:1567–1572.

Shaner NC, Steinbach PA, Tsien RY. 2005. A guide to choosing fluorescent proteins. Nat Meth 2:905–909.

Sharma SV, Lee DY, Li B, Quinlan MP, Takahashi F, Maheswaran S, McDermott U, Azizian N, Zou L, Fischbach MA, et al. 2010. A chromatin-mediated reversible drug-tolerant state in cancer cell subpopulations. Cell 141:69–80.

Shibata T, Giaccia AJ, Brown JM. 2000. Development of a hypoxia-responsive vector for tumor-specific gene therapy. Gene Ther 7:493–498.

Spiller DG, Wood CD, Rand DA, White MRH. 2010. Measurement of single-cell dynamics. Nature 465:736–745.

Tanaka H, Arakawa H, Yamaguchi T, Shiraishi K, Fukuda S, Matsui K, Takei Y, Nakamura Y. 2000. A ribonucleotide reductase gene involved in a p53-dependent cell-cycle checkpoint for DNA damage. Nature 404:42–49.

To TL, Maheshri N. 2010. Noise Can Induce Bimodality in Positive Transcriptional Feedback Loops Without Bistability. Science 327:1142–1145.

Weinberger LS, Shenk T. 2007. An HIV feedback resistor: auto-regulatory circuit deactivator and noise buffer. Plos Biol 5:e9.

Zhang X, Rosenstein BS, Wang Y, Lebwohl M, Wei H. 1997. Identification of possible reactive oxygen species involved in ultraviolet radiation-induced oxidative DNA damage. Free Radic Biol Med 23:980–985.

Chapter 3

Studying memory of cellular stresses in human cells

Abstract[1]

Heterogeneous and long-term responses to transient cellular stimuli may underlie various developmental and disease processes. In particular, the heterogeneous nature of the cellular response to exogenous stresses makes these processes difficult to study in a large population of cells. Transcriptional memory devices, such as those discussed earlier in Chapter 2, allow us to isolate differentially responding subpopulations after exposure to hypoxia, DNA damage, and other stressors. In this Chapter, we discuss the study of long-term effects of hypoxic exposure demonstrating the necessity of a cellular memory device. We also explore the application of the DNA damage memory device to learn about the effects of γ-radiation exposure. Lastly, we modify the memory device to respond to inflammation via the NF-κB signaling pathway. Taken together, these studies show the modularity and broad usefulness of a cellular memory device.

[1] Portions of this chapter were reproduced with permission from Cold Spring Harbor Laboratory Press:
Burrill DR, Inniss MC, Boyle PM, Silver PA. 2012. Synthetic memory circuits for tracking human cell fate. Genes Dev 26:1486–1497.

Studying the long-term effects of transient hypoxic exposure in human cells

Introduction

The role of hypoxia in cancer initiation, progression and prognosis has been recognized for the past 70 years. The observation by Otto Warburg that tumor cells seem to favor glycolysis over aerobic respiration for energy production, even in the presence of oxygen, first suggested the involvement of hypoxia or hypoxic adaptation in this disease(Warburg 1961). Hypoxic cells have since been demonstrated to be present in many solid tumors, correlating with a poor response to treatment and increased chance of metastasis(Chan and Giaccia 2007). Solid tumors grow rapidly and outstrip their blood supply resulting in hypoxic conditions when cells are beyond the diffusion limit of oxygen(Teicher 1994). In addition, the new vessels formed by angiogenesis are often poorly formed and do not provide a consistent supply of oxygen and nutrients leading to cycling hypoxia(Cárdenas-Navia et al. 2008).

It has been shown that hypoxia can influence mutation rates in mammalian cells(Bristow and Hill 2008). Hypoxia and reoxygenation can cause oxidative stress that in turn can cause DNA damage. It is hypothesized that this could result in the accumulation of mutations that may drive tumor progression and metastasis(Bristow and Hill 2008). Recent studies have shown that acute, cycling hypoxia early in tumor development may result in a larger number of metastases later on(Bindra, Crosby, and Glazer 2007). In some cancer models, hypoxia appears to increase the amount of 8-oxo-dG (associated with GC-AT transitions) but has little effect on metastatic development, while in another cancer model, mice exposed to hypoxia show less 8-oxo-dG lesions but increased incidence of metastases(Bindra, Crosby, and Glazer 2007). This indicates that the relationship between hypoxia, DNA damage and metastasis is

more complicated than originally believed.

Aside from potentially causing DNA damage due to oxygen deprivation and reoxygenation, hypoxia has been proposed to impose epigenetic marks on cancer cells(Chen et al. 2006; Shahrzad et al. 2007; Lee et al. 2009; Watson et al. 2009). These changes in gene expression can be the result of chromatin modifications(Kouzarides 2007) or changes in transcriptional profile. Microarray studies have shown that numerous genes are differentially regulated as a result of hypoxic exposure, many of which are involved in pathways regulating cell proliferation, cell division and apoptosis(Fredlund et al. 2008). In addition, it has been demonstrated that in the case of *RUNX3*, a gene often silenced in gastric cancer, exposure to hypoxia results in histone modification, specifically histone deacetylation and methylation of H3K9(Lee et al. 2009). We propose to study whether other genes down regulated by hypoxia are subject to histone modifications or promoter hypermethylation and whether these modifications are inherited through cell division.

Microarray analysis will be used to look for genes that are differentially expressed due to exposure to hypoxia and whose expression remains changed once the cells have been reoxygenated. MCF10A cells will be exposed to hypoxia and allowed to recover in normal oxygen conditions for several days. RNA will be extracted from exposed cells and unexposed control cells that have been passaged at the same time. Transcript levels will be probed using the Human Gene 1.0 chip (Affymetrix). Once a set of differentially expressed genes has been identified, we will investigate whether these changes are the result of chromatin modification, DNA methylation, or transcriptional regulation.

Results and discussion

Preliminary characterization of hypoxic response

To determine which cell line to use to look for long-term effects of hypoxic exposure on the transcriptional profile of cells, we first performed end-point PCR on a panel of candidate cell lines (MCF7, T47D, and MCF10A) to make sure they were responding as expected to hypoxia (Figure 3.1A-C). Cells were exposed to 0.5% oxygen for 24 hours. RNA was then extracted and used to make cDNA. PCR was performed using primers for several known HIF-1 target genes. The product of these reactions was then analyzed by gel electrophoresis. We observed increased expression of *CA-IX* at 24 h relative to unexposed cells in all cell lines. We also observed moderately increased expression of *VEGF* and *GLUT1* at 24h in both MCF7 and MCF10A cells. While we did not observe long-term changes in these genes, we hypothesize that other genes may be affected. MCF7 and MCF10A are both cell lines derived from breast tissue. However, MCF7 is more representative of a cancer, while MCF10A is more "normal" cell type(Christofk et al. 2008). Based on this data, we decided to use MCF10A cells in further experiments, as our results would be more generalizable outside of a disease state.

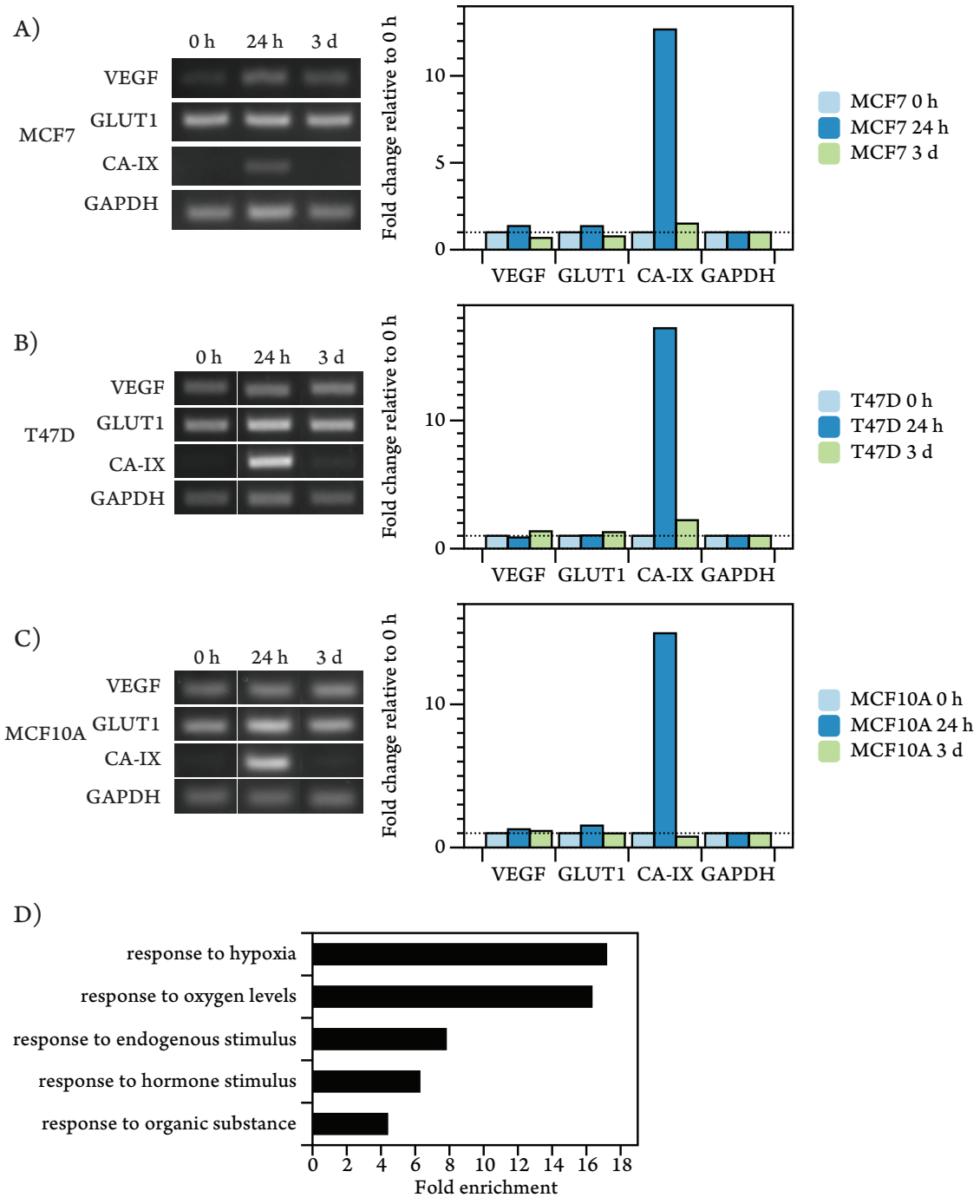

Figure 3.1. Hypoxic exposure causes upregulation of hypoxia responsive genes.

Figure 3.1(continued). Hypoxic exposure causes upregulation of hypoxia responsive genes. Selected cell lines (MCF7, T47D, MCF10A) were exposed to 0.5% O2 for 24 hours and allowed to recover in normoxia. RNA was extracted, converted to cDNA, and end-point PCR was performed and results quantified by ImageJ (A-C). MCF10A was selected for further analysis. RNA from 24 h exposed, and 3 d recovered cells along with corresponding unexposed controls were submitted for microarray analysis. While expected patterns of gene upregulation were seen after 24 h exposure (D) no significant patterns were seen after 3 d recovery.

Microarray analysis of the long-term transcriptional response to hypoxia

To investigate long-term transcriptional changes in response to hypoxic exposure, MCF10A cells were exposed to hypoxia (0.5% O_2) for 24 hours and then allowed to recover in normoxia. RNA was extracted from hypoxic cells immediately after exposure as well as cells that had recovered for 3, 6, and 9 days. RNA was also extracted from unexposed cells that were passaged at the same time. RNA from the hypoxic and 3 day recovered cells was sent to the Dana Farber microarray core for processing for the Human Gene 1.0 ST array (File B.1). The data was annotated and normalized by RMA analysis using the Affymetrix Expression Console software. Differential gene expression was determined using the MATLAB Bioinformatics Toolbox (MathWorks) and P-values were calculated using a permutation t-test of 10 000 permutations. Using a cutoff of fold change ≥ 2 and P-value ≤ 0.05, 79 genes were differentially regulated (66 up, 13 down). These genes were consistent with a typical response to low oxygen. However, using the same cutoffs, no genes were considered differentially regulated after 3 days recovery. When the fold change cutoff was relaxed to 1.5 fold, only 7 genes were differentially regulated (5 up, 2 down). Gene enrichment ontology analysis of the genes upregulated at 24 hours showed enrichment of expected hypoxia pathway genes (Figure 3.1D).

Since it is known that cells can undergo lasting changes in gene expression and chromatin structure after hypoxic exposure, it may be possible that changes are occurring in a small subpopulation of cells. Microarray would most likely not be able to detect this signal over the background of unaffected cells. In future, the hypoxia memory device described earlier in Chapter 2 could be moved to a biologically relevant cell line such as MCF10A. We showed that this synthetic transcriptional circuit allows us to isolate a differentially responding subpopulation. This experiment could then be repeated, comparing memory and non-memory cells.

Conclusions

While we did not observe a long-term transcriptional change due to hypoxic exposure by microarray analysis, previous work suggests that we might see a change in a subpopulation of cells. This result illustrates the advantage of using a synthetic memory device such as the one described in Chapter 2 of this work. Additionally, MCF10A may not be the appropriate cell line to use in this type of study. In future, we could engineer several cell lines with a hypoxia responsive memory device and analyze transcriptional changes using next-generation sequencing methods that can be more sensitive than microarray analysis.

Developing a γ-radiation sensing memory device in human cells

Introduction

One of the challenges present in manned space flight is mitigating the risk of exposure to high levels of radiation and its effect on human cell biology(Rizzo et al. 2012). In particular, astronauts are exposed to galactic cosmic rays (GCR) consisting of protons, helium nuclei, and high energy and charge (HZE) ions. While the immediate health implications of radiation encountered on earth are well studied, near and long-term consequences of GCR exposure are not yet understood(Hellweg and Baumstark-Khan 2007). This uncertainty is one of many challenges that must be resolved before long-term interplanetary travel becomes feasible. Understanding the consequences of prolonged exposure to GCR will help develop appropriate measures to prevent negative effects. Moreover, it would be a major breakthrough to develop a therapeutic strategy to reverse space-travel related radiation damage.

The effects of γ-radiation are often used as a proxy for GCR in estimating the impact of GCR on human health. Moderate doses of γ-radiation cause DNA damage and changes in gene expression, while higher doses increase the risk of developing cancer, and cause cell death leading to acute radiation syndrome (ARS), and tissue damage(Dörr and Meineke 2011). While the immediate impact of higher doses of γ-radiation is clear, the long-term consequences of both high and moderate exposure are more difficult to gauge. Similarly, the cellular response to GCR may depend greatly on the dose and fluence experienced. Additionally, it is not clear how to relate these data about γ-radiation to the potential health effects of GCR.

The field of synthetic biology aims to engineer biological systems in a more predictable and rapid manner to solve previously intractable problems and perform novel functions. This encompasses

everything from designing new genetic circuits, to reengineering complex chemical pathways, or rebuilding entire genomes. In Chapter 2, we describe a synthetic memory device, that can isolate a differentially responding cell population that maintains memory of a given stimulus(Burrill et al. 2012). This memory device is modular and can be re-engineered to respond to a variety of inputs including, doxycycline, hypoxia (low-oxygen), and DNA damage (UV radiation). These devices allow us to isolate a biologically distinct supopulation of cells that maintain growth but show transcriptional differences for many days after exposure to hypoxia and DNA damage.

We propose using the DNA damage sensing memory device integrated in human cells to study the possible long-term effects of γ-radiation exposure. While this device has been characterized using genotoxic chemicals and UV radiation, it should also be activated by γ-radiation(Shen and Maki 2010). This would allow us to study the long-term effect of radiation on gene expression profile and phenotype of these cells. Future work could adapt the device to produce an output such as a therapeutic to attempt to mitigate the effect of DNA damage.

Results and discussion

Characterization of existing DNA damage memory device after γ-radiation exposure

Previously, an integrated memory device responsive to the p53 repair response was built and characterized in U2OS cells using UV radiation (Chapter 2). This cell line was exposed to a range (from 1 Gy to 12.5 Gy) of γ-radiation using a Ce source. To determine whether the engineered cell line was responding normally to γ-radiation we analyzed expression of p53 target genes by RT-PCR. We collected RNA at 24 and 72 hour time-points and performed qRT-PCR to determine whether expression of predicted targets is up-regulated as expected in this cell line (Figure 3.2A). Unexpectedly,

expression of target genes was upregulated most strongly after 72 hours.

The behavior of the memory device was next assessed by both fluorescence microscopy and flow cytometry over several days. As observed when cells were exposed to UV, the trigger was not activated in all cells and the level of response was heterogeneous, however, the time scale of the response to γ-radiation was very different than UV (Figure 3.2B). While we observed a maximal response to UV exposure after 24 hours, at all exposure levels of γ-radiation, we observed the percent of responding cells increasing and reaching a maximum at 72 hours post-exposure. This tells us that the device is responding to p53 signaling in a similar manner to endogenous target genes. In addition, we observed a much smaller percentage of responding cells than when the same cell line was exposed to UV (see data presented in Chapter 2; Figure 2.5).

Investigating memory of γ-radiation exposure

To test whether expression of the memory device could still be maintained through cell division we exposed cells to γ-radiation and allowed them to recover for 72 hours. Based on previous data, we exposed the cells to 10 Gy γ-radiation as was the lowest dose tested that maximized response after 72 hours. Memory and non-memory cells were sorted by FACS and cultured separately in order to observe "memory" behavior by fluorescence microscopy and flow cytometry. However, we determined that when cells are exposed to this level of radiation, the memory cells do not survive the sorting procedure. We then exposed cells to lower amounts of radiation (5 Gy) recovered for 5 days, sorted by FACS, and cultured memory and non-memory cells separately. Memory was observed for up to 10 days post-sorting (Figure 3.2C). As with the DNA damage memory device described in Chapter 2, the memory

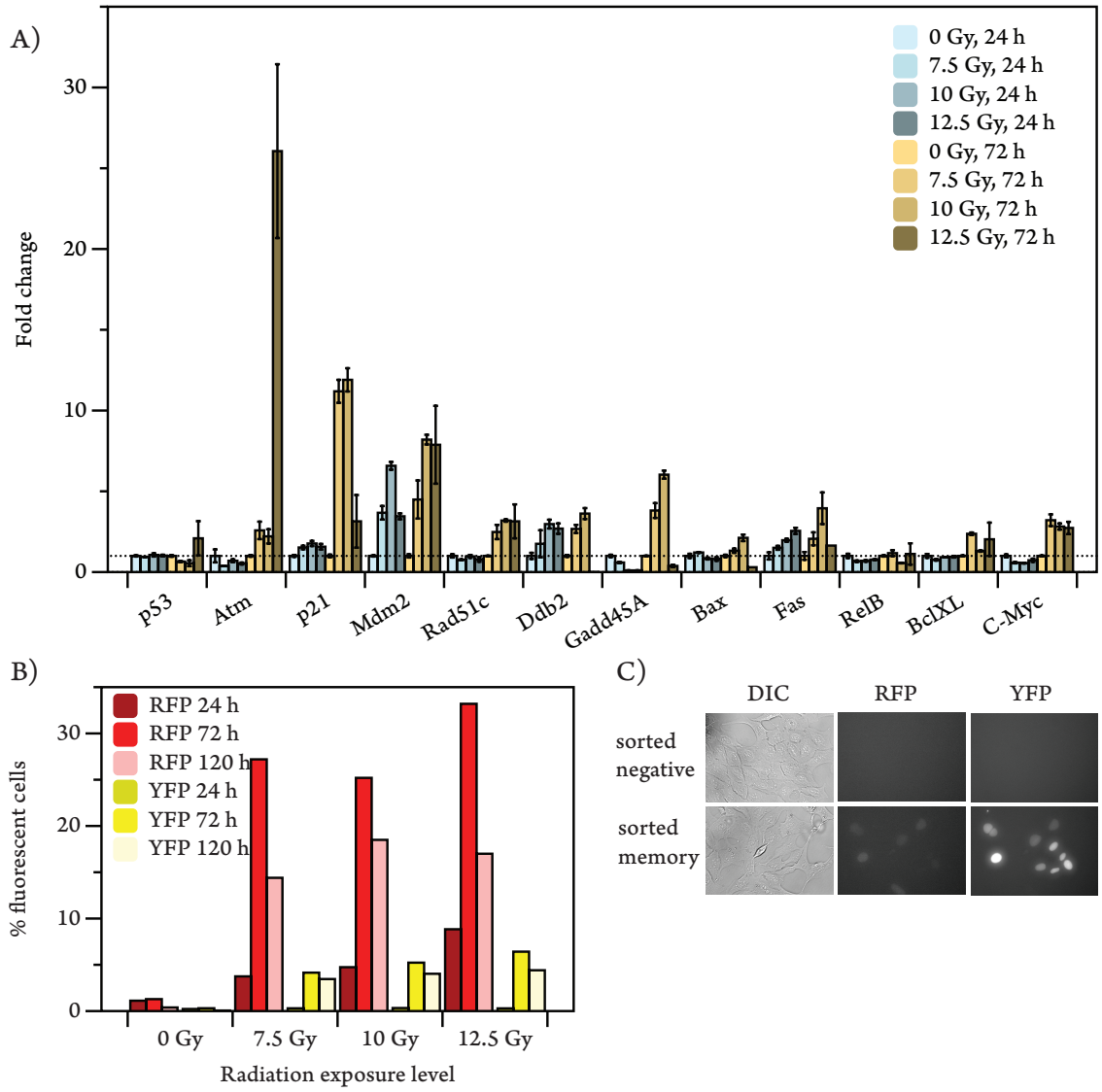

Figure 3.2. DNA damage cell line responds and remembers γ-radiation exposure. (A) The DNA damage memory cell line (MD12.34) described in Chapter 2 was exposed to γ-radiation (0, 7.5, 10, or 12.5 Gy) and allowed to recover for 24 or 72 h. RNA was extracted and analyzed by RT-PCR in triplicate. (B) Cells exposed to γ-radiation and allowed to recover for 24, 72, or 120 h were analyzed by flow cytometry to determine activation of trigger and memory genes. (C) Cells exposed to 5 Gy γ-radiation were allowed to recover for 5 d before cell sorting by FACS. Memory and non-memory (negative) cells were cultured for 10 d before imaging by fluorescence microscopy.

population grew much more slowly that the non-memory population indicating we most likely isolated a differentially responding subpopulation.

Improving response of memory device to γ-radiation

In an effort to improve responsiveness of the memory device to γ-radiation we constructed two alternate trigger constructs (Figure 3.3A), in parallel; the first based on the natural MDM2 promoter region(Batchelor et al. 2011), and the second built on a synthetic Gadd45-based promoter. Gadd45 was chosen as it is reported to be upregulated very quickly after γ-radiation exposure(Kastan et al. 1992). The synthetic promoter consists of six repeats of the p53 binding site from Gadd45 followed by a minimal CMV promoter(Shibata, Giaccia, and Brown 2000). As in the original device, both promoters drive transcription of an artificial transcription factor consisting of a synthetic zinc finger (ZF) DNA-binding domain (Hurt et al. 2003), one copy of the red fluorescent protein (RFP) mCherry (Shaner et al. 2004), the VP64 activation domain (Beerli et al. 1998), and a nuclear localization sequence (NLS) (Kalderon et al. 1984). We transiently transfected these constructs along with the original p53R2-RE trigger into U2OS cells to compare their inducibility by γ-radiation. Cells were exposed to either 10 J/m^2 UV or 5Gy γ-radiation and allowed to recover for 1 d before analysis by flow cytometry. While both the MDM2 promoter and synthetic Gadd45 promoters respond to DNA damage in the form of UV and γ-radiation, the MDM2 promoter showed relatively higher activation by γ-radiation. However, the original synthetic p53R2 promoter is activated in a higher percentage of cells by both forms of radiation. Therefore, we decided to continue using the original device.

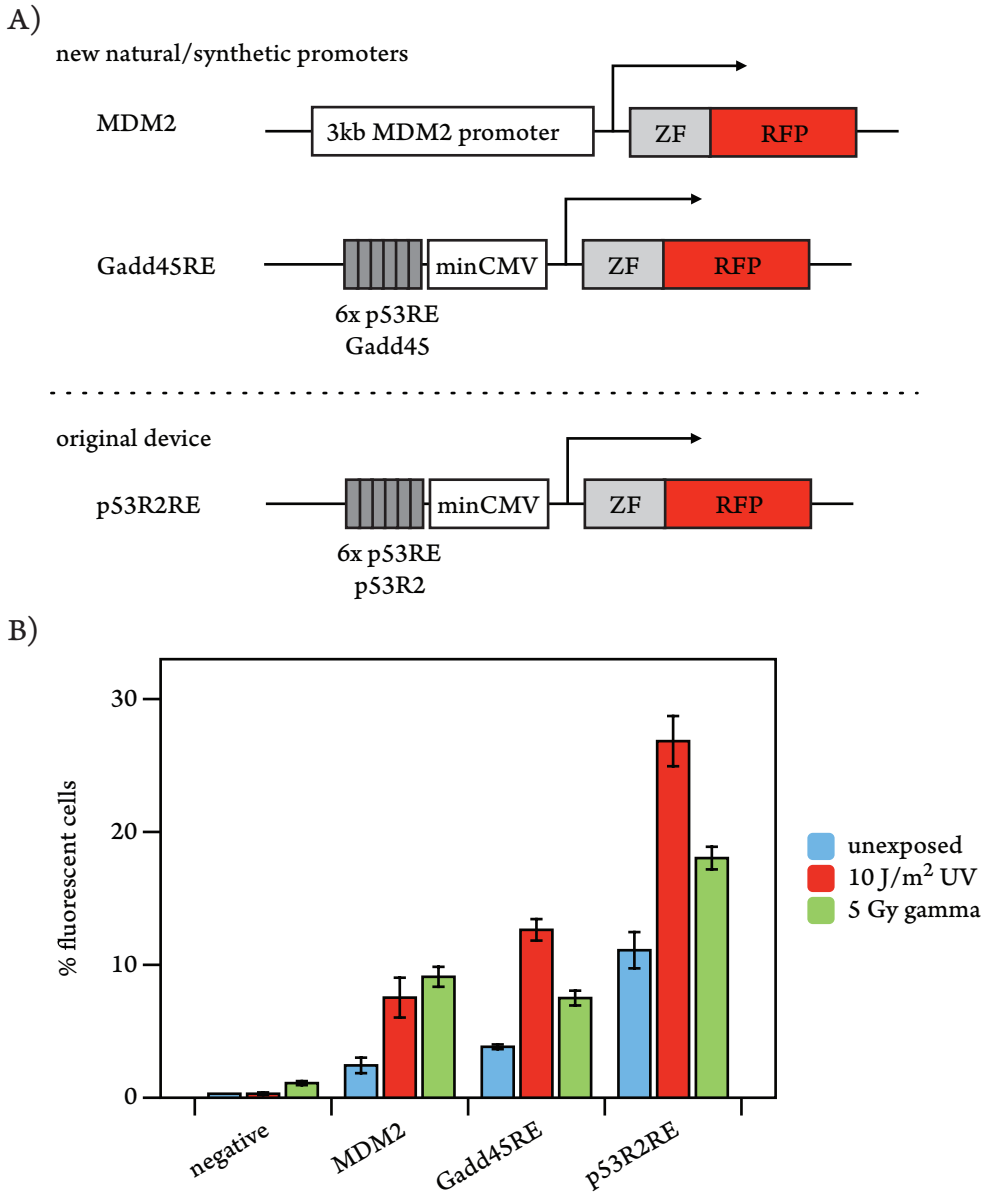

Figure 3.3. Synthetic and natural p53 responsive promoters are activated by γ-radiation. (A) Schematic comparing the new trigger genes to the original DNA damage memory device. The 3kb MDM2 promoter or a synthetic promoter consisting of 6 repeats of the p53RE from the Gadd45 promoter region were cloned in place of the original p53R2RE promoter. (B) The responsiveness to γ-radiation was assayed by transient transfection of trigger constructs into U2OS cells. Cells were transfected, exposed the following day to γ and UV radiation, and analyzed by flow cytometry 24 h later.

Conclusions

We have demonstrated that the DNA damage memory device can be used to detect more diverse types of stimuli than UV radiation as characterized in Chapter 2. We also demonstrated that the synthetic promoter used in previous work is actually quite sensitive. This shows that the memory device can have broad applicability for further studies. In future, we would like to move the DNA damage memory device to more biologically relevant cell types and continue to characterize its responsiveness to different stimuli. This synthetic device will help us gain a greater understanding of the long-term effects of transient exposure to multiple sources of DNA damage.

Development of an inflammation responsive memory device

Introduction

Human disease pathology is complex, involving multiple tissues and organs(Huh et al. 2012). While traditional 2D cell culture systems have been integral in uncovering the architecture of many cellular signaling pathways, these systems are not representative of normal physiology(Huh, Hamilton, and Ingber 2011). For instance, in the context of drug discovery, these culture systems are used for initial screening of drug candidates. Animal studies are then needed to understand the effect of these drug candidates on whole organisms. However, even the best animal model is not a perfect substitute for human physiology and many drugs fail in clinical trials(Huh et al. 2012). Significant progress has been made developing 3D culture systems that more closely mimic the natural environment. As these systems incorporate human cells, they have the potential to become even more useful in the drug development process than animal models. The combination of novel 3D cell culture systems and synthetic memory devices presents an opportunity to gain an even greater understanding of underlying biology and develop a more refined drug discovery platform.

Type 2 diabetes is a complex disease characterized by elevated blood glucose as a result of insulin insensitivity(Novials, Montane, and Cadavez-Trigo 2014). This disease also involves an inflammatory response along with oxidative stress and endoplasmic reticulum (ER) stress which can eventually lead to a loss of beta cell function and cell death(Novials, Montane, and Cadavez-Trigo 2014). The NF-κB signaling pathway is central to the cellular response to all these triggers. NF-κB family transcription factors integrate signal from inflammatory cytokines and metabolic stress (including hyperglycemia), impacting further inflammation, cell survival, immunity, and metabolic pathways(Tornatore et al. 2012). By modifying the DNA damage memory device described earlier to

respond to NF-κB signaling, we can create a synthetic memory device that responds to inflammation and cellular stress in general. Such a device will help us learn about long-term cellular responses to inflammation and stress in a diabetes model. By integrating engineered cells into a 3D culture system, we can also help detect stress responses after drug treatment, thus enabling more effective drug development.

We propose to move the existing DNA damage memory device along with a newly developed inflammation sensing memory device into beta cells to use in a novel drug discovery platform. Initially, these devices will be characterized in the immortalized insulinoma cell line βTC-6(Poitout et al. 1995), but will eventually be integrated in primary rat islet cells and human iPS cells. These synthetic circuits will allow us to gain a deeper understanding of biology of a complex disease like diabetes and could enable more sensitive screening of potential drug candidates.

Results and discussion

Design of an inflammation sensing memory device

To develop an inflammation sensing memory device, we used a similar strategy as described in Chapter 2 for building the hypoxia and DNA damage responsive devices. As we previously demonstrated the modularity of the memory device, it should be possible to modify the promoter of the trigger gene to be activated by an endogenous inflammation responsive pathway. We chose to couple memory to activation of NF-κB, as this signaling pathway is central to inflammatory responses as well as a general stress response pathway(Tornatore et al. 2012). To build a synthetic NF-κB responsive promoter, we chose to put several repeats of known NF-κB response elements (NRE) from the IL-1β gene(Hiscott et al. 1993; Cogswell et al. 1994) or the pNiFty3 promoter (Invitrogen) upstream of a minimal CMV

promoter(Shibata, Giaccia, and Brown 2000) (Figure 3.4A). This promoter mirrors the structure of the original DNA damage responsive promoter. We built four variants of this promoter by using one of two NREs and one of two spacings between NREs in each (Table 3.1). The four promoters were cloned upstream of the same artificial transcription factor described earlier, consisting of a synthetic zinc finger (ZF) DNA-binding domain (Hurt et al. 2003), one copy of the red fluorescent protein (RFP) mCherry (Shaner et al. 2004), the VP64 activation domain (Beerli et al. 1998), and a nuclear localization sequence (NLS) (Kalderon et al. 1984).

Table 3.1. Synthetic NF-κB responsive promoter elements.

Promoter	NRE Variant	Spacer Length	Variant Sequence
NRE1	A	24 bp	A: GGGAAAATCC
NRE2	A	12 bp	
NRE3	B	24 bp	B: GGGACTTTCC
NRE4	B	12 bp	

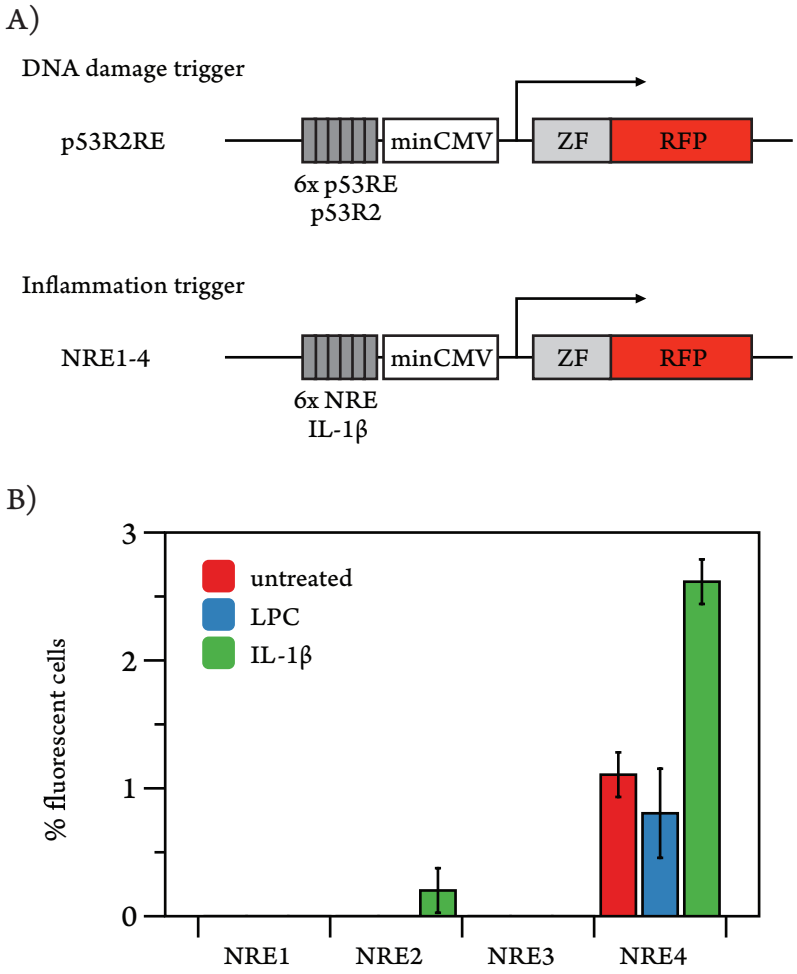

Figure 3.4. Synthetic NF-κB responsive promoter responds to inflammatory stimulus. (A) Schematic comparing the new trigger genes to the original DNA damage memory device. A synthetic promoter consisting of 6 repeats of the NFκB response element from the IL-1β promoter region or the pNiFty3 vector upstream of the minimal CMV promoter was cloned in place of the original p53R2RE promoter. (B) Responsiveness to inflammation-like stimuli was assayed by transient transfection of trigger constructs into βTC-6 cells. Cells were transfected, exposed the following day to LPC and IL-1β, and analyzed by flow cytometry 24 h later.

Characterization of NF-κB responsive trigger genes

We next tested these novel trigger genes by transient transfection. As we are interested in using this device to study inflammatory responses of beta cells in response to drug treatment, we first characterized these constructs in a insulinoma cell line; βTC-6. Cells were plated in 12-well plates and allowed to adhere overnight. Cells were transfected and the following day, they were exposed to LPC (lipopolysaccharide, 20 μg/mL; PMA, 10 ng/mL; db cAMP, 100 μM) or IL-1β (0.1 μg/mL). Three of the four triggers showed little or no expression in response to these stimuli; however, the fourth construct was induced by IL-1β (Figure 3.4B). Expression was also seen after LPC treatment, however levels of activation were comparable to an uninduced control. Thus these preliminary results suggest that we have successfully built an NF-κB responsive trigger gene that may allow us to study long-term effects of inflammatory responses in human cells. Work is ongoing to refine this trigger gene, assemble a complete memory device, and integrate this into the genome. In addition, this circuit, along with the DNA damage memory device, will be tested in primary rat beta cells as well as iPS cells.

Conclusions

While we did not assemble the whole inflammation sensing memory device, we have preliminary results showing that we can create a synthetic NF-κB responsive trigger gene. Future work will refine this promoter and combine the trigger gene with the memory loop gene before integrating these constructs into the genome of βTC-6 cells as well as primary rat islet cells and human iPS cells. This will create a cell line that can help us study the long-term effects of inflammatory signaling. As the NF-κB pathway lies at the intersection of many stress response pathways, this synthetic memory circuit will be useful for studying a variety of disease pathologies.

Materials and Methods

Plasmid constructs

Escherichia coli DH5α was used for all plasmid manipulations. Bacteria were grown in LB-ampicillin media to maintain plasmids; if engineered constructs contained synthetic zinc fingers, media was supplemented with 0.02 mM zinc chloride. DNA fragments were generated by PCR and assembled via restriction cloning or Gibson assembly (Gibson et al. 2009).

Response elements from human p53R2 gene (Ohno et al. 2008), IL-1β gene (Hiscott et al. 1993), or pNiFty3 vector (Invitrogen) were constructed as annealed oligos (Integrated DNA Technologies) and ligated in front a minimal promoter (Shibata, Giaccia, and Brown 2000) to generate the p53R2-RE and NRE1-4 promoters. Human codon-optimized synthetic zinc fingers (Hurt et al. 2003) were commercially synthesized by Mr. Gene (Regensburg, Germany).

For transient transfections, memory devices or triggers were cloned into a pcDNA3.1™ (+)-based vector (Invitrogen) in which the neomycin resistance marker was replaced with puromycin resistance, and the constitutive CMV promoter was deleted (Silver Lab).

Cell culture

MCF7, T47D cells were grown in DMEM media supplemented with 10% fetal bovine serum (FBS) and 1% penicillin and streptomycin. MCF10A cells were grown in DMEM supplemented with 5% horse serum, 20 ng/uL EGF (Peprotech), 0.5 mg/mL hydrocortisone (Sigma), 100 ng/uL cholera toxin (Sigma), 10 ug/mL insulin (Sigma) and 1% penicillin and streptomycin. U2OS cells were grown in McCoy's 5A medium supplemented with 10% tetracycline-screened FBS and 1% penicillin and

streptomycin; βTC-6 cells were grown in DMEM supplemented with 10% FBS and 1% penicillin and streptomycin. All cell lines were grown at 37˚C in a humidified CO_2 incubator.

Transfection of U2OS and βTC-6 cells

Transient transfections were performed by plating 1.2 X 10^5 cells/well in 12-well culture dishes and transfecting with 800 ng plasmid DNA and 2 ul Lipofectamine® 2000 (Invitrogen) in 1 ml of antibiotic-free medium. Cells were exposed the following day to γ or UV radiation, LPC treatment (lipopolysaccharide, 20 μg/mL; PMA, 10 ng/mL; db cAMP, 100 μM) or IL-1β (0.1 ug/mL) (Cogswell et al. 1994) and analyzed by flow cytometry.

Induction of DNA damage, hypoxic and inflammatory response

To induce the DNA damage response in MD12/p53R2-RE cells, 3.0 x 10^5 cells/well were plated in 6-well plates. The following day, plates were exposed to a brief burst of 10 J/m^2 shortwave ultraviolet radiation (UV) (Lahav Lab, Harvard Systems Biology) or varying levels of γ-radiation from a Ce source (Harvard Medical School). To induce hypoxia, 3.0 x 10^6 cells were plated in 10 cm plates. The following day, plates were exposed to hypoxia (0.5% O_2, 5.0% CO_2) in a hypoxic chamber (Kaelin lab, Dana Farber Cancer Institute). When cells were returned to normoxia, media was replaced with appropriate maintenance media. To induce inflammation and NF-κB signaling, cells were exposed to LPC treatment (lipopolysaccharide, 20 μg/mL; PMA, 10 ng/mL; db cAMP, 100 μM) or 0.1 ug/mL IL-1β (Cogswell et al. 1994) for 24 hours.

Fluorescence microscopy

Cells were imaged at 20x with a Nikon TE2000-E inverted fluorescence microscope equipped with a Hamamatsu ORCA-ER camera, and HcRed (RFP) and JP2 (YFP) filters (Silver Lab). Images were acquired and analyzed using Metamorph software.

Flow cytometry and cell sorting

Cells were trypsinized and resuspended in PBS before being loaded in 96 well plates or 5 mL polystyrene tubes (BD Biosciences) on an LSRII (BD Biosciences) with 488-nm (DsRed) and 568-nm (Fitc) lasers (Harvard Systems Biology). 1.0 X 10^4 cells were analyzed for RFP (DsRed) and YFP (FITC) fluorescence and gated based on cell size and granularity. Unexposed cells controlled for basal fluorophore expression. Data was analyzed using FlowJo software.

To sort MD12/p53R2-RE cells, 12, 6-well plates were exposed to γ-radiation and recovered for 3 or 5 d. Cells were then processed as described above, except that 4, 6-well plates of cells were pooled to produce three replicates.

Processed cells were run on a FACS Aria II with a 100 uM nozzle at 20 psi (Harvard Systems Biology). Excitation optics for RFP consisted of a 75 mW 594 nm laser; detection optics included a 630/22 bandpass filter. Excitation optics for YFP consisted of a 15 mW 488 nm laser; detection optics included a 520 nm longpass dichroic mirror and a 530/30 bandpass filter. For microscopy, 200,000 memory and non-memory cells were sorted. Sorted MD12/p53R2-RE cells were seeded in 24-well dishes.

Endogenous pathway induction for RT-PCR

MD12/p53R2-RE and U2OS cells were plated and exposed to γ-radiation or hypoxia, respectively. Whole cell RNA was extracted using the RNeasy Mini Kit (Qiagen), and cDNA was prepared using the SuperScript III First Strand Synthesis System (Invitrogen). Unexposed cells served as controls for background expression.

Differential expression of genes was analyzed by real-time PCR using 0.5 ug RNA of specified cell populations. Primers amplified ~ 100 base pairs (Table B.1). Differential expression was normalized to human gene *ACTB* or *GAPDH*.

Gene expression profiling

U2OS cells were plated in 10 cm plates, exposed to 0.5% O2 for 24 h in triplicate, and allowed to recover for 3, 5, 7, and 9 d. Unexposed cells were plated the same way and passaged at the same time. For each biological replicate, RNA was extracted from exposed and unexposed cells using the RNeasy Mini Kit (Qiagen). For the 0 and 3 d time points, cDNA was prepared, biotinylated, and hybridized to Gene 1.0 ST arrays (Affymetrix). Arrays were scanned and quantified according to standard Affymetrix protocols at the Dana Farber Microarray Core Facility (Dana Farber Cancer Institute).

Identification and analysis of differentially regulated genes

Data was annotated and normalized by RMA-analysis using Affymetrix Expression Console Software. Differential gene expression was determined using the Matlab Bioinformatics Toolbox (MathWorks). P-values were calculated using a permutation t-test of 10,000 permutations. Genes with a fold change ≥ 2 and p-value ≤ 0.05 were considered differentially expressed and analyzed for gene ontology enrichment

via GoStat (http://gostat.wehi.edu.au), with Benjamini correction for multiple hypothesis testing; enrichment was considered significant with $P \leq 0.01$.

Acknowledgements and attributions

We would like to acknowledge the contributions of Caroline Kim and Nicolas Hafner who both helped perform the experimental work presented in this Chapter. Additionally, we would like to thank Jodene Moore in the Systems Biology Flow Cytometry facility for all her help. We would also like to thank the Lahav lab and Weiss lab for providing materials integral to these projects.

Design of the experiments in Chapter 3 was done by myself. Assembly of constructs described in Chapters 3 was performed by Caroline Kim and Nicolas Hafner under my supervision. Exposure of DNA damage memory device to γ-radiation was performed by myself and qRT-PCR was performed by Caroline Kim. Testing of the inflammation memory device was performed by Nicolas Hafner.

References

Batchelor E, Loewer A, Mock C, Lahav G. 2011. Stimulus-dependent dynamics of p53 in single cells. Mol Syst Biol 7:488.

Beerli RR, Segal DJ, Dreier B, Barbas CF. 1998. Toward controlling gene expression at will: specific regulation of the erbB-2/HER-2 promoter by using polydactyl zinc finger proteins constructed from modular building blocks. Proc Natl Acad Sci USA 95:14628–14633.

Bindra RS, Crosby ME, Glazer PM. 2007. Regulation of DNA repair in hypoxic cancer cells. Cancer Metastasis Rev 26:249–260.

Bristow RG, Hill RP. 2008. Hypoxia and metabolism. Hypoxia, DNA repair and genetic instability. Nat Rev Cancer 8:180–192.

Burrill DR, Inniss MC, Boyle PM, Silver PA. 2012. Synthetic memory circuits for tracking human cell fate. Genes Dev 26:1486–1497.

Cárdenas-Navia LI, Mace D, Richardson RA, Wilson DF, Shan S, Dewhirst MW. 2008. The pervasive presence of fluctuating oxygenation in tumors. Cancer Res 68:5812–5819.

Chan DA, Giaccia AJ. 2007. Hypoxia, gene expression, and metastasis. Cancer Metastasis Rev 26:333–339.

Chen H, Yan Y, Davidson TL, Shinkai Y, Costa M. 2006. Hypoxic stress induces dimethylated histone H3 lysine 9 through histone methyltransferase G9a in mammalian cells. Cancer Res 66:9009–9016.

Christofk HR, Vander Heiden MG, Harris MH, Ramanathan A, Gerszten RE, Wei R, Fleming MD, Schreiber SL, Cantley LC. 2008. The M2 splice isoform of pyruvate kinase is important for cancer metabolism and tumour growth. Nature 452:230–233.

Cogswell JP, Godlevski MM, Wisely GB, Clay WC, Leesnitzer LM, Ways JP, Gray JG. 1994. NF-kappa B regulates IL-1 beta transcription through a consensus NF-kappa B binding site and a nonconsensus CRE-like site. J. Immunol. 153:712–723.

Dörr H, Meineke V. 2011. Acute radiation syndrome caused by accidental radiation exposure - therapeutic principles. BMC Med 9:126.

Fredlund E, Ovenberger M, Borg K, Påhlman S. 2008. Transcriptional adaptation of neuroblastoma cells to hypoxia. Biochem Biophys Res Commun 366:1054–1060.

Gibson DG, Young L, Chuang R-Y, Venter JC, Hutchison CA, Smith HO. 2009. Enzymatic assembly of DNA molecules up to several hundred kilobases. Nat Meth 6:343–345.

Hellweg CE, Baumstark-Khan C. 2007. Getting ready for the manned mission to Mars: the astronauts' risk from space radiation. Naturwissenschaften 94:517–526.

Hiscott J, Marois J, Garoufalis J, D'Addario M, Roulston A, Kwan I, Pepin N, Lacoste J, Nguyen H, Bensi G. 1993. Characterization of a functional NF-kappa B site in the human interleukin 1 beta promoter: evidence for a positive autoregulatory loop. Mol Cell Biol 13:6231–6240.

Huh D, Hamilton GA, Ingber DE. 2011. From 3D cell culture to organs-on-chips. Trends Cell Biol 21:745–754.

Huh D, Torisawa Y-S, Hamilton GA, Kim HJ, Ingber DE. 2012. Microengineered physiological biomimicry: Organs-on-Chips. Lab Chip 12:2156.

Hurt JA, Thibodeau SA, Hirsh AS, Pabo CO, Joung JK. 2003. Highly specific zinc finger proteins obtained by directed domain shuffling and cell-based selection. Proc Natl Acad Sci USA 100:12271–12276.

Kalderon D, Roberts BL, Richardson WD, Smith AE. 1984. A short amino acid sequence able to specify nuclear location. Cell 39:499–509.

Kastan MB, Zhan Q, el-Deiry WS, Carrier F, Jacks T, Walsh WV, Plunkett BS, Vogelstein B, Fornace AJ. 1992. A mammalian cell cycle checkpoint pathway utilizing p53 and GADD45 is defective in ataxia-telangiectasia. Cell 71:587–597.

Kouzarides T. 2007. Chromatin modifications and their function. Cell 128:693–705.

Lee SH, Kim J, Kim W-H, Lee YM. 2009. Hypoxic silencing of tumor suppressor RUNX3 by histone modification in gastric cancer cells. Oncogene 28:184–194.

Novials A, Montane J, Cadavez-Trigo L. 2014. Stress and the inflammatory process: a major cause of pancreatic cell death in type 2 diabetes. DMSO:25.

Ohno K, Ishihata K, Tanaka-Azuma Y, Yamada T. 2008. A genotoxicity test system based on p53R2 gene expression in human cells: Assessment of its reactivity to various classes of genotoxic chemicals. Mutation Research/Genetic Toxicology and Environmental Mutagenesis 656:27–35.

Poitout V, Stout LE, Armstrong MB, Walseth TF, Sorenson RL, Robertson RP. 1995. Morphological and functional characterization of βTC-6 cells—an insulin-secreting cell line derived from transgenic mice. Diabetes 44:306–313.

Rizzo AM, Corsetto PA, Montorfano G, Milani S, Zava S, Tavella S, Cancedda R, Berra B. 2012. Effects of Long-Term Space Flight on Erythrocytes and Oxidative Stress of Rodents.Agarwal S, editor. PLoS ONE 7:e32361.

Shahrzad S, Bertrand K, Minhas K, Coomber BL. 2007. Induction of DNA hypomethylation by tumor hypoxia. Epigenetics 2:119–125.

Shaner NC, Campbell RE, Steinbach PA, Giepmans BNG, Palmer AE, Tsien RY. 2004. Improved monomeric red, orange and yellow fluorescent proteins derived from Discosoma sp. red fluorescent protein. Nat Biotechnol 22:1567–1572.

Shen H, Maki CG. 2010. p53 and p21(Waf1) Are Recruited to Distinct PML-Containing Nuclear Foci in Irradiated and Nutlin-3a-Treated U2OS Cells. J. Cell. Biochem. 111:1280–1290.

Shibata T, Giaccia AJ, Brown JM. 2000. Development of a hypoxia-responsive vector for tumor-specific gene therapy. Gene Ther 7:493–498.

Teicher BA. 1994. Hypoxia and drug resistance. Cancer Metastasis Rev 13:139–168.

Tornatore L, Thotakura AK, Bennett J, Moretti M, Franzoso G. 2012. The nuclear factor kappa B signaling pathway: integrating metabolism with inflammation. Trends Cell Biol 22:557–566.

Warburg O. 1961. [On the facultative anaerobiosis of cancer cells and its use in chemotherapy]. Münchener medizinische Wochenschrift (1950) 103:2504–2506.

Watson JA, Watson CJ, McCrohan A-M, Woodfine K, Tosetto M, McDaid J, Gallagher E, Betts D,

Baugh J, O'Sullivan J, et al. 2009. Generation of an epigenetic signature by chronic hypoxia in prostate cells. Hum Mol Genet 18:3594–3604.

Chapter 4

Building a Pulse-Detecting Genetic Circuit

Abstract

The design and engineering of a robust event counter has been a goal in the synthetic biology field for many years. While preliminary counting circuits capable of detecting a few events have been built, designing a reliable and scalable counter is still a difficult task. One difficulty facing event counter function is the ability to define a single event, or pulse, regardless of its duration. To accomplish this, we propose a novel design for a pulse-detecting genetic circuit that responds specifically to the falling edge of a pulse. In this Chapter we discuss the characterization of a dominant negative mutant of cI protein as a potential component of a pulse detecting genetic circuit and describe preliminary characterization of the lambda switch as a functional pulse detector.

Introduction

In previous Chapters, we discussed the development and applications of synthetic cellular memory devices. We showed that these devices can be used to study heterogeneous responses to cellular stresses and discussed their future applications in drug development and tissue engineering. However, memory devices are also a key component of a more complex circuit: a counter(Subsoontorn and Endy 2012). An isolated memory device can be thought of as a 1-counter as it toggles between 2 states. By linking multiple orthogonal memory devices together, we can build counters that can count higher. While unidirectional memory devices like the ones discussed earlier in this dissertation can be used to build a counter, the limit of counting is equal to the number of switches(Subsoontorn and Endy 2012). This makes counting to high numbers challenging, as many orthogonal systems must be designed. Alternatively, reversible or bidirectional memory switches can also be used to build a counter. In this case, we can theoretically count much higher with fewer components.

Building a counter has been a goal in the field of synthetic biology for many years. Such a device would be very useful for studying disease progression in cancer, or learning more about development (Bonnet et al. 2013). A robust counter would also be useful in engineering cells – both eukaryotic and prokaryotic – to perform novel tasks. In complex electrical circuits and computation, counters play an integral role. If we hope to someday program biological systems with the same degree of sophistication, the development of well-characterized and functional counters will be essential. To date, significant progress has been made in building the necessary foundational memory switches. Unidirectional transcriptional memory switches based on both transcriptional positive feedback loops and DNA rearrangement have been studied extensively(Kramer et al. 2004; Ajo-Franklin et al. 2007; Burrill and Silver 2011; Burrill et al. 2012; Lou et al. 2012). In addition, several groups have also developed

transcriptional double-negative feedback loops – toggle switches – and reversible DNA rearrangement based switches creating bidirectional memory(Gardner, Cantor, and Collins 2000; Ham et al. 2008; Bonnet, Subsoontorn, and Endy 2012; Siuti, Yazbek, and Lu 2013). However, only a few circuits with limited counting ability have been created(Friedland et al. 2009).

One obstacle standing in the way of building a robust event counter is the ability to detect a single event regardless of the length of its occurrence. For example, previous counters were sensitive to the length of time they are exposed to inducer; too short and the count is not advanced, too long and the count moves ahead too far(Friedland et al. 2009). This decreases the modularity of the device, as it can be tuned to work in a certain situation but may fail if moved to a different context. We propose to build a pulse detector that responds only to the falling edge of a pulse of stimulus. This would mean, regardless of the length of exposure to inducer, a counter would only advance at the end of the pulse (Figure 4.1). While synthetic circuits have been built that respond to the rising edge of a stimulus by generating a pulse of output(Basu et al. 2004), our design represents the first synthetic biological circuit that detects the end of a pulse of stimulus.

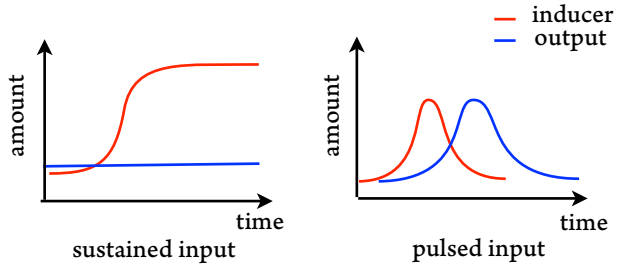

Figure 4.1. A pulse detecting genetic circuit responds to the falling edge of a pulse of stimulus. Our proposed design for a pulse-detecting genetic circuit will have no output when inducer levels are low or high, however, when transitioning from high to low inducer, the circuit should produce a pulse of output.

Our design for the pulse detector is based on the lambda cI repressor protein(Ptashne et al. 1980). This protein has several features that make this circuit possible. The lambda phage has both a lysogenic state – the phage is integrated in the E. coli genome and is replicated during cell division – and a lytic state – the phage produces many new phage particles and lyses the cell. This decision is made based on the stress on the bacterial host caused by environmental conditions. Controlling this behavior is a transcriptional switch consisting of the cI and cro genes transcribed from a divergent promoter (Prm and Pr, respectively)(Ptashne 2004) (Figure 4.2A). While cro represses expression of cI, cI represses cro expression as well as promoting its own expression(Hochschild, Irwin, and Ptashne 1983). However, high levels of cI expression will also shut down the Prm promoter maintaining cI at a moderate level. Thus, when cI is expressed, cro is repressed and the phage remains in a lysogenic state. However, if cro is expressed, cI is repressed and the phage enters the lytic cycle. Importantly for our design, cI normally binds to its operator sequences as a dimer(Ptashne 2004). A lambda phage unable to form lysogens was isolated and found to contain a mutation in the DNA binding domain of the cI protein (N55K)(Nelson and Sauer 1986). It was found that this mutation abolished binding specificity at the operator sequences and the non-specific DNA binding affinity was increased, however it should not interfere with dimerization of the protein. We refer to this protein as dominant-negative cI (cI_{DN}).

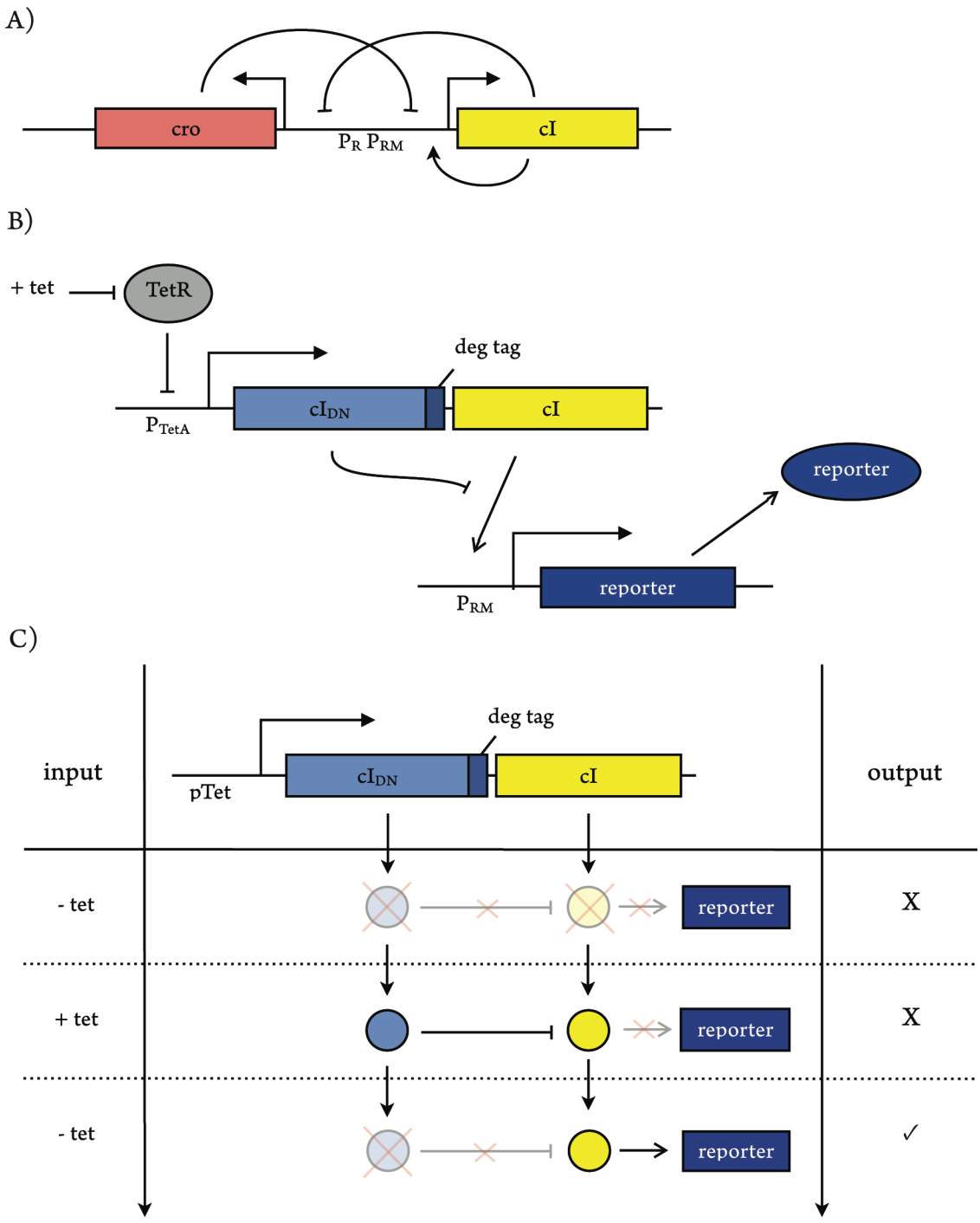

Figure 4.2. Components of the lambda phage switch can be used to build a pulse detecting genetic circuit.

Figure 4.2 (continued). Components of the lambda phage switch can be used to build a pulse detecting genetic circuit. (A) The lambda switch is a bistable switch consisting of a double negative feedback loop where cI and cro repress the other's transcription. In addition, cI also activates its own expression from the Prm promoter. (B) A pulse detecting genetic circuit can be designed by coexpressing a dominant-negative mutant of cI along with wild-type cI, and building a cI reporter using the Prm promoter. By increasing the degradation rate of cI_{DN}, a pulse detector is created. (C) When no inducer is present, neither cI_{DN} nor cI is expressed and there is no output. When inducer is added, both proteins are expressed, cI_{DN} blocks cI function, and no output is detected. However, when inducer is removed, cI_{DN} degrades and cI can activate expression of the reporter gene.

We propose building a pulse detecting genetic circuit by co-expressing a degradation tagged cI_{DN} and wild-type cI from a single inducible promoter (Figure 4.2B). A reporter gene will be expressed from the Prm promoter. Before induction, neither cI_{DN} or cI will be produced and no output is expected from the reporter gene. When the circuit is induced, both cI_{DN} and cI will be produced, cI_{DN} will block cI function and still no reporter expression will be observed. Only when inducer is removed will cI_{DN} degrade leaving cI to dimerize and activate reporter expression (Figure 4.2C). This will produce a novel pulse-detecting circuit that reports on the falling edge of a stimulus.

Results and discussion

Construction of inducible cI and cI_{DN} genes

To engineer a pulse detecting circuit, we first built a small library of inducible cI_{DN} variants and an inducible wild-type cI. To characterize the interaction between cI_{DN} variants and cI protein, we used a reporter plasmid obtained from the Registry of Biological Parts. This plasmid contains a modified Prm promoter driving transcription of a degradation-tagged sfGFP gene(Huang, Holtz, and Maharbiz 2012). The promoter has been modified to eliminate auto-inhibition by high levels of cI so that expression of the reporter will increase with higher levels of cI expression, even if these are beyond the natural level of cI repressor maintenance(Huang, Holtz, and Maharbiz 2012).

In the initial design of the characterization strains, we planned to express cI repressor from the arabinose-inducible pBAD promoter(Guzman et al. 1995). Using gene synthesis, we built a plasmid containing araC and the pBAD promoter followed by the wild-type cI gene. This construct was integrated in the phi80 phage attachment site using the CRIM integration system. This strain was then transformed with the Prm sfGFP reporter plasmid (Figure 4.3A, Table 4.1). Cells containing inducible

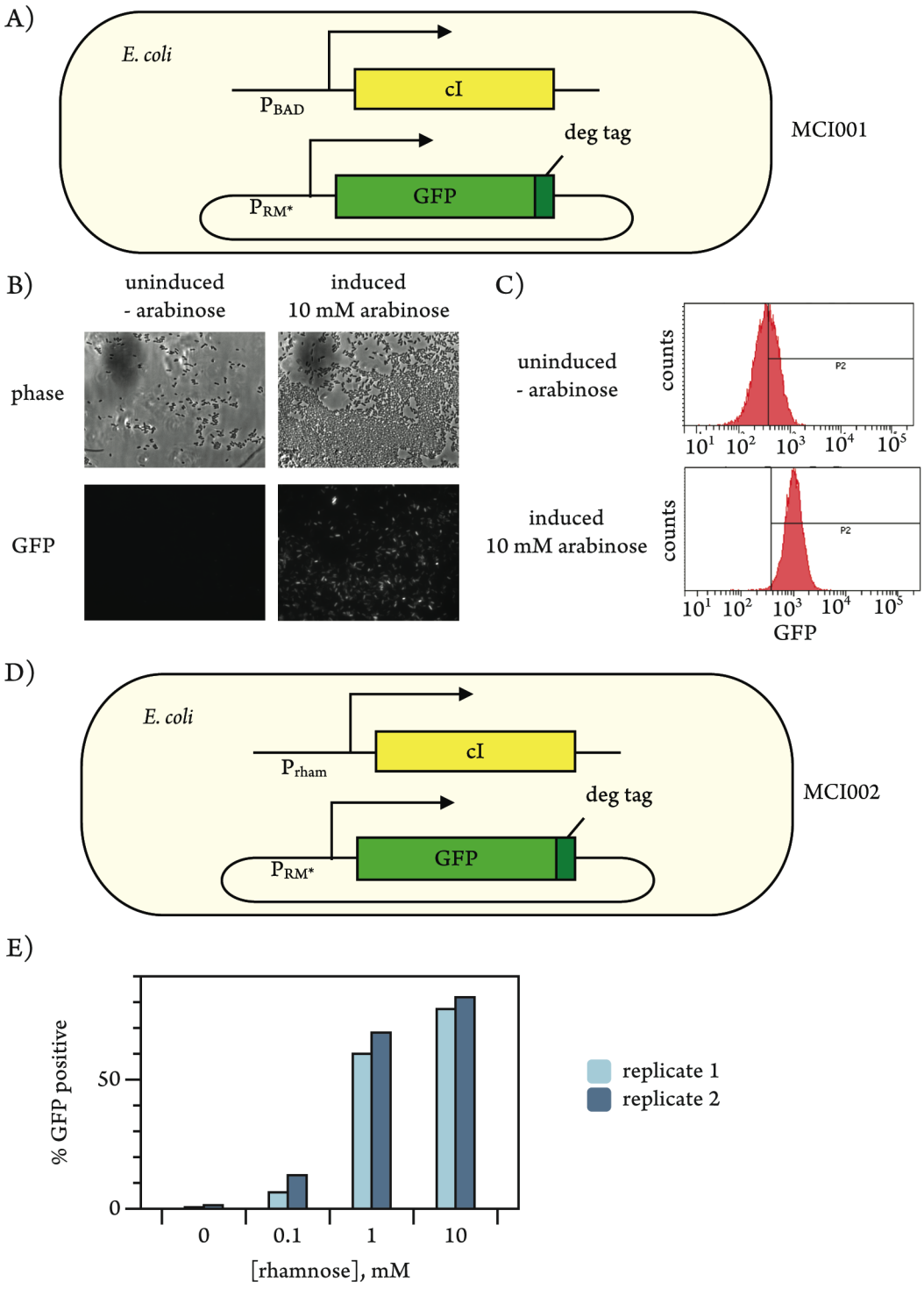

Figure 4.3. A fluorescent reporter system for lambda cI activity.

Figure 4.3 (continued). A fluorescent reporter system for lambda cI activity. (A) A fluorescent reporter of cI activity was built by integrating an arabinose-inducible cI gene into the genome of E. coli. These cells were then transformed with a reporter plasmid carrying sfGFP transcribed from a modified PRM promoter (PRM-GFP)(Huang, Holtz, and Maharbiz 2012). This promoter has mutations in OR3 preventing auto-inhibition by high levels of cI. (B) Cells carrying the PRM-GFP (MCI001) were exposed to 10mM arabinose for 4 h and then imaged by microscopy. Induced cells showed a much higher GFP signal. (C) The induced and uninduced cells were also analyzed by flow cytometry. Induced cells had a significantly higher GFP signal, however, uninduced cells also showed GFP expression. (D) The reporter system was rebuilt by replacing pBAD cI with a rhamnose-inducible cI gene while the reporter plasmid remained unchanged (MCI002). (E) MCI002 cells were induced with varying concentrations of rhamnose for 4 h and analyzed by flow cytometry. The percentage of GFP positive cells increased in a dose dependent manner.

cI and reporter (MCI001) were then grown in the presence and absence of 10 mM arabinose in LB and then analyzed by flow cytometry and microscopy (Figure 4.3B,C). As expected, we observed a significant increase in GFP expression upon induction of cI. However, we also observed expression of GFP, albeit at a much lower lever, in the absence of arabinose. This was most likely due to incomplete repression of the pBAD promoter. Indeed, we observed a significant growth defect in the pBAD cI strain compared to the parent strain even in the absence of reporter plasmid. This suggests that expression of the cI protein is toxic to the cells. The growth difference was suppressed by addition of glucose to the growth media causing tighter repression of the arabinose genes. In addition, we ordered constitutively expressed versions of the cI repressor and not only was production of these constructs seriously delayed, propagation of the resulting plasmids was difficult further supporting the hypothesis that expression of the repressor was toxic.

As the arabinose promoter showed significant leaky expression, we decided to rebuild the inducible cI construct with the rhamnose-inducible pRham promoter(Giacalone et al. 2006). The rhamnose-inducible cI construct was integrated at the araB locus by recombineering. This strain was then transformed with PRM-GFP (Figure 4.3D). Cells containing the rhamnose-inducible cI and the reporter plasmid (MCI002) were then induced with several concentrations of rhamnose and analyzed by flow cytometry (Figure 4.3E). We observed increasing expression of GFP with increasing amounts of rhamnose showing that our reporter system was functioning correctly.

Table 4.1. List of strains used in this study.

Strain name	Host	Genotype	Plasmid	Source
MCI001	BW25113	*attPφ80::gent^R-pBAD->cI^{ind-}*	PRM-GFP	this study
MCI002	BW25113	*araB::CAM^R-pRham->cI^{ind-}*	PRM-GFP	this study
MCI003	BW25113	*araB::CAM^R-pRham->cI^{ind-}, putAP::CAM^R-tetP->* cI_{DN} *1*	PRM-GFP	this study
MCI004	BW25113	*araB::CAM^R-pRham->cI^{ind-}, putAP::CAM^R-tetP->cI_{DN}3*	PRM-GFP	this study
MCI005	BW25113	*araB::CAM^R-pRham->cI^{ind-}, putAP::CAM^R-tetP->cI_{DN}4*	PRM-GFP	this study
PAS132	MG1655	*araB::CAM^R-tetP->cro, mphR:Kan^R-OL-rexBA-cI^{ind-}-OR-cro::lacZ, rpsLK42R*	none	(Kotula et al. 2014)
MCI006	MG1655	*putAP::CAM^R-tetP->cI_{DN}2, mphR:Kan^R-OL-rexBA-cI^{ind-}-OR-cro::lacZ, rpsLK42R*	none	this study
TB10	MG1655		none	(Thomason et al. 2001)
BW25113			none	(Haldimann and Wanner 2001)

We also synthesized several tetracycline inducible cI_{DN} variants: a single mutant (N55K), and a triple mutant (N55K, Y88E, T154E) both with and without degradation tags. While the N55K mutation is reported to interfere with specificity of DNA binding, the Y88E and T154E mutations are novel. We expect that the N55K mutation will affect DNA binding but not dimerization. If a cI_{DN} monomer will bind to other cI_{DN} monomers with the same affinity as wild-type cI monomers, a pool of non-productive cI_{DN} homodimers will form. We selected the Y88E and T154E mutations – these mutations lie at the protein-protein interface in the crystal structure of the cI dimer(Stayrook et al. 2008) – in an effort to discourage homodimerization without affecting heterodimerization, thus, lowering the concentration of cI_{DN} monomer necessary to block cI function (Figure 4.4). Conversely, if these mutations also interfere

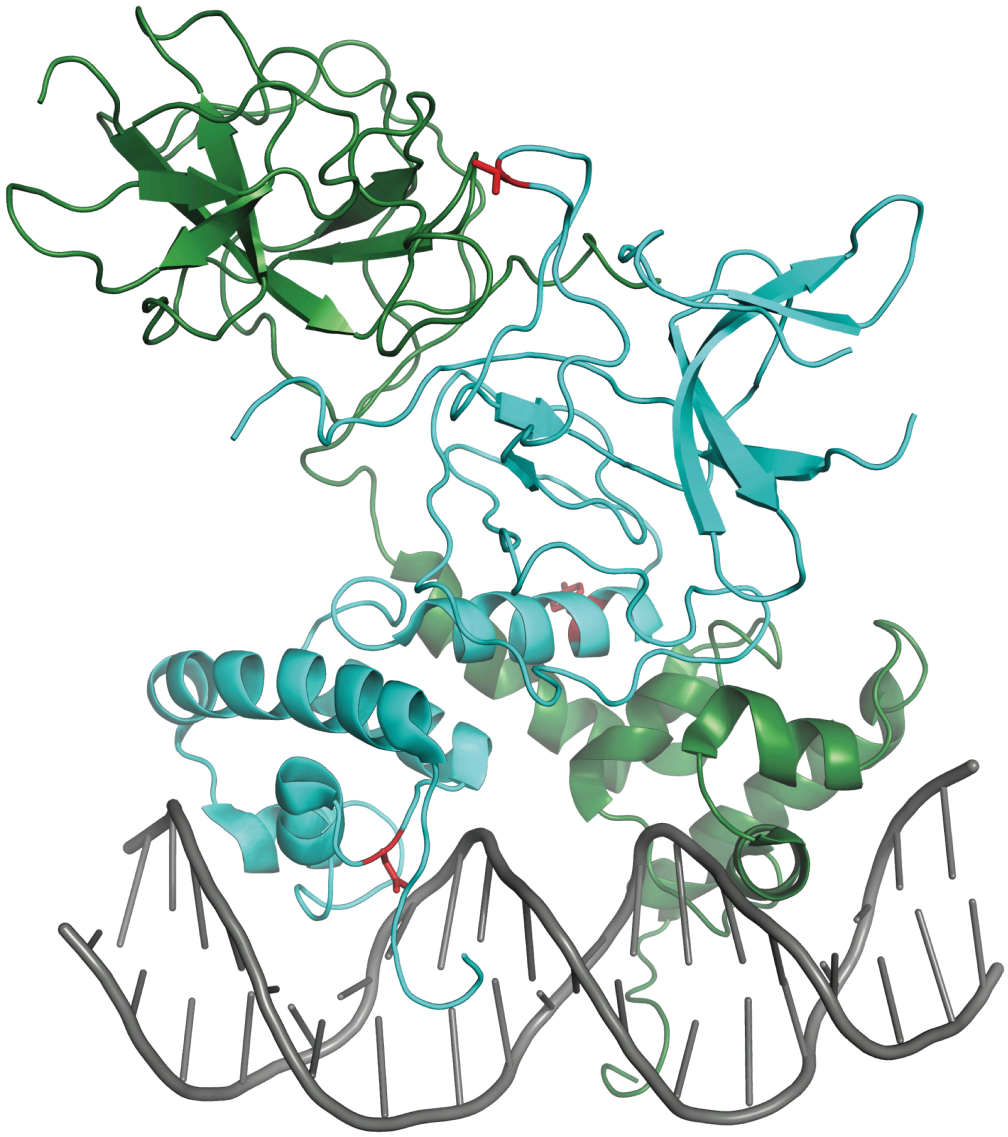

Figure 4.4. Structural model of lambda cI and cI_{DN} heterodimer bound to DNA. In this model of cI dimer bound to DNA(Stayrook et al. 2008), we colored the residues mutated in the cI_{DN} in red, N55K (at the DNA binding interface), Y88E (center) and T154E (top) at the interface between the two monomers.

with dimerization, we would observe a weaker effect on cI function. After synthesis of the single and triple mutants, we proceeded to make all other single and double mutants by site-directed mutagenesis.

Table 4.2. List of cI_{DN} mutants:

cI_{DN} **mutant**	**Mutations**	**Degradation tag**
cI_{DN} 1	N55K	N
cI_{DN} 2	N55K	Y
cI_{DN} 3	N55K, Y88E, T154E	N
cI_{DN} 4	N55K, Y88E, T154E	Y
cI_{DN} 5	N55K, Y88E	N
cI_{DN} 6	N55K, Y88E	Y
cI_{DN} 7	N55K, T154E	N
cI_{DN} 8	N55K, T154E	Y
cI_{DN} 9	Y88E, T154E	N
cI_{DN} 10	Y88E, T154E	Y
cI_{DN} 11	Y88E	N
cI_{DN} 12	Y88E	Y
cI_{DN} 13	T154E	N
cI_{DN} 14	T154E	Y

Characterization of interaction of cI and cI_{DN}

After building a small library of cI_{DN} constructs we began to characterize their ability to interfere with cI function. After integrating the tet-inducible cI_{DN} 1-4 constructs, these were transduced into the rhamnose-inducible cI strain. Resulting strains were transformed with the PRM-GFP(Huang, Holtz, and Maharbiz 2012) (Figure 4.5A). Colonies were grown overnight, back diluted 100-fold and induced with varying concentrations of rhamnose (0, 0.1, 1, and 10 mM) and ATC (0, 1, 10, and 100 ng/mL) for 5 hours. Cells were then pelleted, resuspended in PBS, and analyzed by flow cytometry (Figure 4.5B-G). In all cases, increased expression of GFP was observed with increasing amounts of rhamnose. In addition, addition of 100 ng/mL ATC significantly decreased GFP expression at most levels of ATC

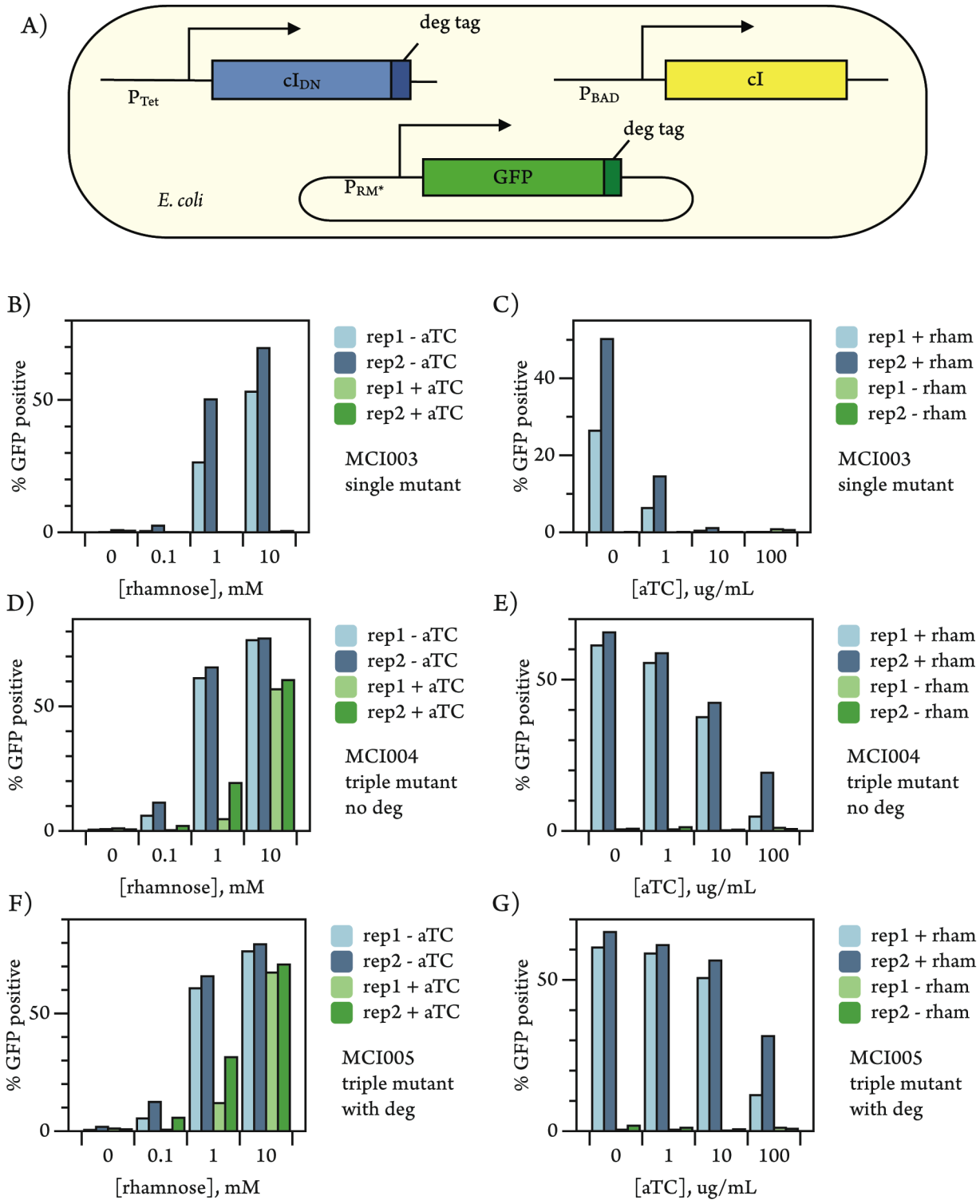

Figure 4.5. cI_{DN} inhibits cI activity in a dose dependent manner.

Figure 4.5 (continued). cI_{DN} inhibits cI activity in a dose dependent manner. (A) Strains were built containing rhamnose-inducible cI, one of several tet-inducible cI_{DN} variants, and reporter plasmid. The single N55K mutant (B,C), triple N55K, Y88E, T154E mutant (D,E), and degradation-tagged triple mutant (F,G) were assayed for their ability to block cI function. Cells were induced with varying concentrations of rhamnose in the absence or presence of 100 ng/uL aTC (B, D, F) and varying concentrations of aTC in the presence or absence of 1 mM rhamnose (C, E, G) and then analyzed by flow cytometry. Two biological replicates were measured for each strain in each condition, and 100,000 cells were measured.

induction. The effect was much stronger in the case of the single mutant (Figure 4.5B), completely eliminating gfp expression at all levels of rhamnose. This repression occurred in a dose dependent manner(Figure 4.5C). Cells were induced with 1 mM rhamnose and increasing concentrations of ATC. As the level of induction of cI_{DN} increased, more repression of gfp was seen. This demonstrates that the cI_{DN} mutants are interfering with wild-type cI function as expected. These results also show that the triple mutant is less effective than the single mutant. This may be due to decreased dimerization, poor protein folding, or decreased stability of the protein. In addition, we observe a weaker effect of the degradation-tagged triple mutant compared to the plain triple mutant. This is expected as the increased degradation rate will result in a lower concentration of cI_{DN} at a given induction level. While we do not currently have the corresponding data for the single mutant, we infer that a similar effect would be observed.

Design of pulse-detecting genetic circuit

In the process of designing the pulse-detecting circuit, we modeled the expected behavior of the circuit using ordinary differential equations (ODEs). Rather than model the induction of the circuit we set the initial parameters for the amount of cI and cI_{DN} protein explicitly. This represents what would happen after a period of constant induction long enough for cI and cI_{DN} concentration to reach steady-state levels. We expect to see no expression of reporter at time 0 in the simulation and over time, a pulse of reporter should appear as cI_{DN} degrades. Indeed, with certain sets of parameters (Tables C.1-C.3) for relative initial concentrations and degradation rates of the two proteins, this behavior is observed. Importantly, while the modeling does not predict specific values, it suggests that we should choose ribosome binding sequences so that cI_{DN} concentration is at least 10 fold higher than cI concentration at

steady state. In addition, the degradation of cI_{DN} must be significantly faster than cI to produce a pulse of output.

State of assembly of pulse detector library

In an effort to build genetic constructs that fulfill the requirements revealed by modeling, we decided to construct a moderately sized library of candidate designs. We chose a standard ssrA degradation tag for cI_{DN} that has been fairly well characterized and shown to be quite strong (Huang, Holtz, and Maharbiz 2012). We placed the cI gene after the cI_{DN} gene in a single operon(Figure 4.1B). This will ensure both proteins are expressed together and the placement of cI_{DN} first in the operon should result in higher expression levels separate from RBS strength. We then designed 24 variants of the RBS for both the cI_{DN} and cI genes to try and tune expression of the two proteins. This library was being built in collaboration with Ginkgo Bioworks by leveraging their automated assembly pipeline. However, the toxicity of spurious cI and cI_{DN} expression made automated assembly of the library problematic and we were not able to assemble an acceptable library of constructs. We are proceeding with building a smaller library manually.

Lambda memory switch as a pulse detector

While the original design for a pulse detecting genetic circuit involved controlling the activity of cI repressor through interaction with a dominant negative mutant, there are other ways of achieving this goal. In our lab, we have taken advantage of the lambda switch to build a robust memory device in *E. coli*(Kotula et al. 2014). The lambda switch was integrated into the genome so that Pr cro read directly into lacZ. In the initial cI state, cells would not express lacZ (Figure 4.6A), however, when cro was

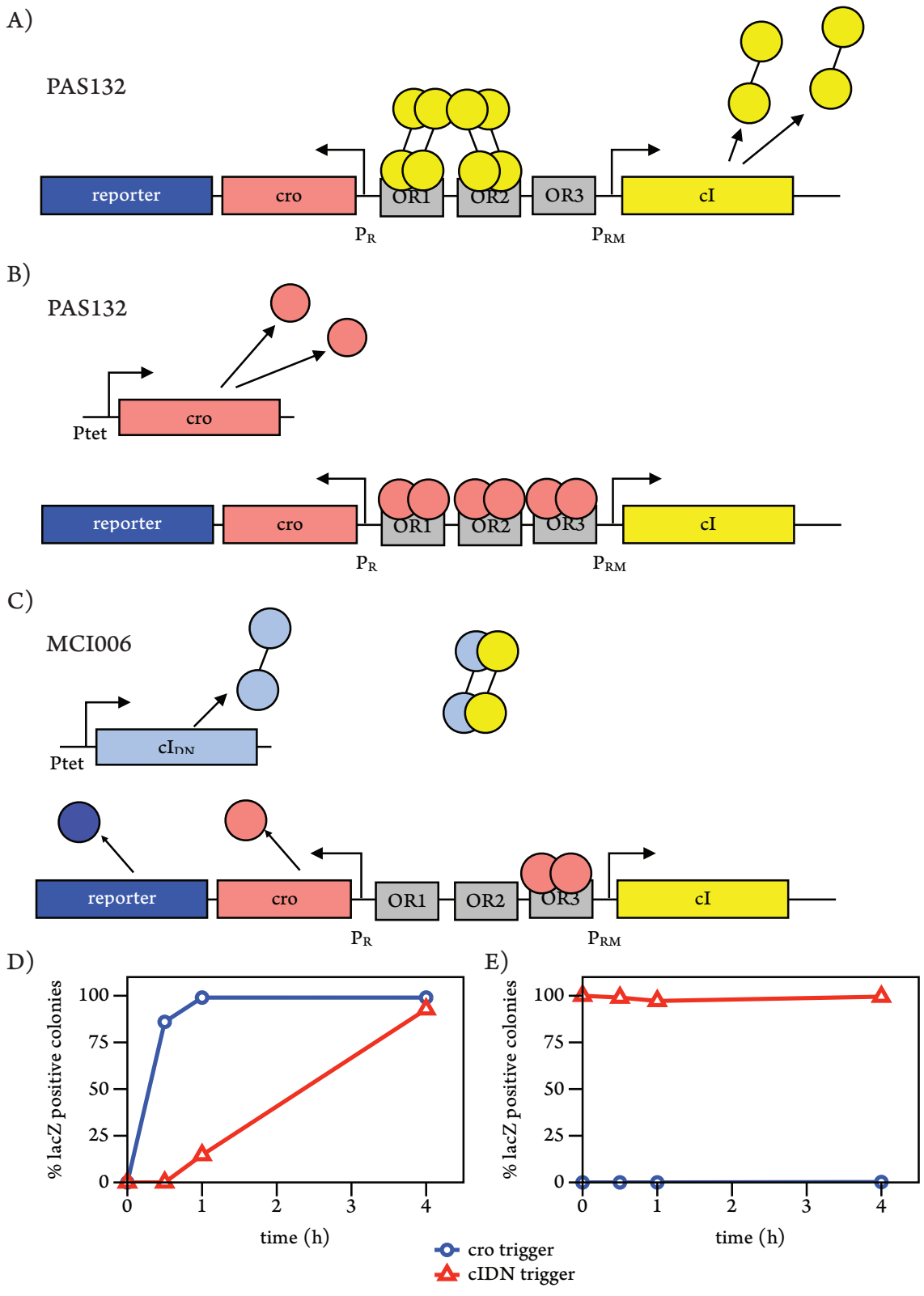

Figure 4.6. The natural lambda switch can function as a pulse detector.

Figure 4.6 (continued). The natural lambda switch can function as a pulse detector. (A) In the basal state of the lambda based memory device (PAS132), cI is expressed repressing cro and lacZ expression. (B) When cro expression is induced from an exogenous tet-inducible promoter, cro is produced to a high enough level to repress expression of cro and lacZ from the Pr promoter. (C) Conversely, when cI_{DN} is expressed from an exogenous tet-inducible promoter (MCI006), it interferes with cI but does not affect the Pr promoter. This allows cro and lacZ to be expressed from the Pr promoter, switching the device to the cro state immediately. (D,E) Cells were induced with 100 ng/mL aTC, aliquots were diluted in PBS and plated on LB plates containing kanamycin without aTC (D) or containing 100 ng/mL aTC (E). On plates without aTC, both the cro trigger and cIDN trigger were able to switch 100% of the population after 4 h. However, when plated on reporter plates containing aTC, cells expressing cI_{DN} are 100% switched, while cells expressing cro remain unswitched.

expressed exogenously from a tetracycline-inducible promoter, cells would switch to the cro state and express lacZ (Figure 4.6B). This switching can be detected by growing cells on plates containing X-gal and looking for blue colonies. They showed that this circuit also specifically reports on aTC exposure when cells are introduced in the gut of a mouse, demonstrating its potential use as a diagnostic probiotic.

During the characterization of this device, it was noted that no switching was observed during induction. LacZ expression was only detected once cells were plated on reporter plates. As mentioned earlier, while cI promotes its own expression from the Prm promoter, it also inhibits its production once levels are too high. Similarly, cro can also inhibit its own expression from the Pr promoter if it is present in high enough amounts; for instance, when expressed from a tetracycline-inducible promoter. This is demonstrated by comparing the switching of the device by expression of cro and expression of cI_{DN}. We integrated the tet-inducible cI_{DN} into PAS132 where pTet cro had been deleted(MCI006). We expect that when cI_{DN} is expressed, it will interfere with cI binding leaving the Pr promoter free allowing expression of cro and lacZ (Figure 4.7C). When induced with aTC, both cro and cI_{DN} induce switching of the device (Figure 4.6D). However, when plated on reporter plates containing aTC, cells expressing cI_{DN} are 100% switched, while cells expressing cro remain white (Figure 4.7E). Thus, the lambda memory switch already functions as a pulse-detecting circuit.

Conclusions

While the construction of the complete pulse-detecting circuit is still ongoing, in this Chapter we have described the characterization of a dominant-negative mutant of cI. This will allow future assembly of more complex circuits. In addition, we demonstrated that an existing device – the lambda memory

switch – already behaves as a pulse detector. These types of devices will allow better control over gene expression in engineered cells in the future.

Materials and Methods

Plasmid construction

Escherichia coli NEB Turbo Competent (NEB), BW23474, and BW23473 were used for all plasmid manipulations. Bacteria were grown in LB media with either 10ug/mL chloramphenicol, 20ug/mL kanamycin, 10ug/mL gentamycin, or 100ug/mL ampicillin to maintain plasmids as appropriate. DNA fragments with were generated by PCR and assembled via Gibson assembly(Gibson et al. 2009). Inducible cI and cI_{DN} constructs were cloned into CRIM plasmids containing the R6Kgamma origin of replication(Haldimann and Wanner 2001) and one of several phage attachment sites. These plasmids can only be propagated in pir+ hosts such as BW23474 and BW23473.

Bacterial strain construction

Constructs built in CRIM plasmids were integrated as described(Haldimann and Wanner 2001). In brief, the recipient E. coli were transformed with a helper plasmid expressing the appropriate integrase, made electrocompetent, and transformed with plasmid containing the construct to be integrated. Cells were then selected on appropriate antibiotic and screened for loss of helper plasmid. Integration was verified by colony PCR and Sanger sequencing.

Later, constructs were built by overlap extension PCR(R Higuchi 1988) and integrated directly into the genome by recombineering(Thomason et al. 2001). Recipient cells were transformed with pKD46, made electrocompetent, and transformed with PCR product. Alternatively, PCR product was

electroporated into TB10 that do not require a helper plasmid. In both cases, cells were then recovered at 30 degrees for 1 h and heat shocked at 42 degrees for 30 min. Cells were then plated on LB plates containing appropriate antibiotics and grown at 37 degrees. Integration was confirmed by colony PCR and Sanger sequencing. Strains containing multiple constructs were made by moving previously integrated constructs into the final strain using P1 transduction.

Flow cytometry

Cells containing PRM-GFP plasmid (Addgene plasmid 40127) were back diluted 1:100 in LB with ampicillin, induced with various concentrations of rhamnose (0, 0.1, 1, 10 mM) and ATC (0, 1, 10, 100 ug/mL) for 5 h. Induced cultures were spun down, resuspended in 1x PBS, and diluted 50 fold in PBS. Cells were later loaded in 96 well plates (BD Biosciences) on an LSRII (BD Biosciences) with a 568-nm (FITC) laser (Harvard Systems Biology). 1.0 X 10^5 cells were analyzed for GFP (FITC) fluorescence and gated based on cell size and granularity. Unexposed cells controlled for basal fluorophore expression. Data was analyzed using FlowJo software.

Microscopy

Cells were imaged at 100x with a Nikon TE2000-E inverted fluorescence microscope equipped with a Hamamatsu ORCA-ER camera, and HcRed (RFP) and JP2 (YFP) filters (Silver Lab). Images were acquired and analyzed using Metamorph software.

Lambda memory switching assay

Strains were grown overnight in LB supplemented with 20 ug/mL kanamycin. Cultures were backdiluted in fresh LB with antibiotics and induced with 100ng/mL aTC. Aliquots of culture were diluted by serial dilution between 10^{-3} to 10^{-6} in PBS then 100 uL were plated on LB plates containing kanamycin and 20 ug/mL X-Gal. Colonies were counted the following day and scored for lacZ expression.

Acknowledgements and attributions

We would like to thank several members of the Silver lab for their support and help with the planning of cloning strategies, design of constructs, and experiments. We especially thank Jordan Kerns and Jonathan Kotula for producing PAS132 and Michael Certo for recognizing its potential as a pulse detector.

Experiments described in Chapter 4 were designed by Jeffrey Way and myself. Assembly of constructs was performed by Leigh Matano, Caroline Kim, and Lauren Kennedy, under my supervision. Inducible wild-type cI and lambda memory strains described in Chapter 4 were produced by S. Jordan Kerns and Jonathan Kotula.

References

Ajo-Franklin CM, Drubin DA, Eskin JA, Gee EPS, Landgraf D, Phillips I, Silver PA. 2007. Rational design of memory in eukaryotic cells. Genes Dev 21:2271–2276.

Basu S, Mehreja R, Thiberge S, Chen M-T, Weiss R. 2004. Spatiotemporal control of gene expression with pulse-generating networks. Proc Natl Acad Sci USA 101:6355–6360.

Bonnet J, Subsoontorn P, Endy D. 2012. Rewritable digital data storage in live cells via engineered control of recombination directionality. Proc Natl Acad Sci USA.

Bonnet J, Yin P, Ortiz ME, Subsoontorn P, Endy D. 2013. Amplifying genetic logic gates. Science 340:599–603.

Burrill DR, Inniss MC, Boyle PM, Silver PA. 2012. Synthetic memory circuits for tracking human cell fate. Genes Dev 26:1486–1497.

Burrill DR, Silver PA. 2011. Synthetic circuit identifies subpopulations with sustained memory of DNA damage. Genes Dev 25:434–439.

Friedland AE, Lu TK, Wang X, Shi D, Church G, Collins JJ. 2009. Synthetic gene networks that count. Science 324:1199–1202.

Gardner TS, Cantor CR, Collins JJ. 2000. Construction of a genetic toggle switch in Escherichia coli. Nature 403:339–342.

Giacalone M, Gentile A, Lovitt B, Berkley N, Gunderson C, Surber M. 2006. Toxic protein expression in Escherichia coli using a rhamnose-based tightly regulated and tunable promoter system. Biotech. 40:355–364.

Gibson DG, Young L, Chuang R-Y, Venter JC, Hutchison CA, Smith HO. 2009. Enzymatic assembly of DNA molecules up to several hundred kilobases. Nat Meth 6:343–345.

Guzman LM, Belin D, Carson MJ, Beckwith J. 1995. Tight regulation, modulation, and high-level expression by vectors containing the arabinose PBAD promoter. J Bacteriol 177:4121–4130.

Haldimann A, Wanner BL. 2001. Conditional-Replication, Integration, Excision, and Retrieval Plasmid-Host Systems for Gene Structure-Function Studies of Bacteria. J Bacteriol 183:6384–6393.

Ham TS, Lee SK, Keasling JD, Arkin AP. 2008. Design and construction of a double inversion recombination switch for heritable sequential genetic memory. PLoS ONE 3:e2815.

Hochschild A, Irwin N, Ptashne M. 1983. Repressor structure and the mechanism of positive control. Cell 32:319–325.

Huang D, Holtz WJ, Maharbiz MM. 2012. A genetic bistable switch utilizing nonlinear protein degradation. J Biol Eng 6:9.

Kotula JW, Kerns SJ, Shaket LA, Siraj L, Collins JJ, Way JC, Silver PA. 2014. Programmable bacteria detect and record an environmental signal in the mammalian gut. Proc Natl Acad Sci USA.

Kramer BP, Viretta AU, Daoud-El-Baba M, Aubel D, Weber W, Fussenegger M. 2004. An engineered epigenetic transgene switch in mammalian cells. Nat Biotechnol 22:867–870.

Lou C, Stanton B, Chen Y-J, Munsky B, Voigt CA. 2012. Ribozyme-based insulator parts buffer synthetic circuits from genetic context. Nat Biotechnol 30:1137–1142.

Nelson H, Sauer RT. 1986. Interaction of mutant λ repressors with operator and non-operator DNA. J Mol Biol 192:27–38.

Ptashne M, Jeffrey A, Johnson AD, Maurer R, Meyer BJ, Pabo CO, Roberts TM, Sauer RT. 1980. How the λ repressor and cro work. Cell 19:1–11.

Ptashne M. 2004. A Genetic Switch. Cold Spring Harbor Laboratory Pr.

R Higuchi BKRKS. 1988. A general method of in vitro preparation and specific mutagenesis of DNA fragments: study of protein and DNA interactions. Nucleic Acids Res 16:7351.

Siuti P, Yazbek J, Lu TK. 2013. Synthetic circuits integrating logic and memory in living cells. Nat Biotechnol.

Stayrook S, Jaru-Ampornpan P, Ni J, Hochschild A, Lewis M. 2008. Crystal structure of the λ repressor and a model for pairwise cooperative operator binding. Nature 452:1022–1025.

Subsoontorn P, Endy D. 2012. Design and Analysis of Genetically Encoded Counters. Procedia Computer Science 11:43–54.

Thomason L, Court DL, Bubunenko M, Costantino N, Wilson H, datta S, oppenheim A. 2001. Recombineering: Genetic Engineering in Bacteria Using Homologous Recombination. Hoboken, NJ, USA: John Wiley & Sons, Inc.

Chapter 5

Conclusion

Where are we now?

While synthetic biologists have been able to achieve ambitious goals, from engineering bacteria and mammalian cells to produce novel compounds(Wang et al. 2009), remember past events(Ajo-Franklin et al. 2007; Burrill and Silver 2011; Bonnet, Subsoontorn, and Endy 2012; Burrill et al. 2012; Kotula et al. 2014), communicate with each other(Bulter et al. 2004), and compute complex logic(Lohmueller, Armel, and Silver 2012; Bonnet et al. 2013; Siuti, Yazbek, and T.K. Lu 2013); as far as rebuilding bacterial genomes(Benders et al. 2010; Gibson et al. 2010), and even an entire eukaryotic chromosome(Annaluru et al. 2014), the field has just begun to cross the threshold from building prototype circuits to creating useful tools. This is not meant to undermine what has already been accomplished. On the contrary, these projects are important and essential milestones on the path to learning to predictably and reliably engineer biological systems. Just as we learn more about the systems we try to build through our failures, we learn more about how to effectively design these systems through trial-and-error. For instance, we initially assumed we could abstract away much of the messiness of biology emphasizing its modularity(Purnick and Weiss 2009), but found this "noise" was actually important to build in to our designs(Daniel et al. 2013). This knowledge, alongside the development of high-throughput screening and selection techniques, led to the strategy of casting a wide net by building and testing every conceivable variant of a circuit. However, it is becoming apparent that a more restrained approach falling somewhere between these two extremes is often the most efficient tactic(Silver et al. 2014).

In this dissertation, we discussed the development of synthetic memory circuits and a pulse detecting circuit. In Chapter 2, we showed that by treating promoters, and protein coding regions as modular units, you could build transcriptional memory circuits triggered by a variety of inputs. While

the building and testing of the initial prototype circuit was difficult and time-consuming, the modularity of this system with respect to the trigger promoter made it a relatively simple matter to modify this device to respond to novel inputs. By changing one element, we were able to change the input from doxycycline exposure, to either hypoxia, or DNA damage. Importantly, we showed that this circuit is useful in the study of long-term and heterogeneous responses to these stimuli. In Chapter 3, we explored further applications for this memory circuit, including the long-term effects of exposure to γ-radiation, and an effort to modify the promoter once again to respond to inflammation. Chapter 4 describes the effort to rationally design a pulse-detecting circuit. By combining, abstraction with modeling of the relevant protein interactions, we showed that it would be possible to design a small library of candidate designs that can be screened for proper function. While the projects in Chapters 2 and 3 rely on our ability to abstract biology into elements such as promoter and transcription factor, Chapter 4 falls more closely into the new paradigm of combining this abstraction with rational design of a limited library of constructs.

What stands in our way?

Even though we understand a lot about transcriptional networks and cellular signaling, creating novel circuits that function as intended both *in vitro* and *in vivo* remains a difficult challenge. In addition, circuits that function reliably in one context can become unpredictable when moved to a different environment, often through changes as subtle as modified growth medium. While natural biological circuits have had the opportunity to evolve robustness to these types of changes, our novel circuits have not had that chance. In an effort to streamline and simplify synthetic genetic networks, we may even be designing out the flexibility needed to build a robust device. Currently, the design of the architecture of

synthetic circuits is mostly done by intuition, or mimicry of natural circuits. It is not unreasonable to assume this is limiting the variety of circuits being developed. To address this issue, as well as to speed up the design process in general, significant effort is being put into the development of computer aided design (CAD) programs(Chandran, Bergmann, and Sauro 2009; Cai, Wilson, and Peccoud 2010; Clancy and Voigt 2010). This would automate the "coding" portion of the design process enabling researchers to define inputs and desired outputs while the software would design the actual genetic network allowing us to test non-intuitive designs.

In addition to the design process, the actual building and delivery of our designed circuits also remains challenging. While techniques for efficiently assembling several small pieces (several kb to hundreds of kb) of DNA have become commonplace in many academic labs(Gibson et al. 2009), as designs become more complex, assembly of large numbers of constructs (library preparation), and large-scale constructs (> 1 Mb) are still beyond the reach of most researchers. However, as with earlier assembly techniques, recent breakthroughs in the construction of whole genomes(Benders et al. 2010) and chromosomes(Annaluru et al. 2014) will open the door for others. In addition, the falling cost of synthesis and creation of synthetic biology companies focused on bulk production of constructs will enable researchers to test large numbers of designs more quickly. As libraries and individual constructs become larger, efficient delivery to the cell becomes more challenging as well. In the end, the current roadblocks and obstacles in the design and building of novel synthetic circuits are mostly technical in nature, so we can anticipate they will eventually be solved. Hopefully, in the near future, testing of candidate designs will be the rate-limiting step for synthetic biologists. The most important question we need to ask is not how, but what do we want to design and why?

Where do we go from here?

In this dissertation, we have demonstrated that synthetic biology has the potential to help us answer questions that would be difficult to investigate by traditional means. For instance, we used synthetic memory circuits to learn more about long-term and heterogeneous responses to transient stimuli. Building synthetic circuits also lets us learn more about the natural circuits that inspire them. However, the potential of synthetic biology is greater than just as a tool for learning about biology. For example, we could develop engineered cellular therapies that would be programmable "smart" therapeutics. These could be nanostructures or other vectors for delivering drugs to specific tissues or cell types, or even engineered cells, such as T-cells, delivered directly into the blood stream(Ruder, T. Lu, and Collins 2011; Ausländer and Fussenegger 2012). Synthetic biology approaches could eventually be used to program stem cell differentiation to engineer tissues. Bacteria can be modified to become engineered probiotics that can diagnose or potentially treat disease. It is easy to be optimistic about the future of synthetic biology. Its potential seems bounded only by our imagination. However, this optimism must be tempered with the knowledge that we still have technical hurdles and obstacles to overcome.

References

Ajo-Franklin CM, Drubin DA, Eskin JA, Gee EPS, Landgraf D, Phillips I, Silver PA. 2007. Rational design of memory in eukaryotic cells. Genes Dev 21:2271–2276.

Annaluru N, Muller H, Mitchell LA, Ramalingam S, Stracquadanio G, Richardson SM, Dymond JS, Kuang Z, Scheifele LZ, Cooper EM, et al. 2014. Total Synthesis of a Functional Designer Eukaryotic Chromosome. Science 344:55–58.

Ausländer S, Fussenegger M. 2012. From gene switches to mammalian designer cells: present and future prospects. Trends Biotechnol.

Benders GA, Noskov VN, Denisova EA, Lartigue C, Gibson DG, Assad-Garcia N, Chuang R-Y, Carrera W, Moodie M, Algire MA, et al. 2010. Cloning whole bacterial genomes in yeast. Nucleic Acids Res 38:2558–2569.

Bonnet J, Subsoontorn P, Endy D. 2012. Rewritable digital data storage in live cells via engineered control of recombination directionality. Proc Natl Acad Sci USA.

Bonnet J, Yin P, Ortiz ME, Subsoontorn P, Endy D. 2013. Amplifying genetic logic gates. Science 340:599–603.

Bulter T, Lee SG, Wong WW, Fung E, Connor MR, Liao JC. 2004. Design of artificial cell-cell communication using gene and metabolic networks. Proc Natl Acad Sci USA 101:2299–2304.

Burrill DR, Inniss MC, Boyle PM, Silver PA. 2012. Synthetic memory circuits for tracking human cell fate. Genes Dev 26:1486–1497.

Burrill DR, Silver PA. 2011. Synthetic circuit identifies subpopulations with sustained memory of DNA damage. Genes Dev 25:434–439.

Cai Y, Wilson ML, Peccoud J. 2010. GenoCAD for iGEM: a grammatical approach to the design of standard-compliant constructs. Nucleic Acids Res 38:2637–2644.

Chandran D, Bergmann FT, Sauro HM. 2009. TinkerCell: modular CAD tool for synthetic biology. J Biol Eng 3:19.

Clancy K, Voigt CA. 2010. Programming cells: towards an automated "Genetic Compiler." Curr Opin Biotechnol [Internet] 21:572–581. Available from: http://www.ncbi.nlm.nih.gov/sites/entrez?Db=pubmed&Cmd=Retrieve&list_uids=20702081&dopt=abstractplus

Daniel R, Rubens JR, Sarpeshkar R, Lu TK. 2013. Synthetic analog computation in living cells. Nature 497:619–623.

Gibson DG, Glass JI, Lartigue C, Noskov VN, Chuang R-Y, Algire MA, Benders GA, Montague MG, Ma L, Moodie MM, et al. 2010. Creation of a bacterial cell controlled by a chemically synthesized genome. Science 329:52–56.

Gibson DG, Young L, Chuang R-Y, Venter JC, Hutchison CA, Smith HO. 2009. Enzymatic assembly of DNA molecules up to several hundred kilobases. Nat Meth 6:343–345.

Kotula JW, Kerns SJ, Shaket LA, Siraj L, Collins JJ, Way JC, Silver PA. 2014. Programmable bacteria detect and record an environmental signal in the mammalian gut. Proc Natl Acad Sci USA.

Lohmueller JJ, Armel TZ, Silver PA. 2012. A tunable zinc finger-based framework for Boolean logic computation in mammalian cells. Nucleic Acids Res 40:5180–5187.

Purnick PEM, Weiss R. 2009. The second wave of synthetic biology: from modules to systems. Nat Rev Mol Cell Biol 10:410–422.

Ruder WC, Lu T, Collins JJ. 2011. Synthetic biology moving into the clinic. Science 333:1248–1252.

Silver PA, Way JC, Arnold FH, Meyerowitz JT. 2014. Synthetic biology: Engineering explored. Nature 509:166–167.

Siuti P, Yazbek J, Lu TK. 2013. Synthetic circuits integrating logic and memory in living cells. Nat Biotechnol.

Wang HH, Isaacs FJ, Carr PA, Sun ZZ, Xu G, Forest CR, Church GM. 2009. Programming cells by multiplex genome engineering and accelerated evolution. Nature 460:894–898.

Appendix A

Supplementary Information for Chapter 2

Supplementary figures[1]

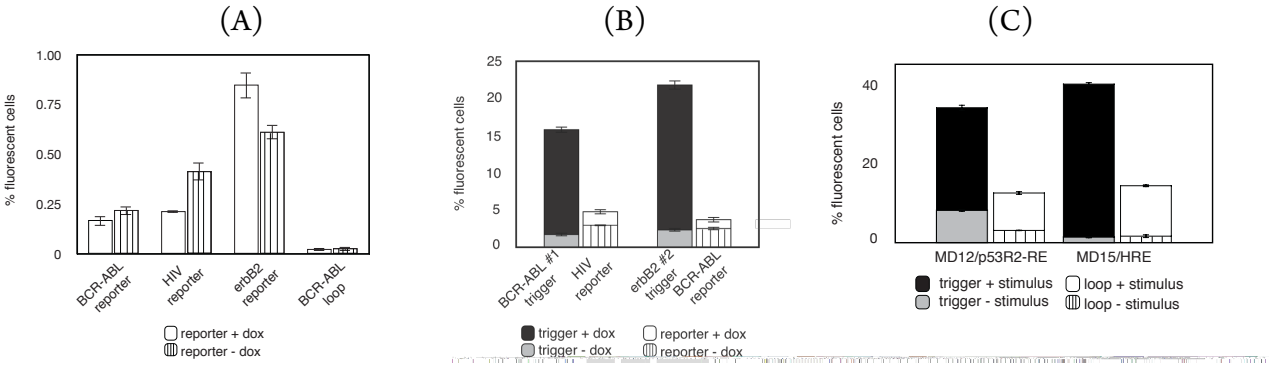

Figure A.1. Transient transfections. (A) Reporters and loops were transfected to detect basal activity. (B) Reporters and loops were mismatched and transfected to determine orthogonality. (C) p53R2-RE and HRE triggers and loops were co-transfected.

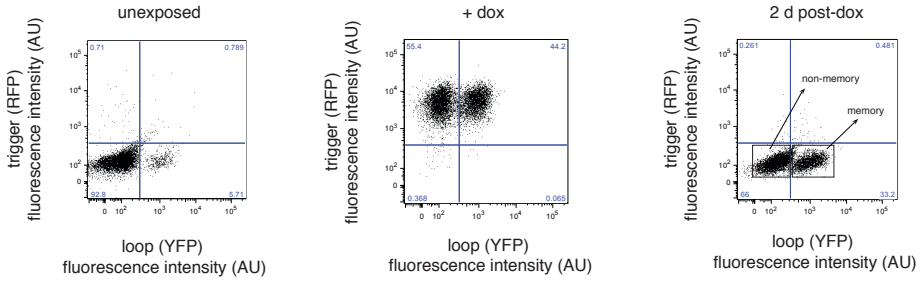

Figure A.2. Representative FACS scatter plots demonstrating how MD10/TetOx2 was analyzed by flow cytometry. "+dox": 24 h dox exposure. "2 d post-dox": 48 h recovery from dox exposure.

[1] Portions of this chapter were reproduced with permission Cold Spring Harbor Laboratory Press:
Burrill DR, Inniss MC, Boyle PM, Silver PA. 2012. Synthetic memory circuits for tracking human cell fate. Genes Dev 26:1486–1497.

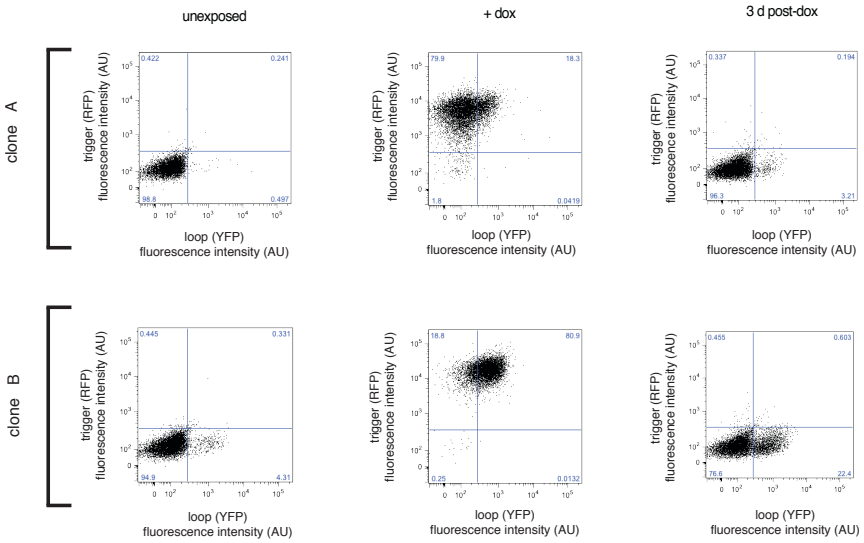

Figure A.3. Selected MD10/ TetOx2 clones behaved similarly. Each row of FACS plots represents a clone.

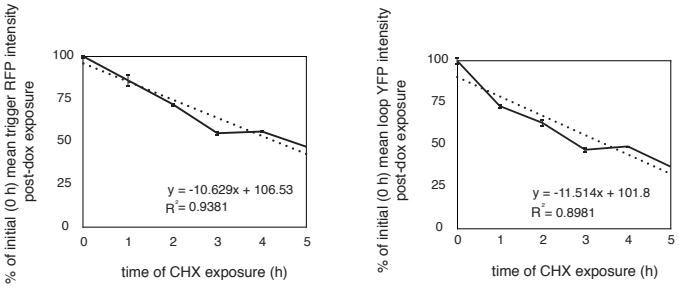

Figures A.4. RFP (left) and YFP (right) degrade at similar rates. MD10/TetOx2 was exposed to dox to induce fluorophore expression and then exposed to cycloheximide (CHX) to observe protein decay. Aliquots were fixed each hour and fluorescence was measured by FACS. Decay was measured as a percentage of starting intensities at time 0 h of CHX exposure.

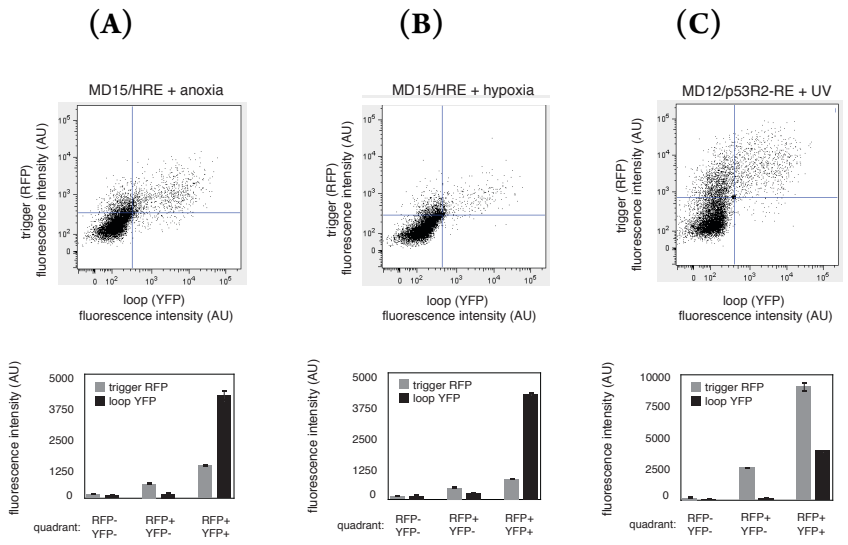

Figure A.5. FACS scatter plots (top row) showing distribution of fluorescence intensity when MD15/HRE and MD12/p53R2-RE are activated by (A) anoxia, (B) hypoxia, or (C) UV. Fluorescence intensities in each quadrant are shown below each scatter plot. Error bars represent the mean ± SE for three biological replicates.

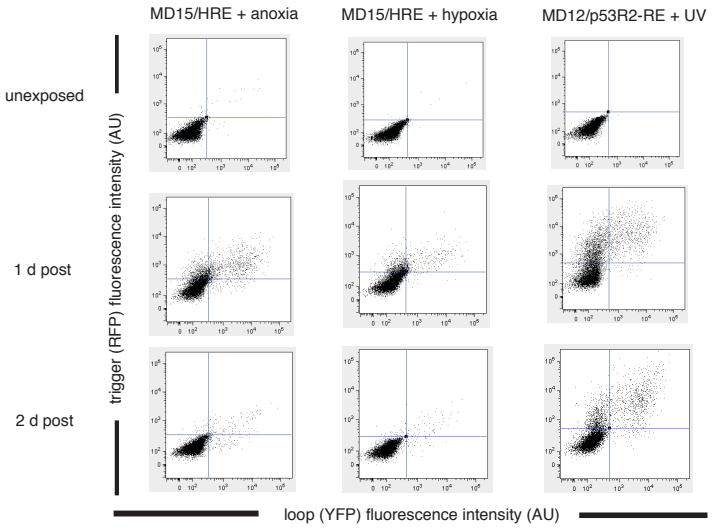

Figure A.6. FACS scatter plots showing distribution of fluorescence intensities when MD15/HRE and MD12/p53R2-RE are activated by anoxia, hypoxia, or UV and recovered for 2 d.

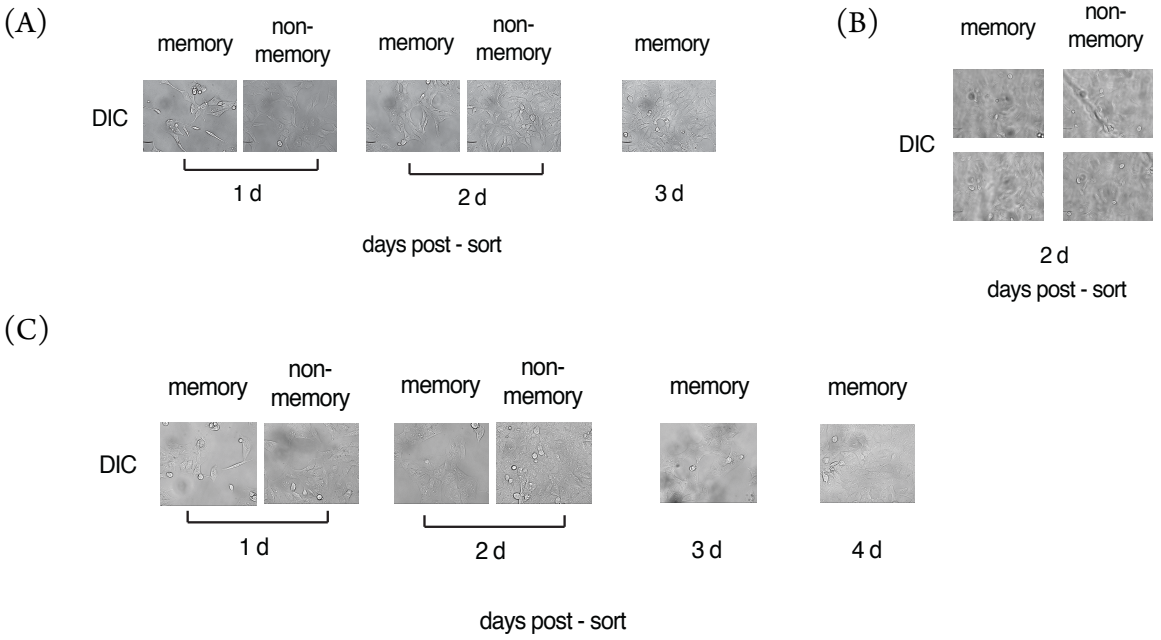

Figure A.7. Growth and viability of stable cell lines. (A) MD15/HRE memory cells were sorted 1 d post-hypoxia and growth was compared at subsequent time-points. (B) MD10/TetOx2 cells and (C) MD12/p53R2-RE were sorted 2 d post-UV or dox, and growth was compared at subsequent time-points.

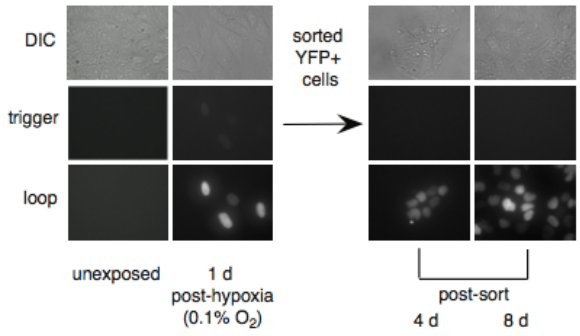

Figure A.8. MD15/HRE transmits memory of hypoxia through cell division. Cells were exposed to hypoxia, sorted 1 d post-exposure for YFP+ cells, and followed by microscopy for 8 d.

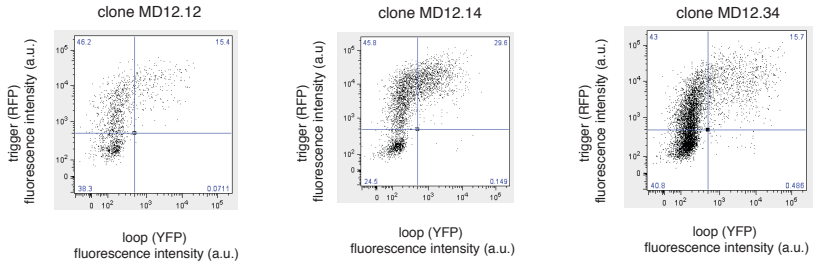

Figure A.9. FACS scatter plots of MD12/p53R2-RE clones.

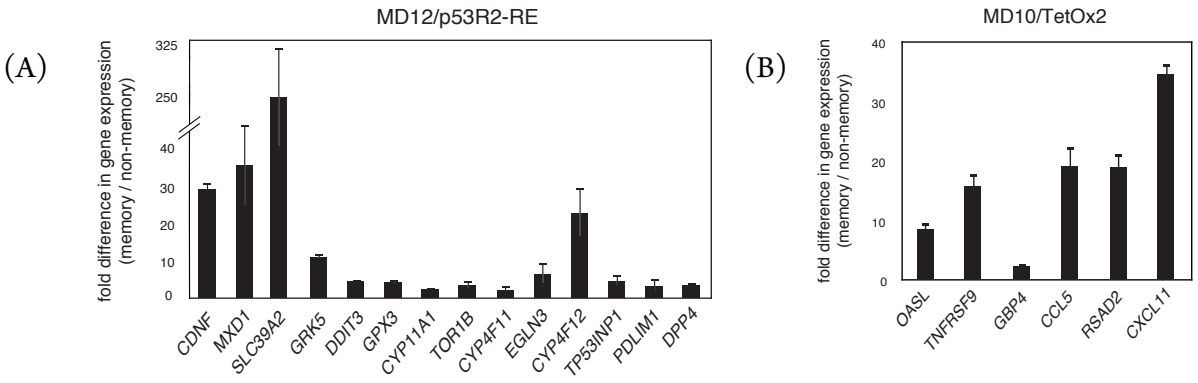

Figure A.10. qPCR validation of up-regulated genes in memory versus non-memory cells. (A) MD12/p53R2-RE and (B) MD10/TetOx2 cells were sorted 3 d post-UV or dox in biological triplicate, and RNA was extracted. Values represent mean fold difference in gene expression between memory and non-memory sub-populations ± SE across three biological replicates.

Supplementary Tables

Table A.1. Transient transfection guidelines.

construct	amount (ng)	construct	amount (ng)
trigger	400	reporter or loop	400
Flp-In T-REx™ vector	400	reporter or loop	400
trigger-spacer-reporter	800	-----	-----
trigger-spacer-loop	800	-----	-----

Table A.2. Media requirements for stable cell lines.

integrated construct	U2OS cell type	antibiotic	selection concentration (ug/mL)	maintenance concentration (ug/mL)
MD10/TetOx2	Flp-In T-REx™	hygromycin puromycin blasticidin	300 3 15	100 1 15
MD12/p53R2-RE	plain	puromycin	3	1
MD15/HRE	plain	puromycin	3	1

Table A.3. Primer sequences used for real-time PCR.

Gene	Sequences (5'- 3', forward first, reverse second)
ACTB	tccctggagaagagctacga, aggaaggaaggctggaagag
OASL	tttctgcccatccttcagcgagc, ggacctggctttcacatactgctgg
TNFRSF9	ccgacctctctccgggagcat, tgcggagagtgtcctggctct
GBP4	ctcgaggatccaggcgcagg, ctggataacctggtgtgggcactg
CCL5	tacattgcccgcccactgcc, gggtgacaaagacgactgctggg
CXCL10	tggcacactagccccacgtt, tgctgagactggaggttcctctgc
RSAD2	accctgtccgctggaaagtgttc, gcaggacacttctttgtggcgct
CXCL11	tgctacagttgttcaaggcttcccc, cactgcttttaccccagggccta
CDNF	ttgcgccgggcttttggtct, ctttacatacttcacagtcggcccc
MXD1	gctccgactccgacagggaaat, atgctgccccgctcgtcaga
SLC39A2	agccagaggtcatcaccggcta, gctgatctgttctgcaccatgaact
GRK5	ggaggggctgcagaggtca, cgcgggggtctggaacgaag
DDIT3	atgttaaagatgagcgggtggcagc, ttgaacactctctcctcaggttcca
GPX3	tcgcagagccggggacaaga, tggtgagggctccgtactcg
CYP11A1	agcagggagcgacccggtat, acgttgccgagcttctcccttag
TOR1B	ccgctcaacgcttcggctct, gccagcccagccgtgtaagg
ABCB1	accagataaaagagaggtgcaacgg, tcccggcccggattgactga
CYP4F11	acaagtggagccgccaccg, acatgtccagtctggcgctgc
EGLN3	cgtggatcgggggcaacgag, gcaagccaccattgccttagacct
CYP4F12	actcgacccagatgtcggcca, ttgggtgcaatggcagctgagg
TP53INP1	agcccaagtagtcccagagtgga, tccactgggaagggcgaaagc
PDLIM1	tgaaccccaggaggtcctgcac, aggcgaggcggtaaagggca
DPP4	gagtgactccaccgcccgga, cacggtgtcttcatcgtcggc
P53R2	tccctcagcgcccgtagctt, atgatctctcatcctgatccagccc
P21	gcactcagaggaggcgccatgt, tcgctgtccactgggccgaa
APAF1	gcgagacagagccctgcacc, gctgtcaaccatgagccaagcct
DDB2	aggacgcgatggctcccaaga, ctaggaccggagcccttcgca
BAX	agcaaactggtgctcaaggccc, gtctcacccaaccaccctggtct
GADD45A	aagctgctcaacgtcgacccc, tctcgcagcaaaacgcctgga
MDM2	cgcgccccgtgaaggaaact, gcacatttgcctgctcctcacca
Maspin	ttctgcccagacacggtcgc, ccattgcgggcctggagtcac
P53	gccagactgccttccgggtc, gggacggcaaggggacaga
TP53INP1	agcccaagtagtcccagagtgga, tccactgggaagggcgaaagc
VEGF	**aaggaggagggcagaatcat, cacacaggatggcttgaaga**
CA-IX	**tggaagaaatcgctgaggaaggct, agcactcagcatcactgtctggtt**
GLUT1	**atcgtggccatctttggctttgtg, ctggaagcacatgcccacaatgaa**
EPO	**cgggcatgggcactcccttg, agaggccagcccccatcctg**
TF	gtgccagagtttccgcgacca, cgtttgccgcaatggccctga
TFR	acggaggacgcgctagtgttct, ttgccgagccaggctgaacc
NOS2	ggacccgcaccactacaggc, gtggcacggctggatgtcgg
ENO1	tgggtacccggagcacggag, tgaacttctagccactgggtctcgt

Supplementary Files

File A.1. Time-lapse video of MD10/TetOx2. Cells were plated, exposed to dox for 1 d, and recovered for 1 d. Cells were then imaged every hour for 3 d. Phase, RFP, and YFP channels were overlaid using Metamorph software. Cells can be seen dividing and transmitting memory to daughter cells, as well as when the circuit does not remain active after division.

File A.2. Transcriptional profiling array analysis of MD12/p53R2-RE and MD10/TetOx2.

Appendix B

Supplementary Information for Chapter 3

Supplementary Tables

Table B.1. qRT-PCR primer sequences

Primer name	Sequence
p53 qPCR F	CAGCACATGACGGAGGTTGT
p53 qpCR R	TCATCCAAATACTCCACACGC
Atm qPCR F	ATCTGCTGCCGTCAACTAGAA
Atm qPCR R	GATCTCGAATCAGGCGCTTAAA
p21 qPCR F	TGTCCGTCAGAACCCATGC
p21 qPCR R	AAAGTCGAAGTTCCATCGCTC
Mdm2 qPCR F	GAATCATCGGACTCAGGTACATC
Mdm2 qPCR R	TCTGTCTCACTAATTGCTCTCCT
Rad51C qPCR F	TTTGGTGAGTTTCCCGCTGTC
Rad51C qPCR R	AACTTCTTTGCTAAGCTCGGAG
Ddb2 qPCR F	ACCTCCGAGATTGTATTACGCC
Ddb2 qPCR R	TCACATCTTCTGCTAGGACCG
Gadd45A qPCR F	GAGAGCAGAAGACCGAAAGGA
Gadd45A qPCR R	CACAACACCACGTTATCGGG
Bax qPCR F	CCCGAGAGGTCTTTTTCCGAG
Bax qPCR R	CCAGCCCATGATGGTTCTGAT
Fas qPCR F	AGATTGTGTGATGAAGGACATGG
Fas qPCR R	TGTTGCTGGTGAGTGTGCATT
RelB qPCR F	CCATTGAGCGGAAGATTCAACT
RelB qPCR R	CTGCTGGTCCCGATATGAGG
BclXL qPCR F	GAGCTGGTGGTTGACTTTCTC
BclXl qPCR R	TCCATCTCCGATTCAGTCCCT
C-Myc qPCR F	TCCCTCCACTCGGAAGGAC
C-Myc qPCR R	CTGGTGCATTTTCGGTTGTTG
Gapdh qPCR F	ACAACTTTGGTATCGTGGAAGG
Gapdh qPCR R	GCCATCACGCCACAGTTTC

Supplementary Files

File B.1. Transcriptional profiling array analysis of MCF10A exposed to 0.5% O_2 for 24 h and recovered for 3 d.

Appendix C

Supplementary Information for Chapter 4

Supplementary Tables

Table C.1. Model Equations

d(pRM_D0)/dt = 1/cell*(-ReactionFlux6)
d(lacZ_mRNA)/dt = 1/cell*(ReactionFlux9 + ReactionFlux10 + ReactionFlux11 - ReactionFlux14)
d(lacZ_pro)/dt = 1/cell*(ReactionFlux12 - ReactionFlux13)
d(cI_wt)/dt = 1/cell*(- -2*ReactionFlux1 - ReactionFlux2 - ReactionFlux4)
d(cI_DN)/dt = 1/cell*(-ReactionFlux2 - -2*ReactionFlux3 - ReactionFlux5)
d(pRM_D1)/dt = 1/cell*(ReactionFlux6 - ReactionFlux7)
d(pRM_D2)/dt = 1/cell*(ReactionFlux7 - ReactionFlux8)
d(cI_dimer)/dt = 1/cell*(ReactionFlux1 - ReactionFlux6 - ReactionFlux7 - ReactionFlux8)
d(cI_mixed)/dt = 1/cell*(ReactionFlux2)
d(cI_DN_dimer)/dt = 1/cell*(ReactionFlux3)

Table C.2. Model Fluxes

ReactionFlux1 = cI_dimerize.kdimF*cI_wt*cI_wt-cI_dimerize.kdimR*cI_dimer
ReactionFlux2 = cI_hetero.kdimF*cI_wt*cI_DN-cI_hetero.kdimR*cI_mixed
ReactionFlux3 = cI_DN_dimerize.kdimF*cI_DN*cI_DN-cI_DN_dimerize.kdimR*cI_DN_dimer
ReactionFlux4 = kdeg*cI_wt
ReactionFlux5 = kdeg2*cI_DN
ReactionFlux6 = kbind0F*cI_dimer*pRM_D0-kbind0R*pRM_D1
ReactionFlux7 = kbind1F*cI_dimer*pRM_D1-kbind1R*pRM_D2
ReactionFlux8 = kbind2F*cI_dimer*pRM_D2-kbind2R
ReactionFlux9 = basal_txn_D0.ktxn*pRM_D0
ReactionFlux10 = basal_txn_D1.ktxn*pRM_D1
ReactionFlux11 = activated_txn.ktxn*pRM_D2
ReactionFlux12 = ktln*lacZ_mRNA
ReactionFlux13 = kdeg_pro*lacZ_pro
ReactionFlux14 = kdeg_mRNA*lacZ_mRNA

Table C.3. Model Parameters

cI_dimerize.kdimR = 1
cI_dimerize.kdimF = 0.05
cI_hetero.kdimF = 0.05
cI_hetero.kdimR = 1
cI_DN_dimerize.kdimF = 0.05
cI_DN_dimerize.kdimR = 1
kdeg = 0.01
kdeg2 = 1
kbind0F = 0.33
kbind0R = 1
kbind1F = 0.66
kbind1R = 1
kbind2F = 0.03
kbind2R = 1
basal_txn_D0.ktxn = 10
basal_txn_D1.ktxn = 10
activated_txn.ktxn = 110
ktln = 1
kdeg_pro = 0.01
kdeg_mRNA = 10
cell = 1

Appendix D

Burrill DR[1], Inniss MC[1], Boyle PM, Silver PA. 2012. Synthetic memory circuits for tracking human cell fate. Genes Dev 26:1486–1497.[*]

[1]These authors contributed equally to this work

[*] Reprinted from *Genes and Development*, with permission from Cold Spring Harbor Laboratory Press

Synthetic memory circuits for tracking human cell fate

Devin R. Burrill,[1,3] Mara C. Inniss,[1,3] Patrick M. Boyle,[1] and Pamela A. Silver[1,2,4]

[1]Department of Systems Biology, Harvard Medical School, Boston, Massachusetts 02115, USA; [2]The Wyss Institute of Biologically Inspired Engineering, Boston, Massachusetts 02115, USA

A variety of biological phenomena, from disease progression to stem cell differentiation, are typified by a prolonged cellular response to a transient environmental cue. While biologically relevant, heterogeneity in these long-term responses is difficult to assess at the population level, necessitating the development of biological tools to track cell fate within subpopulations. Here we present a novel synthetic biology approach for identifying and tracking mammalian cell subpopulations. We constructed three genomically integrated circuits that use bistable autoregulatory transcriptional feedback to retain memory of exposure to brief stimuli. These "memory devices" are used to isolate and track the progeny of cells that responded differentially to doxycycline, hypoxia, or DNA-damaging agents. Following hypoxic or ultraviolet radiation exposure, strongly responding cells activate the memory device and exhibit changes in gene expression, growth rates, and viability for multiple generations after the initial stimulus. Taken together, these results indicate that a heritable memory of hypoxia and DNA damage exists in subpopulations that differ in long-term cell behavior.

[*Keywords*: synthetic circuit; memory; bistability; human cell fate; DNA damage; hypoxia]

Supplemental material is available for this article.

Received February 6, 2012; revised version accepted May 22, 2012.

Biological heterogeneity exists in most cell populations; even isogenic populations exhibit some natural cell-to-cell variability in parameters including gene expression and cell morphology (Bishop et al. 2006). Heterogeneity can result from factors such as noise in gene expression and signal transduction, epigenetic modifications, and cell age (Avery 2006; Bishop et al. 2006). A consequence of this diversity is that not all cells in a population will respond identically to a given stimulus. Biological systems can take advantage of such heterogeneity to produce specific cell types (e.g., differentiation) or optimize fitness in fluctuating environments (e.g., immunity) (Acar et al. 2008). Conversely, heterogeneity can leave some cell subpopulations more sensitive to drug treatment (e.g., chemotherapy) or disease states (e.g., metastasis) (Murray-Zmijewski et al. 2008). Distinct cell fates can be heritably encoded using multiple gene regulatory strategies, including epigenetic marks, stable cytoplasmic factors, and transcriptional autoregulatory circuits (Burrill and Silver 2011). Thus, biological diversity can produce cell subpopulations harboring different memories of an experienced stimulus.

By the very nature of its heterogeneity, memory of a biological decision is difficult to study. Population-level data can obscure subpopulations (Bishop et al. 2006), and single-cell experiments remain expensive, technically difficult, and hard to scale (Spiller et al. 2010). Studies of biological memory require a technique for tracking a cellular decision through cell division. Recombinase systems are commonly used to confer a permanent genomic mark in lineage-tracing studies; however, DNA rearrangement and recombinase expression can have off-target effects that negatively affect genomic fidelity (Forni et al. 2006). Furthermore, tunable, rewriteable DNA recombinase-based memory has only recently been demonstrated in bacteria (Bonnet et al. 2012) and has yet to be developed in eukaryotic cells.

One solution is the application of synthetic, transcriptional autoregulatory circuits to track heritable, differential responses to a stimulus. In this circuit design, a stimulus induces transcription of a trigger gene expressing a transactivator, which binds the promoter of a second gene. The second gene produces more of the same transactivator, initiating a positive feedback loop, or memory (Fig. 1A). Memory is self-sustainable when the input exceeds the circuit's bistable threshold for feedback, allowing the circuit to switch to an alternative state that is transmitted through cell division. Examples of this in nature include the cell cycle and cell differentiation (Burrill and Silver 2010), and synthetic versions have been built in bacteria, yeast, and mammalian cells (for review, see Haynes and Silver 2009; Burrill and Silver 2010). In recent work, we

[3]These authors contributed equally to this work.
[4]Corresponding author
E-mail pamela_silver@hms.harvard.edu
Article is online at http://www.genesdev.org/cgi/doi/10.1101/gad.189035.112.

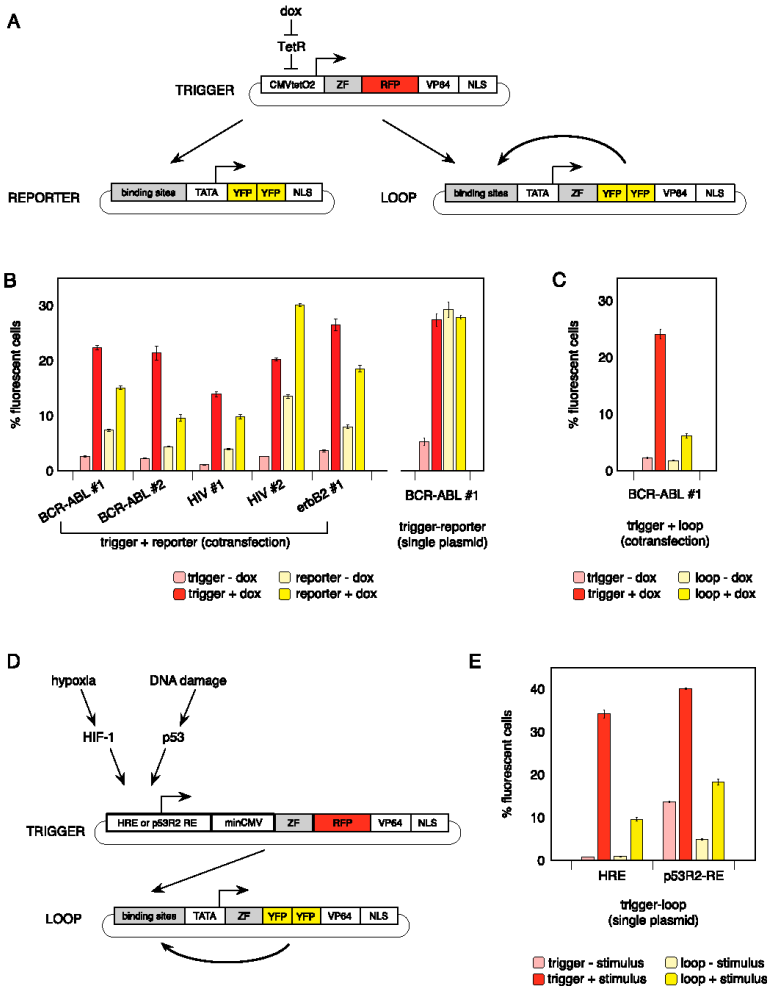

Figure 1. Design and testing of trigger and loop genes. (*A*) Schematic of dox trigger, reporter, and loop genes. (*B*) Synthetic ZFs (BCR-ABL #1 and 2, HIV #1 and 2, and erbB2 #1) were tested as transactivators via cotransfection with corresponding reporters. BCR-ABL #1 was also tested on a single plasmid with its corresponding reporter gene. (*C*) The BCR-ABL #1 trigger and loop were tested via cotransfection on separate plasmids. (*D*) The BCR-ABL #1 trigger was adapted to be sensitive to hypoxia or DNA damage. (*E*) The HRE and p53R2-RE triggers were tested on a single plasmid with their corresponding loop genes. (*B*,*C*,*E*) FACS determined the percent of cells positive for trigger RFP and reporter or loop YFP. Values represent mean ± SE; $n = 3$.

constructed a memory circuit in yeast that detects DNA repair, allowing for isolation of cells that initiated a repair response above the circuit's bistable threshold (Burrill and Silver 2011). Strongly responsive cells exhibited a heritable damage response that was distinct from less-responsive cells for many generations.

Here we report the construction and implementation of synthetic memory circuits in human cells to track differential cellular decisions following a global stimulus. Activation of the device was linked to endogenous hypoxia and DNA damage response pathways, as these stressors elicit heterogeneous responses at the single-cell level (Bristow and Hill 2008; Murray-Zmijewski et al. 2008). A synthetic memory device that responds to low oxygen (O_2) concentrations could help study the sustained effects of hypoxic exposure during tumor formation.

Hypoxia stabilizes the HIF-1 transcription factor, which can activate or silence target genes as well as increase genomic instability by mediating the bypass of DNA repair checkpoints (Chen et al. 2006; Bristow and Hill 2008; Denko 2008; Lee et al. 2009; Lu et al. 2011). Tumors can harbor cell subpopulations that have been exposed to acute or chronic hypoxia and subsequently reoxygenated, and these tumors are associated with a more aggressive disease (Bristow and Hill 2008). A memory device activated by HIF-1 could potentially detect, isolate, and track these subpopulations within the heterogeneous tumor microenvironment to determine their specific contributions toward tumor development and metastasis.

Like hypoxia, DNA damage also produces a complex array of biological responses at the single-cell level. Linking a memory circuit to native DNA damage pathways could help identify how DNA damage responses are transmitted to subsequent generations and impact long-term cell behavior. The variable activation of the tumor suppressor p53 largely determines a single cell's response to DNA damage (Murray-Zmijewski et al. 2008). A memory device triggered at the level of a p53-induced repair factor, such as the ribonucleotide reductase p53R2, would facilitate the isolation and tracking of progeny whose ancestors underwent a repair response strong enough to activate the memory loop, versus those that did not (Tanaka et al. 2000). This could reveal how a cell's specific history of DNA damage translates into long-term biological consequences.

Collectively, our work illustrates a synthetic biology approach for studying cell heterogeneity and fate. The described genomically integrated devices enable the investigation of biological questions that require inheritance of a genetic circuit through cell division. The modularity of our system is demonstrated by the construction of memory circuits that respond to diverse and relevant stimuli. Our studies reveal the existence of a heritable biological memory of DNA damage and hypoxia, providing unique insight into protracted responses to transient stimuli.

Results

Characterizing memory circuit components via transient transfection

To engineer a memory device, we first designed a set of fluorescently labeled synthetic transcriptional activators (triggers) and their corresponding reporter genes (Fig. 1A). Each trigger gene consisted of a synthetic zinc finger (ZF) DNA-binding domain (Hurt et al. 2003), one copy of the red fluorescent protein (RFP) mCherry (Shaner et al. 2004), the VP64 activation domain (Beerli et al. 1998), and a nuclear localization sequence (NLS) (Kalderon et al. 1984), all under the control of a doxycycline (dox)-inducible CMV-TetOx2 promoter with a human kozak sequence. ZFs were mammalian codon-optimized versions of those previously engineered by Hurt et al. (2003) to bind specifically to target DNA sequences in a BCR-ABL translocation (BCR-ABL #1 and #2), the erbB2 gene (erbB2 #1), or the HIV promoter (HIV #1 and #2). Each reporter gene had six tandem copies of DNA-binding sites for a given ZF upstream of a minimal promoter (composed of a TATA sequence and human kozak sequence), and its protein-coding region encoded two copies of the yellow fluorescent protein (YFP) variant Venus (Shaner et al. 2005) tagged with an NLS (Fig. 1A). In the presence of dox, trigger genes were expected to express RFP and a functional transactivator that should bind to its corresponding reporter binding sites, producing a YFP signal.

To evaluate the functionality of our constructs in human cell culture, triggers and reporters were built on separate plasmids and transiently cotransfected in a human U2OS cell line that expresses the Tet repressor (Supplemental Table S1). Following the addition of dox, trigger RFP and reporter YFP coexpression was monitored by fluorescence-activated cell sorting (FACS) (Fig. 1B). All triggers activated transcription of their target reporters by at least twofold. The HIV #2 reporter exhibited the most leaky expression, with >10.0% of cells expressing YFP in the absence of dox. Trigger/reporter pairs were specific and orthogonal to one another, as minimal YFP expression was observed when reporters alone (Supplemental Fig. S1A) or mismatched trigger/reporter combinations (Supplemental Fig. S1B) were transfected. Thus, all triggers were capable of producing a functional transcriptional circuit.

This set of synthetic transactivators provided the components to construct autoregulatory loops intended to confer memory of a stimulus to a single cell and its progeny. In our proposed device, an input causes synthesis of an RFP-labeled transactivator, which activates expression of a 2xYFP-labeled transactivator (Fig. 1A). This protein binds to its own promoter and, given certain parameters, continues to self-activate in the absence of stimulus, resulting in sustained YFP expression. For simplicity, all memory devices were built with the BCR-ABL #1 domain, although the above transient experiments suggested that all tested ZFs would provide similar results.

Since tracking long-term memory requires a stably integrated device, a trigger–reporter circuit was assembled on a single plasmid and tested by transient transfection for circuit activation to determine whether the circuit could be integrated in one step. On a single plasmid, the dox memory device demonstrated constitutive reporter YFP expression in the absence of dox, likely due to *cis*-activation caused by enhancer elements in the trigger's CMV-TetOx2 promoter (Fig. 1B; Boshart et al. 1985). However, the dox device demonstrated inducible expression of the loop gene when the trigger and loop were cotransfected on separate plasmids (Fig. 1C).

We next aimed to construct memory circuits capable of recording exposure to dox, hypoxia, or DNA damage. The hypoxia-inducible promoter we used was based on one previously engineered by Shibata et al. (2000) and is composed of five copies of HIF-1 binding sites, known as hypoxia-responsive elements (HREs), ligated to a minimal human CMV promoter. This promoter is activated when a cell triggers the HIF-1 pathway in response to hypoxia (Fig. 1D). A DNA damage-inducible promoter (p53R2-RE) was generated by linking four copies of the p53-binding site in p53R2 (Ohno et al. 2008) to a minimal human

CMV promoter (Shibata et al. 2000). This promoter is activated when a cell executes a p53R2-mediated repair response (Fig. 1D).

Unlike the dox device, the HRE and p53R2-RE triggers do not contain strong enhancer elements and can be assembled as a single construct with the loop gene. When the hypoxia and DNA damage devices were transfected as a single plasmid and exposed to the hypoxia mimic cobalt chloride ($CoCl_2$) or the DNA-damaging agent neocarzinostatin (NCS), respectively, RFP and YFP were coexpressed in a significant percentage of cells above basal levels (Fig. 1E). These observations were similar whether or not the circuits were built on one plasmid (Supplemental Fig. S1C). Thus, we determined that while a dox memory cell line would require two integrations, only one was necessary to produce DNA damage and hypoxia memory cell lines. To test the capacity of the loop element to retain memory of dox, hypoxia, or DNA damage exposure, we proceeded to genomically integrate the circuits.

An integrated dox memory device

The dox trigger and loop were randomly integrated as separate genes to create the cell line MD10/TetOx2 (Supplemental Table S2). Dox exposure resulted in trigger RFP and loop YFP expression in 99.8% and 42.7% of cells, respectively, as determined by FACS (Fig. 2A) and fluorescence microscopy (Fig. 2B). Upon the removal of dox, trigger RFP turned off in most cells within 1 d, while loop YFP achieved a bimodal distribution, such that two distinct memory and non-memory subpopulations coexisted (Supplemental Fig. S2). YFP expression persisted in a large percentage of cells for at least 3 d (about four generations), suggesting heritable memory loop activity (Fig. 2B). These traits were not specific to MD10/TetOx2, as multiple alternative clones were analyzed and demonstrated similar behavior (Supplemental Fig. S3).

Sustainable memory behavior in a subpopulation of dividing cells was further revealed in time-lapse fluorescence microscopy of cells recovering from dox exposure (Fig. 2C; Supplemental File S1). Distribution of YFP intensity in the memory subpopulation was constant over time, suggesting persistent protein production (Fig. 3A). Furthermore, spontaneous loop activation in the absence of dox was not observed when MD10/TetOx2 was cultured for 9 d (~10 generations), indicating that any loop activity was due solely to dox exposure (Fig. 3B). To rule out a difference in RFP and YFP protein degradation rates as causal of the observed memory behavior, cells were

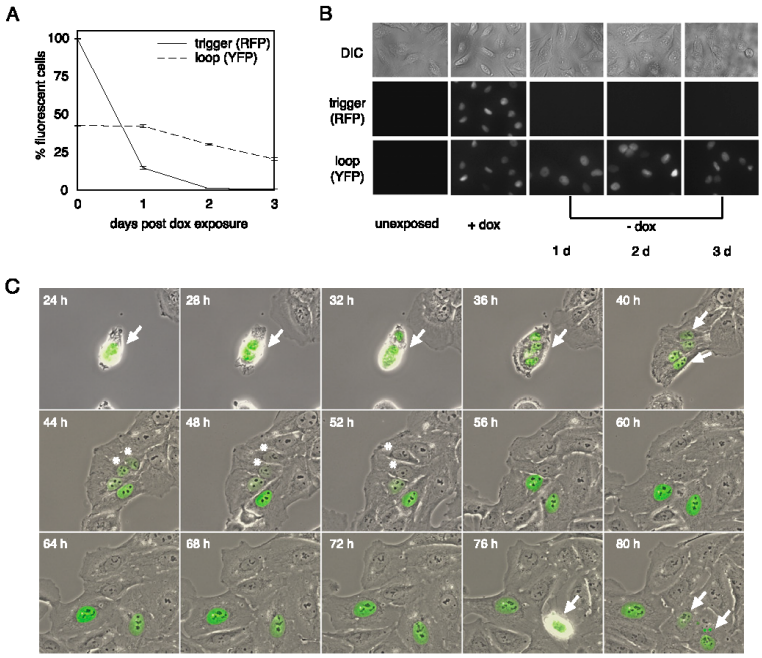

Figure 2. MD10/TetOx2 transmits memory of dox exposure. Memory behavior was analyzed by FACS (*A*) and fluorescence microscopy (*B*). FACS determined the percent of cells positive for trigger RFP and loop YFP. Values represent mean ± SE; $n = 3$. (*C*) Fluorescence microscopy montage of MD10/TetOx2, 24–28 h post-dox exposure. Phase, RFP, and YFP channels were overlaid. (Arrows) Dividing memory cells; (*) cells in which the circuit does not remain active after division.

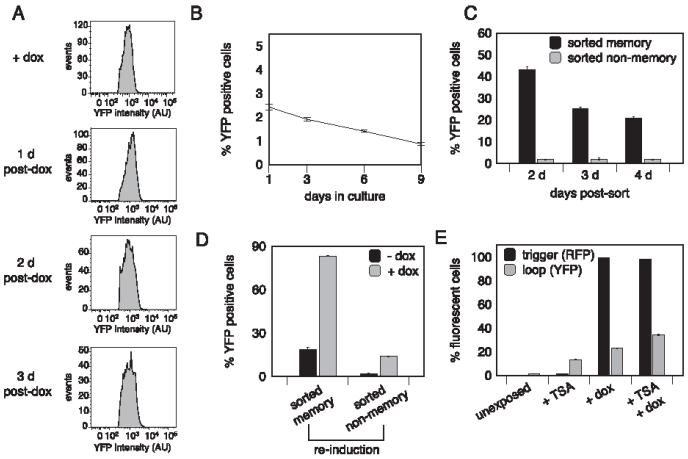

Figure 3. Further characterization of MD10/TetOx2. (*A*) FACS plots of the YFP intensity of the memory cell subpopulation versus the event rate at several time points post-dox exposure. (*B*) Unexposed cells were tracked via FACS to determine the rate of spontaneous loop activation. (*C*) Memory and non-memory cells were sorted 2 d post-dox exposure and tracked by FACS to determine the percent of cells positive for loop YFP. (*D*) Sorted memory and non-memory cells were reinduced 3 d post-sort with dox, and FACS determined the percent of cells positive for loop YFP. (*E*) Cells were exposed to TSA, dox, or TSA + dox to identify epigenetic silencing of the device. FACS determined the percent of cells positive for trigger RFP and loop YFP. (*A–E*) Values represent mean ± SE; $n = 3$.

exposed to dox to activate fluorophore expression, and cycloheximide was then added to inhibit protein biosynthesis. RFP and YFP degradation rates were determined to be approximately equivalent: 10.6 versus 11.5 arbitrary intensity units per hour, respectively (Supplemental Fig. S4). Thus, loop YFP protein persisted by positive feedback and not by protein stability. We concluded that MD10/TetOx2 was capable of recording dox exposure and transmitting memory of this response to progeny.

To investigate the independent behavior of memory and non-memory cells, cell sorting based on YFP expression was used to physically separate and expand the two cell populations for biological analysis. Over a period of 3 d, sorted memory cells behaved similarly to unsorted memory cells, in that the percentage that maintained loop expression decreased over time (Fig. 3C). Sorted memory cells were re-exposed 3 d post-sort to dox, at which time 20.2% were still expressing the loop, but only 83.3% reactivated the loop (Fig. 3D). Furthermore, sorted non-memory cells largely failed to reinduce the loop (Fig. 3D). These observations suggested that epigenetic silencing might play a role in permanently deactivating the memory loop. To test this, trichostatin A (TSA)—a histone deacetylase inhibitor—was applied to unsorted MD10/TetOx2 cells before dox exposure to reverse gene silencing. While the number of cells expressing the trigger did not change, 12.5% more cells activated the memory loop if first exposed to TSA (Fig. 3E), indicating that decreased loop activity over time could be due to epigenetic silencing. This may also explain why only 42.7% of cells initially activated the loop. Every selected MD10/TetOx2 clone exhibited this behavior, suggesting that the loop became silenced during the selection process. Despite this effect, this cell line exhibits persistent inducible memory loop expression in a significant percentage of cells, allowing for tracking of the cellular response to dox through cell division.

An integrated hypoxia memory device

To track memory of hypoxia through cell division, the stable cell line MD15/HRE was constructed via random genomic integration of the HRE trigger and loop as a single plasmid. While $CoCl_2$ induced a hypoxic response in transient experiments, it was not appropriate for long-term cell tracking due to its deleterious effect on cell viability and possible nonspecific activity as a hypoxia mimic. Alternatively, an anaerobic chamber caused less cell death and created an anoxic environment in which MD15/HRE could be easily characterized, since the HRE promoter is maximally active under anoxic conditions (Shibata et al. 2000). As fluorophores require O_2 to fold properly, any trigger or loop protein produced during anoxia was not fluorescent, necessitating a recovery period before analysis. After 1 d of anoxic exposure and 1 d of recovery, the trigger was expressed in 21.5% of cells at a low intensity, since the anoxic response had likely subsided by that time, and the loop was activated in 10.8% of cells, as determined by FACS (Fig. 4A) and fluorescence microscopy (Fig. 4B). Loop-expressing cells were expected to have activated the trigger's anoxia-inducible promoter above the bistable threshold required for loop expression. A scatterplot of single-cell RFP versus YFP intensities post-anoxia shows that higher RFP expression corresponds to higher YFP expression, as measured by

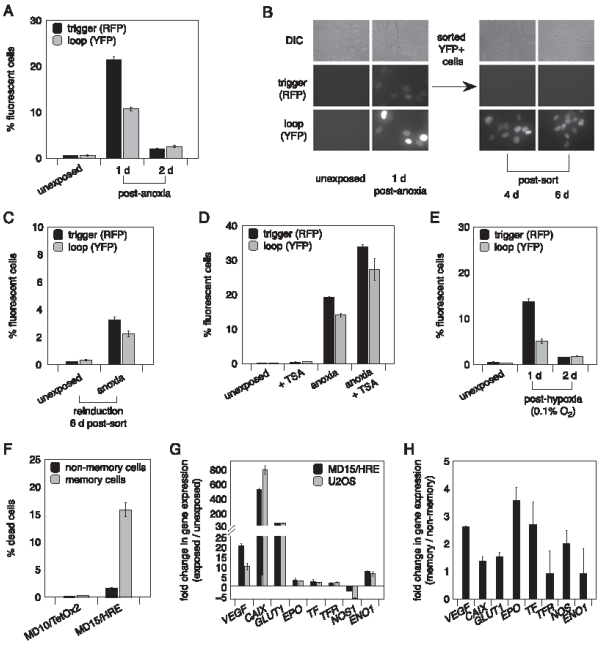

Figure 4. MD15/HRE device identifies a subpopulation with a unique memory of low O_2 exposure. (*A*) Cells were exposed to anoxia and tracked by FACS for 2 d. (*B*) Cells were exposed to anoxia and recovered for 1 d. Memory cells (YFP+) were sorted and followed by microscopy for 6 d. (*C*) Cells were exposed to anoxia and recovered for 1 d. Non-memory cells were sorted and re-exposed to anoxia 6 d post-sort. (*D*) Cells were exposed to TSA, anoxia, or TSA + anoxia to identify epigenetic silencing of the device. (*E*) Cells were exposed to hypoxia and tracked by FACS for 2 d. (*A*,*C*,*D*,*E*) FACS determined the percent of cells positive for trigger RFP and loop YFP. Values represent mean ± SE; n = 3. (*F*) Cells were exposed to hypoxia and recovered for 1 d. MD10/TetOx2 was exposed to dox and recovered for 1 d. Cell death was measured in memory versus non-memory cells by FACS. Values represent mean ± SE; n = 3. (*G*) MD15/HRE and U2OS cells were exposed to hypoxia, and HIF target gene expression was measured. Values represent mean fold expression change over unexposed cells ± SE; n = 3. (*H*) Cells were exposed to hypoxia and recovered for 1 d. Memory and non-memory cells were sorted, and HIF target gene expression was measured in each subpopulation. Values represent mean fold expression change in memory versus non-memory cells ± SE; n = 2.

FACS (Supplemental Fig. S5A). Thus, loop expression results from stronger trigger activation in response to anoxia.

During the first 2 d post-exposure, we observed a decrease in the memory subpopulation as a fraction of the total population (Fig. 4A). We hypothesized that memory cells, having activated a stronger response to anoxia, were likely more susceptible to growth defects and being diluted out of the population. This made it difficult to observe by FACS whether memory of anoxia indeed persisted through cell division in a subpopulation of cells (Supplemental Fig. S6). However, when memory cells were isolated from their non-memory counterparts via cell sorting and observed by fluorescence microscopy, a significant proportion of sorted memory cells expressed the loop for at least 6 d (about five generations) post-sort and grew in clusters, indicating active maintenance of memory through cell division (Fig. 4B).

To determine whether epigenetic silencing contributed to the observed decrease in the percentage of memory cells when the two subpopulations were cocultured, sorted non-memory cells were reinduced 6 d post-sort. Only 3.3% and 2.5% of sorted nonmemory cells reactivated the trigger and loop, respectively (Fig. 4C). In addition, when TSA was applied to unsorted MD15/HRE cells prior to anoxic exposure, 8.8% and 13.5% more cells activated the trigger and loop, respectively (Fig. 4D), indicating that epigenetic silencing was occurring in this cell line. We also noted that the slower growth of memory cells contributed to a decrease in the percentage of loop-expressing cells. When equal numbers of sorted memory and non-memory cells were plated 1 d post-exposure, memory cells exhibited a growth defect, reaching confluency 1 d later than non-memory cells (Supplemental Fig. S7A). This phenotype was not caused by synthetic gene expression, as no growth difference was observed between sorted MD10/TetOx2 memory and non-memory cells (Supplemental Fig. S7B). In sum, epigenetic silencing and slow growth likely caused the observed decline in memory cells when memory and non-memory cells were cocultured.

To interrogate the biological relevance of the subpopulations captured by the circuit, hypoxia (0.1% O_2) was next used to activate the MD15/HRE device. While the trigger's HRE promoter is known to be less active under increasing O_2 conditions, hypoxia is commonly used to mimic a tumor microenvironment and plays a significant biological role in disease and development (Bristow and Hill 2008). As expected, hypoxia activated the device in fewer cells (13.6% trigger RFP-positive and 5.1% loop YFP-positive) than anoxia, presumably due to the higher O_2 concentration (Fig. 4E; Supplemental Fig. S5B). However, in cells that were activated, memory behavior similar to that under anoxic conditions was observed: Unsorted memory cells were quickly diluted out (Fig. 4E; Supplemental Fig. S6), while sorted memory cells grew in clonal populations for at least 8 d (about seven generations) (Supplemental Fig. S8). A viability assay using the dead cell stain SYTOX Blue (Invitrogen) revealed that memory

cells remained less viable than non-memory cells 1 d post-hypoxic exposure: 15.9% death versus 1.68% death, respectively, as compared with MD10/TetOx2 memory and non-memory cells (Fig. 4F). This difference in viability not only contributed to dilution of the memory population over time, but was also indicative of memory and non-memory subpopulations having distinct biological responses to hypoxia.

To investigate these responses, we first established that endogenous pathways responsive to low O_2 concentrations were similarly functional in MD15/HRE and its background strain, U2OS. Both cell lines were exposed to hypoxia, and HIF target gene expression was measured by real-time PCR (Fig. 4G; Ke and Costa 2006). Since gene activation patterns were similar in both cell lines, we concluded that MD15/HRE responded to hypoxia with normal gene regulation. While this experiment examined hypoxic responses of the population as a whole, we next assessed whether expression of target genes was specifically up-regulated in memory cells, as compared with non-memory cells. Since memory cells had surpassed the circuit's bistable threshold for loop expression, they were expected to have responded more strongly to hypoxia. Memory and non-memory cells were sorted 1 d post-hypoxic exposure, and HIF target gene expression was compared by real-time PCR (Fig. 4H). Indeed, a subset of HIF target genes was up-regulated in memory cells. Some target genes were not up-regulated, which was likely due to the fact that exposed cells needed to recover for 1 d for fluorophores to develop to allow for FACS analysis, during which time the initial transcriptional response to hypoxia subsided. Nevertheless, these results demonstrate that the synthetic circuit integrated in the cell line MD15/HRE is capable of sensing and tracking subpopulations that differ in their responses to hypoxia.

An integrated DNA damage memory device

To follow memory of DNA damage, the stable cell line MD12/p53R2-RE was generated via random genomic integration of the p53R2-RE trigger and loop as a single plasmid. While NCS was used as a DNA-damaging agent in transient experiments, it was not amenable to long-term cell tracking due to its highly deleterious effects on cell viability. Alternatively, a brief burst of 10 J/m^2 shortwave ultraviolet radiation (UV) allowed greater cell viability (Latonen et al. 2001; Sharma et al. 2010). UV exposure resulted in trigger and loop activation in 20.2% and 8.3% of cells, respectively, as determined by FACS (Fig. 5A), and higher trigger activation corresponded with greater loop activation (Supplemental Fig. S5C); this behavior was similar for all positive selected clones (Supplemental Fig. S9). Fluorescence microscopy indicated that memory persisted for at least 2 d post-exposure in a subpopulation of cells (Fig. 5B); however, a significant decrease in the percentage of cells expressing the loop was observed during the first 2 d post-exposure.

While this characteristic precluded FACS analysis of sustained memory, fluorescence microscopy revealed that loop expression was maintained in small clonal populations

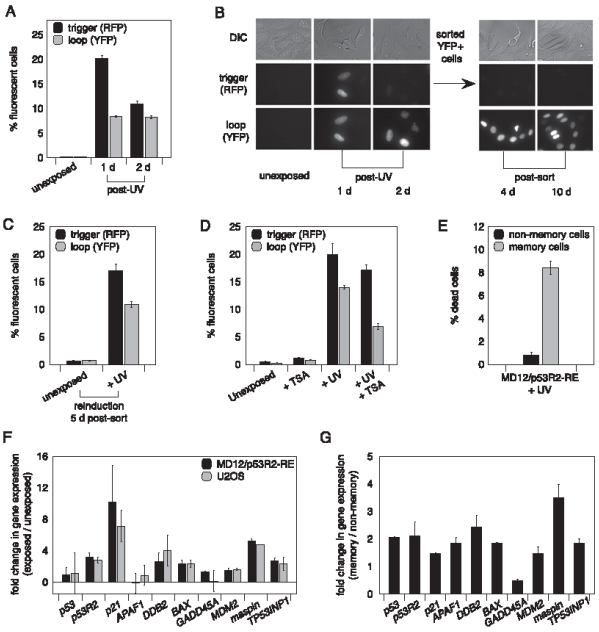

Figure 5. MD12/p53R2-RE device identifies a subpopulation with unique memory of DNA damage. (*A*) Cells were exposed to UV and tracked by FACS for 2 d. (*B*) Cells were exposed to UV and recovered for 1 d. Memory cells (YFP+) were sorted and followed by microscopy for 10 d. (*C*) Cells were exposed to UV and recovered for 1 d. Non-memory cells were sorted and re-exposed to UV 5 d post-sort. (*D*) Cells were exposed to TSA, UV, or TSA + UV to identify epigenetic silencing of the device. (*A*,*C*,*D*) FACS determined the percent of cells positive for trigger RFP and loop YFP. Values represent mean ± SE; n = 3. (*E*) Cells were exposed to UV and recovered for 2 d. Cell death was measured in memory versus non-memory cells by FACS. Values represent mean ± SE; n = 3. (*F*) MD12/p53R2-RE and U2OS cells were exposed to UV, and p53 target gene expression was measured. Values represent mean fold expression change over unexposed cells ± SE; n = 3. (*G*) Cells were exposed to UV and recovered for 1 d. Memory and non-memory cells were sorted, and p53 target gene expression was measured in each subpopulation. Values represent mean fold expression change in memory versus non-memory cells ± SE; n = 2.

when memory cells were isolated 2 d post-UV exposure (Fig. 5B; Supplemental Fig. S6). The loop was expressed in a subpopulation of cells for at least 10 d (about eight generations) post-sort. This indicated that a subpopulation successfully activated the device above the bistable threshold for loop expression, permitting tracking of memory and non-memory cells. Gene dysfunction was not a contributing factor to the observed memory population decrease, as sorted non-memory cells were able to reinduce both the trigger and loop to levels comparable with their initial induction (Fig. 5C). Furthermore, epigenetic silencing of the device did not likely affect its function over time: Exposure to TSA alone caused no significant induction of the device, and pretreatment with TSA did not increase the number of cells that responded to subsequent UV exposure (Fig. 5D).

These results implied that the proportion of memory cells—having executed a stronger DNA damage response—decreased post-damage due to a growth defect or cell death, resulting in dilution of the population over time by the more rapidly growing or viable non-memory cells. When equal numbers of sorted memory and non-memory cells were plated and observed for 4 d by fluorescence microscopy, non-memory cells reached confluency 2 d sooner than memory cells (Supplemental Fig. S7C). This slow growth phenotype could account for memory cells being diluted out of the population over time when memory and non-memory cells are grown together. Using the dead cell stain SYTOX Blue, we also determined that memory cells were less viable than non-memory cells 2 d post-UV exposure: 8.4% cell death versus 0.8%, respectively (Fig. 5E). Altogether, these data suggest that memory and non-memory cells maintained different growth and viability phenotypes after UV exposure.

We next asked whether unique gene expression profiles characterized how distinct subpopulations responded initially to DNA damage. Endogenous response pathways were similarly functional in MD12/p53R2-RE and its background strain post-UV exposure, as measured by p53 target gene expression using real-time PCR (Fig. 5F; Brady and Attardi 2010). Furthermore, a subset of target genes was specifically up-regulated in memory cells (Fig. 5G). Memory and non-memory subpopulations were sorted 1 d post-UV exposure, and p53 target gene expression was compared by real-time PCR. Since exposed cells required 1 d of recovery before sorting, not all target genes were up-regulated at the indicated time point. In sum, these results verify that the synthetic circuit is capable of differentiating between subpopulations that uniquely respond to DNA damage.

To assess whether specific initial responses translated into each subpopulation maintaining distinct long-term expression profiles, we performed gene expression profiling of memory and non-memory cells multiple days after UV exposure. After 3 d of recovery from UV treatment, memory and non-memory cells were sorted. The expression signature of memory cells was distinct from their non-memory counterparts: 127 genes were up-regulated and 31 genes were down-regulated in memory cells (fold change $\geq$2.0, corrected P-value $\leq$0.05) (Supplemental File S2). Bioinformatics analysis identified the transcriptional pattern of oxidative stress and general stress responses in memory cells (Fig. 6A): Up-regulated genes were enriched for those responsive to external stimulus ($P = 1.48 \times 10^{-3}$), wounding ($P = 1.56 \times 10^{-3}$), hydrogen peroxide ($P = 3.41 \times 10^{-3}$), stress ($P = 3.89 \times 10^{-3}$), reactive oxygen species (ROS) ($P = 6.05 \times 10^{-3}$), and chemical stimulus ($P = 9.29 \times 10^{-3}$). Enrichments were validated by real-time PCR (Supplemental Fig. S10A). To eliminate any transcriptional effects caused by expression of a synthetic device, profiling of MD10/TetOx2 sorted memory versus non-memory cells was also performed, and common genes were removed from the MD12/p53R2-RE data analysis (Supplemental Fig. S10B; Supplemental File S2).

While the microarray data defined a set of genes that were uniquely expressed in memory cells multiple days post-DNA damage, it did not inform on the expression level of those genes at earlier time points. To address this question, we tested the expression of four up-regulated genes—*CDNF*, MAX dimerization protein 1 (*MXD1*), *SCL39A2*, and *GRK5*—1 d after UV exposure (Fig. 6B). Interestingly, all four tested genes showed significant up-regulation in memory cells, as compared with non-memory cells. Thus, these genes were expressed both 1 d and 3 d after UV exposure. This suggested that UV-mediated DNA damage produced a transcriptional response that was maintained over time in memory and non-memory cells. Since differences in not only gene expression, but also viability and growth, were shown to persist for multiple days, we concluded that the MD12/p53R2-RE circuit is capable of capturing subpopulations with distinct long-term memories of DNA damage.

Discussion

Building a prototype memory circuit in mammalian cells

In this study, we present the successful engineering and implementation of synthetic memory devices in human cells. The construction of a prototype, dox-inducible circuit (MD10/TetOx2) revealed behavioral qualities of an integrated, transcription-based device that could inform further applied systems. In all isolated clones, most cells activated the trigger in response to dox, and a significant

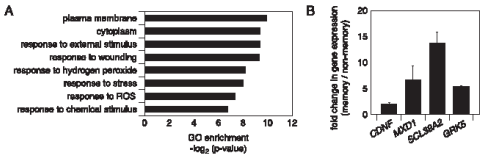

Figure 6. MD12/p53R2-RE device identifies a subpopulation with a unique transcriptional profile. (*A*) Gene ontology enrichment of genes up-regulated in memory cells 3 d post-UV exposure. (*B*) Cells were exposed to UV and recovered for 1 d. Memory and non-memory cells were sorted, and gene expression was measured in each subpopulation. Values represent mean fold expression change in memory versus non-memory cells ± SE; $n = 2$.

fraction activated the memory loop. Moreover, a subpopulation of loop-expressing cells transmitted the memory protein to daughter cells for multiple generations. These cells likely activated the circuit above its bistable threshold. The MD10/TetOx2 circuit provides one of the first synthetic examples of what is required to create a bistable mammalian memory switch based on positive feedback.

While a significant percentage of cells maintained loop expression post-exposure, this population decreased over time. Indeed, time-lapse fluorescence microscopy revealed that some daughter cells failed to inherit memory protein from loop-expressing mother cells. As this was observed for all selected clones, the genomic integration location was unlikely to be causative. However, we hypothesize that epigenetic silencing resulted in memory loop deactivation, and stochastic noise in memory loop protein segregation during cell division might also have played a role. If a daughter cell randomly fails to receive a sufficient amount of loop protein to maintain feedback, it will switch to a non-memory state that is propagated in future progeny. This behavior has been observed for both natural and synthetic transcriptional autoregulatory circuits (Becskei et al. 2001; Weinberger and Shenk 2007; To and Maheshri 2010). Producing more loop protein before cell division, by either increasing the synthesis rate or reducing the rate of cell division, is expected to minimize any loss of memory over time (Ajo-Franklin et al. 2007). However, for certain uses—such as drug dosage in a clinical setting—short-term memory loop expression could be desirable.

Integrating synthetic circuits with endogenous pathways

To demonstrate its potential to report on biological phenomena, the MD10/TetOx2 device was reconfigured to respond to endogenous hypoxia and DNA damage response pathways. Memory cells were identified as descendants of cells that experienced HIF-1 or p53R2 activity above the circuit's bistable threshold, while non-memory cells were those that responded more weakly, such that the loop was not activated. The formation and defining characteristics of these memory cells, versus their non-memory counterparts, could vary depending on cell state, DNA-damaging or hypoxic agents, length of exposure, and time of recovery. Furthermore, a given stressor likely produces many subpopulations with uniquely protracted responses. Our goal was to use the described circuits to identify how an initial response translated into sustained biological characteristics that distinguished what we defined as memory and non-memory cell subpopulations.

Interestingly, the hypoxia and DNA damage memory devices behaved quite differently from the dox memory device. MD10/TetOx2 responded to dox by activating the trigger to similar levels in all cells and the memory loop to similar levels in 42.7% of cells (Supplemental Fig. S2). In contrast, MD15/HRE and MD12/p53R2-RE responded to hypoxia or DNA damage with variable activation of the trigger and loop (Supplemental Fig. S5). Furthermore, while memory of dox exposure was sustained in a significant number of cells, memory of hypoxia and DNA damage persisted in a small subset.

Behavioral differences were likely due to the more heterogeneous activation of hypoxia and DNA damage signaling pathways. MD10/TetOx2 induction occurs when the tet repressor can no longer bind the trigger's promoter due to the presence of dox, resulting in strong, homogeneous trigger and loop expression (Supplemental Fig. S2). In contrast, MD15/HRE and MD12/p53R2-RE activation is dependent on signals transduced by biological pathways composed of numerous proteins, each with its own degree of biological noise. Unlike the dox-inducible trigger, HIF-1 and p53 should not be uniformly activated within a population (Bristow and Hill 2008; Murray-Zmijewski et al. 2008), resulting in heterogeneous trigger and loop activation (Supplemental Fig. S5). MD15/HRE and MD12/p53R2-RE thus permit the isolation of unique subpopulations after hypoxia or DNA damage.

The utility of the hypoxia and DNA damage memory devices in detecting biologically distinct subpopulations was assessed in multiple ways. We determined that in initial response to hypoxia or UV, HIF and p53 target gene expression was elevated in MD15/HRE and MD12/p53R2-RE cells that activated both the trigger and loop, as compared with cells that only activated the trigger. This result indicated that the devices work as intended: Cells with a stronger response are capable of overcoming the bistable threshold of the circuit, such that the loop is expressed. We also established that a stronger response translated into long-term phenotypes, including slow growth and poor viability. Memory cells exhibited these characteristics for multiple generations past the point of exposure, as compared with their non-memory counterparts.

Finally, gene expression profiling revealed that DNA-damaged memory cells had a persistent gene expression signature that was different from that of non-memory cells. The memory cell expression profile was largely enriched for genes responsive to oxidative stress, as well as stress in general, including DNA damage-inducible transcript (*DDIT3*), glutathione peroxidase 3 (*GPX3*), *MXD1*, egl nine homolog 3 (*EGLN3*), and tumor protein p53-inducible nuclear protein 1 (*TP53INP1*). UV radiation is known to cause significant intracellular production of ROS and reactive nitrogen species as well as alter the levels of intracellular antioxidant enzymes (Zhang et al. 1997; Birch-Machin and Swalwell 2010). Our study shows that transcriptional responses to UV-induced oxidative damage persist through multiple generations in a subpopulation of cells. It is possible that this differential maintenance of gene expression translates into differences in vulnerability to future damage or disease and may also dictate the mechanisms by which each subpopulation protects the fate of its progeny.

Conclusions

The memory devices presented here have the potential to illuminate previously undescribed biological phenomena. The hypoxia and DNA damage memory circuits could be used in further analyses, such as deep-sequencing or

epigenetic mapping, of differentially responsive subpopulations to create a more detailed picture of how a cell's history contributes to its biological future. Differentially regulated genes in memory cells could potentially serve as targets in future work toward defining how the inherited expression profile is maintained. This approach could implicate genes that play a role in disease development. The work might also be translated to a xenograft model in mice to study the in vivo heterogeneous effects of DNA damage and hypoxia through the development of a solid tumor. It would be interesting to identify whether these transient stimuli produce subpopulations that are more or less prone to disease development. Given their modular nature, the circuits could potentially produce outputs other than fluorophores. For example, in the future, a memory device could be used in a clinical setting by modifying the loop to produce a therapeutic drug in response to a transient stimulus. The loop could also be altered to create a useful tissue-engineering tool that produces morphogens or growth factors for differentiation control in tissue engineering. While these proposed applications will require significant retooling and testing of the device, their pursuit will help advance and define the utility of synthetic circuits.

Our work demonstrates that complex biological problems can be investigated with synthetic circuits. To date, development of new synthetic devices has been hindered by a slow design cycle and poor device robustness, particularly in mammalian cell culture (Burrill et al. 2011). Streamlining the mammalian design cycle is critical as synthetic biology strives to better integrate with complex human applications such as stem cell therapy and tissue engineering. Continuing to build mammalian devices will undoubtedly provide invaluable data for more comprehensive quantitative models, which will allow better predictions of function at the preliminary design stage and thereby reduce the number of tested iterations of a device. Synthetic devices destined for clinical applications must also demonstrate faithful performance; constructing genomically integrated devices, as with our memory circuits, is an important first step. Improving mammalian cell design remains an essential task for synthetic biology as the field continues to engage in the engineering of increasingly complex cell types.

Materials and methods

Plasmid constructs

Escherichia coli DH5α was used for all plasmid manipulations. Bacteria were grown in LB-ampicillin medium to maintain plasmids; if engineered constructs contained synthetic ZFs, medium was supplemented with 0.02 mM zinc chloride. DNA fragments with universal cloning sites (EcoRI, NotI, XbaI, SpeI, and PstI) were generated by PCR and assembled via BioBrick DNA assembly (Phillips and Silver 2006).

A CMV-TetOx2 promoter fragment (from pcDNA5/FRT/TO, Invitrogen) ligated in front of a human kozak sequence produced a dox-inducible promoter. A HRE promoter was provided by the Brown laboratory (Shibata et al. 2000). Response elements from the human p53R2 gene (Ohno et al. 2008) were constructed as annealed oligos (Integrated DNA Technologies) and ligated in front a minimal promoter (Shibata et al. 2000) to generate a p53R2-RE promoter. Human codon-optimized synthetic ZFs (Hurt et al. 2003) were commercially synthesized by Mr. Gene GmbH.

For transient transfections, triggers and reporters were cloned as NotI/SpeI fragments into the Flp-In T-REx vector in which the constitutive CMV promoter was deleted (Invitrogen, Silver Laboratory). For MD10/TetOx2 (clone MD10.21), trigger and memory loop genes were cloned as separate fragments into a pcDNA3.1 (+)-based vector (Invitrogen) in which the neomycin resistance marker was replaced with hygromycin or puromycin resistance, respectively, and the constitutive CMV promoter was deleted (Silver Laboratory). For MD15/HRE (clone 15.21) and MD12/p53R2-RE (clone 12.34), trigger and loop genes were cloned as one fragment into the puromycin-resistant pcDNA3.1 (+)-based vector (Invitrogen, Silver Laboratory).

Memory device design strategy

Devices were built in two stages. First, multiple gene circuits were designed and tested via transient transfection. In these plasmid-based experiments, multiple designs were characterized to identify elements that generated the most effective circuit activation and least basal activity. Selected prototypes were then genomically integrated to produce the final stable devices, which are characterized in greater detail in this study.

Cell culture and transfection

Plain U2OS and U2OS Flp-In T-REx cells (Blacklow Laboratory) were grown in McCoy's 5A medium supplemented with 10% tetracycline-screened fetal bovine serum (FBS) and 1% penicillin and streptomycin; T-REx cells were further supplemented with 15 μg/mL blasticidin and 200 μg/mL zeocin. Cells were grown at 37°C in a humidified CO_2 incubator.

Transient transfections were performed by plating 1.2×10^5 cells per well in 12-well culture dishes and transfecting with 800 ng of total plasmid DNA and 2 μL of Lipofectamine 2000 (Invitrogen) in 1 mL of antibiotic-free medium (Supplemental Table S1). Medium was changed 4 h post-transfection, and cells were exposed 20 h later to 1 μg/mL dox (Sigma-Aldrich), 0.5 μg/mL NCS (Sigma-Aldrich), or 100 μM $CoCl_2$ (Sigma-Aldrich) for 24 h and analyzed by FACS.

Stable cell lines were generated by plating 3.0×10^5 cells per well in six-well culture dishes and transfecting with 2 μg of plasmid DNA and 5 μL of Lipofectamine 2000 in 2 mL of antibiotic-free medium. Medium was changed 4 h post-transfection, and cells were exposed to selection medium the following day (Supplemental Table S2). After 5 d of selection, medium was changed to maintenance antibiotic concentrations (Supplemental Table S2). Clones were picked and screened for inducible expression via 1 μg/mL dox, 0.5 μg/mL NCS, or 100 μM $CoCl_2$. Positive clones were expanded and maintained as stable lines.

Induction of MD15/HRE and MD12/p53R2-RE cell lines

To analyze MD15/HRE behavior, 3.0×10^6 cells were plated in 10-cm plates. The following day, plates were exposed to anoxia (0% O_2, ~2.0% H_2) in an anaerobic chamber (Wyss Institute for Biologically Inspired Engineering) for 1 d in CO_2-independent medium (Invitrogen) or hypoxia (0.1% O_2, 5.0% CO_2) in a hypoxic chamber (Kaelin laboratory, Dana Farber Cancer Institute). When cells were returned to normoxia, the medium was replaced with the appropriate maintenance medium. To analyze MD12/p53R2-RE behavior, 3.0×10^5 cells per well were plated

in six-well plates. The following day, plates were exposed to a brief burst of 10 J/m^2 UV (Lahav laboratory, Harvard Systems Biology).

Flow cytometry and cell sorting

Prior to FACS analysis, cells were fixed in 4% paraformaldehyde/1× PBS solution for 10 min, resuspended in 200 μL of 1× PBS, and stored at 4°C. Cells were later loaded in 96-well plates or 5-mL polystyrene tubes (BD Biosciences) on an LSRII (BD Biosciences) with 488-nm (DsRed) and 568-nm (Fitc) lasers (Harvard Systems Biology). Cells (1.0×10^4) were analyzed for RFP (DsRed) and YFP (FITC) fluorescence and gated based on cell size and granularity. Unexposed cells controlled for basal fluorophore expression. Data were analyzed using FlowJo software.

To sort MD10/TetOx2 cells, three six-well plates were exposed to dox, washed with 1× PBS, and moved to three T-150 flasks for 2 d. Cells were then trypsinized, spun at 1100 rpm for 5 min, washed with 1× PBS, spun a second time, resuspended in 3 mL of 1× PBS/1% FBS, and filtered. To sort MD12/p53R2-RE cells, 12 six-well plates were exposed to UV and recovered for 2 d. Cells were then processed as described above, except that four six-well plates of cells were pooled to produce three replicates. To sort MD15/HRE cells, nine 10-cm plates were exposed to anoxia or hypoxia and recovered for 1 d. Cells were then processed as described above, except that three 10-cm plates were pooled to produce three replicates.

Processed cells were run on a FACS Aria II with a 100 μM nozzle at 20 psi (Harvard Systems Biology). Excitation optics for RFP consisted of a 75-mW 594-nm laser; detection optics included a 630/22 bandpass filter. Excitation optics for YFP consisted of a 15-mW 488-nm laser; detection optics included a 520-nm longpass dichroic mirror and a 530/30 bandpass filter. For microscopy, 2.0×10^5 memory and non-memory cells were sorted. Sorted MD10/TetOx2 and sorted MD15/HRE cells were seeded in 12-well dishes; sorted MD12/p53R2-RE cells were seeded in 24-well dishes.

Fluorescence microscopy

For short-term microscopy, cells were imaged at 20× with a Nikon TE2000-E inverted fluorescence microscope equipped with a Hamamatsu ORCA-ER camera and HcRed (RFP) and JP2 (YFP) filters (Silver Laboratory). Images were acquired and analyzed using Metamorph software.

For long-term imaging, 5.0×10^4 cells per well were seeded in a 12-well glass-bottom culture dish (MatTek) and exposed to dox for 1 d. Wells were next washed with medium. Cells were allowed to recover for 1 d and then imaged every hour for 3 d using a Plan Apo 20× 0.75 NA objective lens on a Nikon TE200E motorized inverted microscope equipped with a Hamamatsu ORCA-ER cooled CCD camera; Prior Proscan II motorized stage and shutters; EXFO X-cite 120-XL fluorescence illuminator; a 37°C, 5% CO_2 custom-built microscope enclosure incubation chamber; and mCherry (RFP) and YFP filter sets (Nikon Imaging Center, Harvard Medical School). Images were acquired and analyzed using Metamorph software.

Cycloheximide assay

MD10/TetOx2 cells were plated in 12-well dishes and exposed to dox in triplicate. After 24 h of incubation, cells were exposed to 100 μM cycloheximide (Sigma-Aldrich) for 8 h. Three wells were fixed in 4% PFA/1× PBS per hour and later analyzed by FACS. The same procedure was applied to regular T-REx cells.

Histone deacetylase inhibitor assay

MD10/TetOx2 cells were plated in 12-well dishes, MD12/p53R2-RE cells were plated in six-well dishes, and MD15/HRE cells were plated in 10-cm plates. Cells were exposed in triplicate to 50 ng/mL TSA (Sigma-Aldrich) for 16 h and then washed and exposed in triplicate to dox, UV, or anoxia. Three wells were fixed in 4% PFA/1× PBS and later analyzed by FACS.

SYTOX Blue assay

MD15/HRE cells were plated in 10-cm plates, were exposed to hypoxia, and recovered for 1 d. MD10/TetOx2 cells were plated in six-well plates, were exposed to dox, and recovered for 1 d. MD12/p53R2-RE cells were plated in six-well plates, were exposed to UV, and recovered for 2 d. To analyze viability, cells were trypsinized, spun at 1100 rpm for 5 min, and resuspended in 10 mL of 1× PBS. Five hundred microliters from each plate was stained with 1 μM SYTOX Blue dead cell stain (Invitrogen), incubated for 5 min, and analyzed by FACS using the AmCyan filter. Unexposed cells were treated similarly to control for basal levels of cell death.

Endogenous pathway induction

MD15/HRE and MD12/p53R2-RE were plated and exposed to UV or hypoxia, respectively. Whole-cell RNA was extracted using the RNeasy minikit (Qiagen), and cDNA was prepared using the SuperScript III first strand synthesis system (Invitrogen). Unexposed cells served as controls for background expression.

Gene expression profiling

MD10/TetOx2 and MD12/p53R2-RE cells were plated in six-well plates; exposed to dox or UV in triplicate, respectively; and allowed to recover for 3 d. Cells were then processed as described above for cell sorting. For each biological replicate, 2.0×10^5 memory and non-memory cells were sorted, and RNA was extracted using the RNeasy minikit (Qiagen). cDNA was prepared, biotinylated, and hybridized to Gene 1.0 ST arrays (Affymetrix). Arrays were scanned and quantified according to standard Affymetrix protocols at the Dana Farber Microarray Core Facility (Dana Farber Cancer Institute). Data sets have been submitted to the Gene Expression Omnibus database (record GSE38189).

Identification and analysis of differentially regulated genes

Data were annotated and normalized by RMA analysis using Affymetrix Expression Console software. Differential gene expression was determined using the MATLAB Bioinformatics Toolbox (MathWorks). *P*-values were calculated using a permutation *t*-test of 1.0×10^4 permutations. Genes with a fold change ≥2 and *P*-value ≤0.05 were considered differentially expressed and analyzed for gene ontology enrichment via GoStat (http://gostat.wehi.edu.au), with Benjamini correction for multiple hypothesis testing; enrichment was considered significant with $P \leq 0.01$. Differentially expressed genes were validated by real-time PCR using 0.5 μg of RNA of specified cell populations. Primers amplified ~100 base pairs (Supplemental Table S3). Differential expression was normalized to the human gene *ACTB*.

Acknowledgments

We owe special thanks to D. Drubin for initiating this project. We further thank D. Ducat, C. Agapakis, Q. Wang, K. Haynes, J. Lohmueller, T. Armel, E. Wintermute, W. Senapedis, the Lahav

laboratory (Harvard Systems Biology), C. Shen, W. Kaelin, J. Way, K. Joung, and J. Hurt for thoughtful contributions to this manuscript and sharing reagents. Technical expertise was generously provided by J. Moore and A. Kressler (Harvard Systems Biology Flow Cytometry Facility), the Dana Farber Cancer Institute Microarray Core and Flow Cytometry Core, and J. Waters and L. Piedmont (Nikon Imaging Center at Harvard Medical School). D.R.B. is supported by the National Science Foundation (NSF) Synthetic Biology Engineering Research Center (SynBERC), M.C.I. is supported by the Natural Sciences and Engineering Research Council of Canada, P.M.B. is supported by the Harvard University Center for the Environment and NSF SynBERC, and P.A.S. is supported by the National Institutes of Health, the Wyss Institute for Biologically Inspired Engineering, and the Defense Advanced Research Projects Agency.

References

Acar M, Mettetal JT, van Oudenaarden A. 2008. Stochastic switching as a survival strategy in fluctuating environments. *Nat Genet* **40:** 471–475.

Ajo-Franklin CM, Drubin DA, Eskin JA, Gee EPS, Landgraf D, Phillips I, Silver PA. 2007. Rational design of memory in eukaryotic cells. *Genes Dev* **21:** 2271–2276.

Avery SV. 2006. Microbial cell individuality and the underlying sources of heterogeneity. *Nat Rev Microbiol* **4:** 577–587.

Becskei A, Séraphin B, Serrano L. 2001. Positive feedback in eukaryotic gene networks: Cell differentiation by graded to binary response conversion. *EMBO J* **20:** 2528–2535.

Beerli RR, Segal DJ, Dreier B, Barbas CF. 1998. Toward controlling gene expression at will: Specific regulation of the erbB-2/HER-2 promoter by using polydactyl zinc finger proteins constructed from modular building blocks. *Proc Natl Acad Sci* **95:** 14628–14633.

Birch-Machin MA, Swalwell H. 2010. How mitochondria record the effects of UV exposure and oxidative stress using human skin as a model tissue. *Mutagenesis* **25:** 101–107.

Bishop AL, Rab FA, Sumner ER, Avery SV. 2006. Phenotypic heterogeneity can enhance rare-cell survival in 'stress-sensitive' yeast populations. *Mol Microbiol* **63:** 507–520.

Bonnet J, Subsoontorn P, Endy D. 2012. Rewritable digital data storage in live cells via engineered control of recombination directionality. *Proc Natl Acad Sci* **109:** 8884–8889.

Boshart M, Weber F, Jahn G, Dorsch-Häsler K, Fleckenstein B, Schaffner W. 1985. A very strong enhancer is located upstream of an immediate early gene of human cytomegalovirus. *Cell* **41:** 521–530.

Brady CA, Attardi LD. 2010. p53 at a glance. *J Cell Sci* **123:** 2527–2532.

Bristow RG, Hill RP. 2008. Hypoxia and metabolism. Hypoxia, DNA repair and genetic instability. *Nat Rev Cancer* **8:** 180–192.

Burrill DR, Silver PA. 2010. Making cellular memories. *Cell* **140:** 13–18.

Burrill DR, Silver PA. 2011. Synthetic circuit identifies subpopulations with sustained memory of DNA damage. *Genes Dev* **25:** 434–439.

Burrill DR, Boyle PM, Silver PA. 2011. A new approach to an old problem: Synthetic biology tools for human disease and metabolism. *Cold Spring Harb Symp Quant Biol* doi: 10.1101/sqb.2011.76.010686.

Chen H, Yan Y, Davidson TL, Shinkai Y, Costa M. 2006. Hypoxic stress induces dimethylated histone H3 lysine 9 through histone methyltransferase G9a in mammalian cells. *Cancer Res* **66:** 9009–9016.

Denko NC. 2008. Hypoxia, HIF1 and glucose metabolism in the solid tumour. *Nat Rev Cancer* **8:** 705–713.

Forni PE, Scuoppo C, Imayoshi I, Taulli R, Dastrù W, Sala V, Betz UAK, Muzzi P, Martinuzzi D, Vercelli AE, et al. 2006. High levels of Cre expression in neuronal progenitors cause defects in brain development leading to microencephaly and hydrocephaly. *J Neurosci* **26:** 9593–9602.

Haynes KA, Silver PA. 2009. Eukaryotic systems broaden the scope of synthetic biology. *J Cell Biol* **187:** 589–596.

Hurt JA, Thibodeau SA, Hirsh AS, Pabo CO, Joung JK. 2003. Highly specific zinc finger proteins obtained by directed domain shuffling and cell-based selection. *Proc Natl Acad Sci* **100:** 12271–12276.

Kalderon D, Roberts BL, Richardson WD, Smith AE. 1984. A short amino acid sequence able to specify nuclear location. *Cell* **39:** 499–509.

Ke Q, Costa M. 2006. Hypoxia-inducible factor-1 (HIF-1). *Mol Pharmacol* **70:** 1469–1480.

Latonen L, Taya Y, Laiho M. 2001. UV-radiation induces dose-dependent regulation of p53 response and modulates p53-HDM2 interaction in human fibroblasts. *Oncogene* **20:** 6784–6793.

Lee SH, Kim J, Kim W-H, Lee YM. 2009. Hypoxic silencing of tumor suppressor RUNX3 by histone modification in gastric cancer cells. *Oncogene* **28:** 184–194.

Lu Y, Chu A, Turker MS, Glazer PM. 2011. Hypoxia-induced epigenetic regulation and silencing of the BRCA1 promoter. *Mol Cell Biol* **31:** 3339–3350.

Murray-Zmijewski F, Slee EA, Lu X. 2008. A complex barcode underlies the heterogeneous response of p53 to stress. *Nat Rev Mol Cell Biol* **9:** 702–712.

Ohno K, Ishihata K, Tanaka-Azuma Y, Yamada T. 2008. A genotoxicity test system based on p53R2 gene expression in human cells: Assessment of its reactivity to various classes of genotoxic chemicals. *Mutat Res Genet Toxicol Environ Mutagen* **656:** 27–35.

Phillips IE, Silver PA. 2006. A new biobrick assembly strategy designed for facile protein engineering. http://hdl.handle.net/1721.1/32535.

Shaner NC, Campbell RE, Steinbach PA, Giepmans BNG, Palmer AE, Tsien RY. 2004. Improved monomeric red, orange and yellow fluorescent proteins derived from *Discosoma* sp. red fluorescent protein. *Nat Biotechnol* **22:** 1567–1572.

Shaner NC, Steinbach PA, Tsien RY. 2005. A guide to choosing fluorescent proteins. *Nat Methods* **2:** 905–909.

Sharma SV, Lee DY, Li B, Quinlan MP, Takahashi F, Maheswaran S, McDermott U, Azizian N, Zou L, Fischbach MA, et al. 2010. A chromatin-mediated reversible drug-tolerant state in cancer cell subpopulations. *Cell* **141:** 69–80.

Shibata T, Giaccia AJ, Brown JM. 2000. Development of a hypoxia-responsive vector for tumor-specific gene therapy. *Gene Ther* **7:** 493–498.

Spiller DG, Wood CD, Rand DA, White MRH. 2010. Measurement of single-cell dynamics. *Nature* **465:** 736–745.

Tanaka H, Arakawa H, Yamaguchi T, Shiraishi K, Fukuda S, Matsui K, Takei Y, Nakamura Y. 2000. A ribonucleotide reductase gene involved in a p53-dependent cell-cycle checkpoint for DNA damage. *Nature* **404:** 42–49.

To TL, Maheshri N. 2010. Noise can induce bimodality in positive transcriptional feedback loops without bistability. *Science* **327:** 1142–1145.

Weinberger LS, Shenk T. 2007. An HIV feedback resistor: Auto-regulatory circuit deactivator and noise buffer. *PLoS Biol* **5:** e9. doi: 10.1371/journal.pbio.0050009.

Zhang X, Rosenstein BS, Wang Y, Lebwohl M, Wei H. 1997. Identification of possible reactive oxygen species involved in ultraviolet radiation-induced oxidative DNA damage. *Free Radic Biol Med* **23:** 980–985.

Appendix E

Boyle PM[1], Burrill DR[1], Inniss MC[1], Agapakis CM[1], Deardon A[2], Dewerd JG[2], Gedeon MA[2], Quinn JY[2], Paull ML[2], Raman AM[2], Theilmann MR[2], Wang L[2], Winn JC[2], Medvedik O, Schellenberg K, Haynes KA, Viel A, Brenner TJ, Church GM, Shah JV, & Silver PA. 2012. A BioBrick compatible strategy for genetic modification of plants. J Biol Eng 6:8[*]

[1]These authors contributed equally to this work
[2]These authors contributed equally to this work

JOURNAL OF BIOLOGICAL ENGINEERING

A BioBrick compatible strategy for genetic modification of plants

Boyle *et al.*

BioMed Central

Boyle *et al. Journal of Biological Engineering* 2012, **6**:8
http://www.jbioleng.org/content/6/1/8

Boyle et al. Journal of Biological Engineering 2012, 6:8
http://www.jbioleng.org/content/6/1/8

JOURNAL OF BIOLOGICAL ENGINEERING

METHODOLOGY Open Access

A BioBrick compatible strategy for genetic modification of plants

Patrick M Boyle[1†], Devin R Burrill[1†], Mara C Inniss[1†], Christina M Agapakis[1,7†], Aaron Deardon[2], Jonathan G DeWerd[2], Michael A Gedeon[2], Jacqueline Y Quinn[2], Morgan L Paull[2], Anugraha M Raman[2], Mark R Theilmann[2], Lu Wang[2], Julia C Winn[2], Oliver Medvedik[3], Kurt Schellenberg[4], Karmella A Haynes[1,8], Alain Viel[3], Tamara J Brenner[3], George M Church[5,6], Jagesh V Shah[1*] and Pamela A Silver[1,5*]

Abstract

Background: Plant biotechnology can be leveraged to produce food, fuel, medicine, and materials. Standardized methods advocated by the synthetic biology community can accelerate the plant design cycle, ultimately making plant engineering more widely accessible to bioengineers who can contribute diverse creative input to the design process.

Results: This paper presents work done largely by undergraduate students participating in the 2010 International Genetically Engineered Machines (iGEM) competition. Described here is a framework for engineering the model plant *Arabidopsis thaliana* with standardized, BioBrick compatible vectors and parts available through the Registry of Standard Biological Parts (www.partsregistry.org). This system was used to engineer a proof-of-concept plant that exogenously expresses the taste-inverting protein miraculin.

Conclusions: Our work is intended to encourage future iGEM teams and other synthetic biologists to use plants as a genetic chassis. Our workflow simplifies the use of standardized parts in plant systems, allowing the construction and expression of heterologous genes in plants within the timeframe allotted for typical iGEM projects.

Keywords: iGEM, Synthetic biology, Arabidopsis, Plant biotechnology

Background

Selective breeding has long been used to modify plant characteristics such as growth rate, seed size, and flavor [1]. For much of agricultural history, the targeted traits reflected the needs of local growers and consumers, creating a vast array of crop varieties. Advances in the field of genetics and the advent of recombinant DNA technology accelerated our ability to manipulate food crops [1-5]. In particular, the introduction of multiple genes (termed *gene stacking* in plants) has made plants accessible to synthetic biology applications [6-11]. In contrast to previous developments in agricultural technology, genetic modification of plants has been primarily performed for the benefit of large-scale monocultures of agricultural crops.

This work aims to create a standardized, modular system for the production of genetically enhanced plants to facilitate their adoption by diverse users. Ideally, a plant engineering system is customizable, yet has convenient standard features that minimize the need to re-invent common steps such as transferring genetic material into the plant. We demonstrate the feasibility of small-scale engineering projects in the model organism, *Arabidopsis thaliana* (Arabidopsis), using a BioBrick-modified plant vector system (Figure 1), performed within the time constraints of the iGEM competition.

Using BioBrick compatible plant vectors, we sought to modify the taste of Arabidopsis, specifically enhancing the sweetness of a bitter plant without altering sugar content. Several naturally occurring proteins are 100–3000 times sweeter than sugar by weight [12]. Brazzein, monellin, thaumatin, pentadin, mabinlin, and curculin are sweet proteins found in a variety of African and South Asian fruits, with no sequence similarity or common features

* Correspondence: jagesh_shah@hms.harvard.edu; pamela_silver@hms.harvard.edu
†Equal contributors
[1]Department of Systems Biology, Harvard Medical School, Boston, MA02115USA
Full list of author information is available at the end of the article

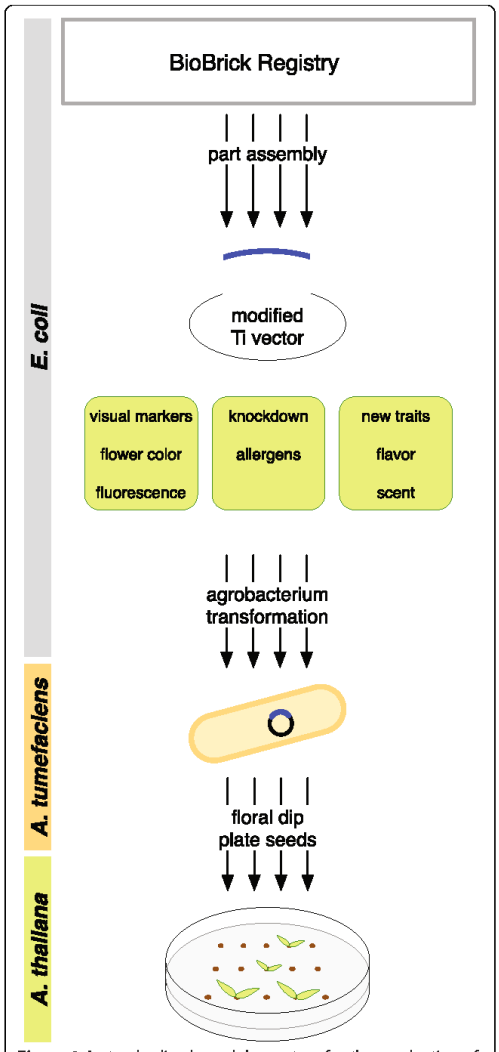

Figure 1 A standardized, modular system for the production of genetically-modified plants. Genetic parts (such as those obtained from the BioBrick Registry) were assembled and inserted into modified vectors (Open, Expression, or Reporter) in *E. coli*. These parts may be assembled to build constructs to impact a wide variety of plant phenotypes. Once assembled, these vectors were transformed into *Agrobacterium*. Using the floral dip procedure, *Agrobacterium* infected Arabidopsis, thereby transferring the assembled construct. Once seeds were produced, they were plated on selective media to obtain transgenic plants carrying the assembled construct.

[13]. Brazzein, isolated from the West African fruit *Pentadiplandra brazzeana*, is the smallest of these proteins with only 54 amino acids. It is exceptionally heat stable and was previously expressed heterologously in *Escherichia coli* (*E. coli*) [13], *Zea mays* [14], and *Lactobacillus lactis* [15].

Miraculin, isolated from the berries of the West African plant *Synsepalum dulcificum*, does not taste sweet on its own. Rather, it acts as a flavor-inverter by binding to taste receptors on the tongue in a pH-dependent manner, causing sour foods to taste sweet [16]. A 1 μM miraculin solution is sufficient to activate this inversion, where 20 mM citrate corresponds to the sweetness of 300 mM sucrose [17]. Miraculin is a glycosylated homodimer that has been heterologously expressed in lettuce [18], tomato [19], and even *E. coli* [17], indicating that endogenous *S. dulcificum* glycosylation is not required for functional expression.

Beyond creative gastronomy, we imagine this system being used to enhance the nutritional content of edible plants or help allergy sufferers enjoy the benefits of fresh home-grown produce (Figure 1). The development of efficient transformation techniques for many plants remains a key hurdle for commercial and personal agriculture. However, flexible genetic customization of plants also requires a system of easily transferable, standardized components such as those presented here. We hope this work will lead to techniques that yield a diversity of produce tailored to individual, community, and local environmental needs.

Results

Design of BioBrick compatible vectors for Arabidopsis transformation

Arabidopsis is readily transformed by *Agrobacterium*: when a plant is injured, *Agrobacterium* migrates to the wound site and transfers the T-DNA region of its tumor-inducing (Ti) plasmid into the plant cell [20]. The T-DNA localizes to the nucleus and integrates into the plant's chromosomal DNA. A series of vectors (the pORE series) have been developed from *Agrobacterium*'s Ti plasmid to allow transformation of heterologous DNA into plants via *Agrobacterium* [20]. pORE vectors come equipped with a multiple cloning site (MCS) containing twenty-one unique restriction endonuclease sites. Reporters or promoters are included to create expression vectors, reporter vectors, or vectors that can carry an exogenous promoter or open reading frame. This vector series offers either glufosinate resistance via the *pat* gene, or kanamycin resistance via the *nptII* gene, to enable the selection of successfully transformed plants.

We developed a new set of six BioBrick DNA assembly compatible plant transformation vectors based on the pORE series (Table 1). Vectors V1 and V2 (modified Open vectors) contain no promoter or reporter gene, allowing integration of constructs under the control of a chosen

Table 1 Features of BioBrick plant vectors

Vector	BioBrick Registry ID	Bacterial Resistance	Plant Resistance	Promoter	Reporter	Original pORE vector
V1	BBa_K382000	kan	pat	none	none	pORE O1
V2	BBa_K382001	kan	nptII	none	none	pORE O2
V3	BBa_K382002	kan	pat	pENTCUP2	none	pORE E3
V4	BBa_K382003	kan	nptII	pENTCUP2	none	pORE E4
V5	BBa_K382004	kan	nptII	none	gusA	pORE R1
V6	BBa_K382005	kan	nptII	none	smGFP	pORE R3

promoter (Figure 2A, Table 1). Vectors V3 and V4 (modified Expression vectors) contain the constitutive pENTCUP2 promoter upstream of the MCS (Figure 2B, Table 1), while V5 and V6 (modified Reporter vectors) contain no promoter but have either the reporter gusA or soluble modified GFP (smGFP) downstream of the cloning site (Figure 2C, Table 1). Each vector contains an MCS that is compatible with three widely used BioBrick standards (RFC 10, 20, 23, www.partsregistry.org).

Expression of standardized flavor protein genes in industrial microorganisms

We first tested the expression of standardized miraculin and brazzein genes in *E. coli* and the yeast *Saccharomyces cerevisiae* (*S. cerevisiae*), since the introduction of exogenous genes is faster in these organisms. Full-length miraculin and brazzein genes were commercially synthesized and codon-optimized for expression in Arabidopsis. BioBrick compatible restriction enzyme sites bracketed each open reading frame. Constructs were tagged at either the N- or C-terminus with the Strep-II tag [21] for western blot analysis. Miraculin (Figure 3A) and brazzein (Figure 3B) were expressed from an IPTG-inducible T7 promoter in *E. coli*. Monomeric miraculin was expressed at very low levels at approximately 24 kDa regardless of tag location, which is consistent with previous work [17]. Brazzein was highly expressed in the same system at about 12 kDa, regardless of tag location, as has been previously observed [13]. Brazzein was also highly expressed from the constitutive TEF and copper-inducible CUP1 promoters in *S. cerevisiae* (Figure 3C). The higher molecular weight of the Strep-II tagged brazzein observed by western blot in yeast, compared to *E. coli* (~35 kDa versus 12 kDa) is likely due to yeast-specific glycosylation of the brazzein protein [22]. While expression of the miraculin gene was not verified in yeast, integration of both miraculin and brazzein constructs in Arabidopsis was attempted.

Expression of flavor proteins in Arabidopsis

We successfully introduced two different BioBrick plant vectors into Arabidopsis and selected for seeds carrying genomically-integrated miraculin and brazzein transgenes. Miraculin- or brazzein-encoding DNA under control of the pENTCUP2 promoter and NosT transcriptional terminator on either the V3 (glufosinate resistance) or V4 (kanamycin resistance) BioBrick vector was introduced into Arabidopsis via *Agrobacterium*-mediated transformation [23]. Transformed seeds were selected on MS-agar, and resistant plants were moved to soil and allowed to produce seeds. T1 generation seeds were collected and re-plated on selective plates. Resistant plants were once again moved to soil and allowed to produce T2 generation seeds. While integration of both the miraculin and brazzein genes into the plant genome was verified by PCR (Figure 4A), only miraculin RNA expression was detected by end-point PCR (Figure 4B). Miraculin expression could not be verified by western blot as the antibody showed significant background binding. However, the RNA expression data indicates that miraculin mRNA is expressed in our transgenic plants.

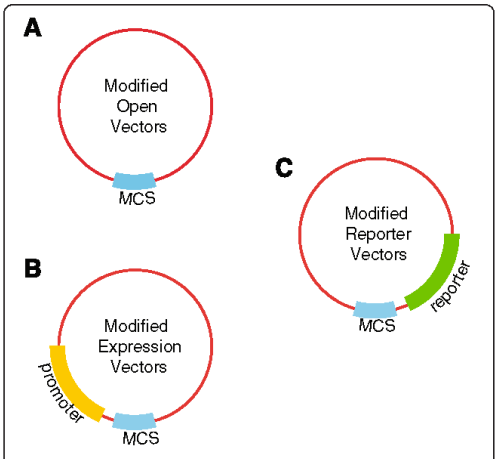

Figure 2 Schematic of BioBrick plant vectors. (A) Modified Open vectors are based on vectors pORE O1 and O2 [14]. They are designed for general insertion of a construct. **(B)** Modified Expression vectors are based on vectors pORE E3 and E4 [14]. They contain an inducible promoter preceding the BioBrick MCS, to permit user-controlled expression of the inserted construct. **(C)** Modified Reporter vectors are based on vectors pORE R1 and R2 [14]. They contain a reporter gene following the BioBrick MCS, such that expression of the reporter follows that of the inserted construct.

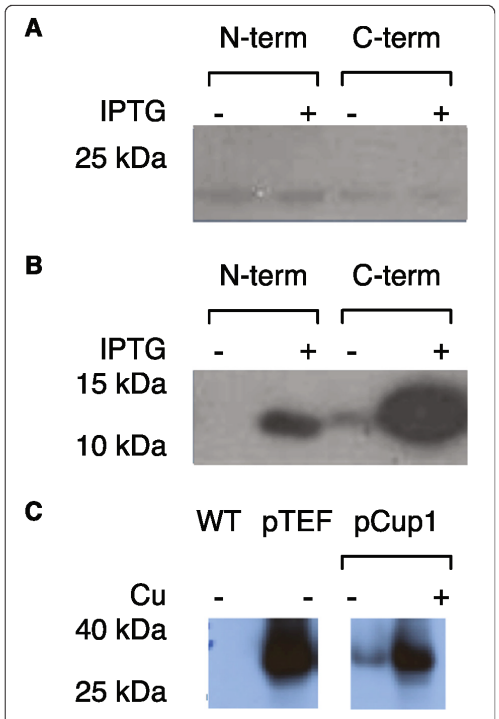

Figure 3 BioBrick miraculin and brazzein protein expression in bacteria and yeast. (A) Miraculin and **(B)** brazzein BioBricks were expressed from an IPTG-inducible promoter in *E. coli* with an N- or C-terminal Strep-II tag. Miraculin was expressed at low levels, with only a faint band appearing at 24 kDa. Brazzein was well expressed in an IPTG-dependent manner. **(C)** Brazzein BioBrick was expressed in yeast from pTEF or pCup1 promoters with a C- terminal Strep-II tag. Brazzein appeared larger in yeast vs. *E. coli*, most likely due to glycosylation of brazzein in yeast.

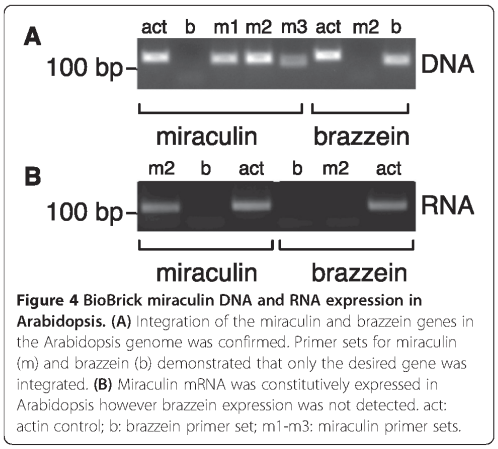

Figure 4 BioBrick miraculin DNA and RNA expression in Arabidopsis. (A) Integration of the miraculin and brazzein genes in the Arabidopsis genome was confirmed. Primer sets for miraculin (m) and brazzein (b) demonstrated that only the desired gene was integrated. **(B)** Miraculin mRNA was constitutively expressed in Arabidopsis however brazzein expression was not detected. act: actin control; b: brazzein primer set; m1-m3: miraculin primer sets.

Discussion and conclusions

Genetic engineering of plants at the industrial and laboratory scale is well established. Technological advances have yielded crops that reduce food production costs through resistance to pests, herbicide, drought, and flood [24]. Additionally, modification of crops (e.g., rice) to contain pro-vitamins can help treat health issues such as vitamin A deficiency in countries where staple foods do not provide the necessary nutrients [24,25]. However, advances in small-scale experimental horticulture, farming, and gardening have been impeded by the lack of readily available modular parts for the genetic modification of plants. Access to standardized plant vectors in the Registry of Standard Biological Parts will facilitate the design of small-scale plant engineering projects.

We have modified existing plant integration vectors to make them compatible with the BioBrick assembly standard 23 [26], demonstrated that they can be used to integrate transgenes in Arabidopsis, and showed successful integration and expression of the taste modifying gene miraculin. All constructs have been submitted to the Registry of Biological Parts (www.partsregistry.org) and are available as a resource for the synthetic biology and plant engineering communities. These include vectors modified from the pORE vector series [20], plant-specific regulatory elements (e.g., promoters, terminators), resistance markers, and the coding sequence of miraculin. The vector series features variations containing the constitutive promoter pENTCUP2 (V3 and V4), visible reporters gusA or smGFP (V5 and V6), or a simple multiple cloning site (V1 and V2), allowing expression of a gene from a promoter of choice.

In addition to using these vectors to express exogenous proteins, we have considered integrating constructs expressing hairpin RNAs [27] or artificial microRNAs [28] to knock down the expression of endogenous genes. This strategy is particularly powerful in that synthesizing a DNA sequence to match any gene transcript of choice allows the regulation of potentially any plant protein. For instance, this approach could be used reduce allergenic protein levels [29]. Alternatively, microRNAs could be targeted to metabolic regulators so that key metabolites, such as pigments or nutrients, are allowed to accumulate [30] and enhance the color or nutritional content of the plant. Modification of existing vectors to conform to a BioBrick assembly standard allows them to be integrated into a BioBrick cloning based workflow. In addition to simplifying the construction of more complex genetic devices, adhering to an assembly standard allows for the possibility of automation of the assembly process.

We hope that availability of plant integration vectors compatible with a common assembly standard will

facilitate the use of plants as a chassis in synthetic biology. Local-scale design of food plants, in which the grower selects traits desired in their community, can be made possible through the availability of standardized, modular genetic parts. Personalized engineering of plants to modify flavor, nutritional value, or allergenicity could create a new class of designed foods that are grown and consumed at a local scale. We encourage the iGEM community to continue to explore these concepts via plant engineering.

A significant barrier to the adoption of local-scale plant engineering is the uncertain regulatory landscape for the deployment of genetically modified organisms. This landscape has been defined by large-scale commercial agriculture. As the tools of synthetic biology become more accessible, efforts by small groups such as our own will continue to challenge existing regulatory frameworks. We hope that our concept of genetic engineering tools in the hands of local growers will spur discussion and debate on how to responsibly regulate the synthetic biology scenarios of the near future.

Materials and methods

Plasmids and cloning

Gene assembly was performed in *E. coli* DH5α using BioBrick assembly standard 23 [26], and all described parts were submitted to the BioBrick Registry. Arabidopsis pORE series vectors were provided by The Arabidopsis Information Resource (TAIR) and engineered to support BioBrick cloning through PCR-based methods (see Additional file 1: Table S1). pORE Open Series vectors O1 and O2 were digested with SpeI and SacII and ligated with an annealed oligonucleotide insert with NheI and SacII overhangs containing the BioBrick Multiple Cloning Site (MCS) to create vectors V1 and V2. pORE Expression Series vectors E3 and E4 were digested with HindIII and SpeI and ligated with an insert PCR-amplified from the expression vectors containing a HindIII site upstream of the pENTCUP2 promoter and the BioBrick MCS and an NheI site downstream to create vectors V3 and V4. pORE Reporter Series vectors R1, containing the gusA reporter, and R3, containing the smGFP reporter, were digested with HindIII and SpeI and ligated with inserts containing the reporter gene PCR-amplified with primers containing a HindIII site followed by the BioBrick MCS upstream and NheI downstream, yielding vectors V5 and V6.

Brazzein and miraculin were codon-optimized for expression in Arabidopsis, commercially synthesized (Mr. Gene, Regensburg, Germany), and assembled with the pENTCUP2 promoter and NosT transcriptional terminator. Completed constructs were subcloned from BioBrick assembly vector V0120 to BioBrick modified pORE vectors through digestion with EcoRI and PstI.

Plant maintenance

Wild-type Col-0 *Arabidopsis thaliana* seeds were sterilized by washing with 70% ethanol, 0.1% Triton X-100, followed by two 95% ethanol washes and two sterile dH_2O washes. Seeds were then plated on 1X Murashige & Skoog (MS) media with 0.7% agar supplemented with 150 uM carbenicillin and placed in the dark at 4°C for three days before moving to an incubator with 16 h illumination at 20°C and 8 h dark at 15°C per day to allow seeds to germinate. Once plants produced secondary leaves, they were moved to soil and allowed to mature and produce seeds. Seeds were collected and stored at 4°C.

Plant transformation

Agrobacterium-mediated transformation was performed according to previously reported techniques [23]. Briefly, *Agrobacterium* was made electro-competent by washing in cold sterile water and resuspending in 10% glycerol. Vector DNA was dialyzed to remove excess salt, and electroporated into *Agrobacterium*. Kanamycin-resistant colonies were grown in YEB media, spread on YEB plates, and allowed to form a lawn. Lawns were scraped and suspended in a solution of 20% YEB, 4% sucrose (w/v), and 0.024% Silwet L-77 surfactant (Helena Chemical Company, Collierville, TN). Wild-type Col-0 Arabidopsis flowers were dipped in the *Agrobacterium* solution and allowed to grow and develop seed pods. Seeds were collected from mature plants and selected on 1x MS media with 0.7% agar supplemented with 5 mg/L glufosinate or 50 μg/ml kanamycin.

E. coli and yeast protein expression

In BL21(DE3) *E. coli*, StrepII-tagged brazzein and miraculin were inserted at multiple cloning site 1 of a BioBrick-modified pET-duet vector [31]. Cells were grown to mid-log phase and induced with a final concentration of 1 mM IPTG. Protein expression was measured by western blot.

In PSY580a yeast *S. cerevisiae*, StrepII-tagged brazzein was cloned with the constitutive TEF promoter or the copper-inducible CUP1 promoter and integrated at the LEU2 locus. Transformants were grown in YEPD media with 0.3 mM $CuSO_4$ to induce protein expression, which was measured by western blot.

Verification of genomic transgenes

Genomic DNA was extracted from Arabidopsis using the DNEasy kit (Qiagen) and amplified by PCR (see Additional file 1: Table S2). Whole cell RNA was collected using the plant RNEasy kit (Qiagen). cDNA was synthesized with the SuperScript III First-Strand synthesis kit (Invitrogen). qPCR was performed with primer pairs (see Additional file 1: Table S2) amplifying 100 base pair

amplicons within target genes to identify expression of heterologous genes or endogenous gene knockdown.

SDS-page and western blotting

Protein samples were extracted from Arabidopsis, *E. coli*, and yeast and normalized using the Bradford assay (Bio-Rad, Hercules, CA). Samples were diluted into SDS-PAGE loading buffer and loaded onto a 4–20% Tris/glycine/SDS acrylamide gel. α-Strep-tag II antibody (HRP-conjugated, Novagen, Gibbstown, NJ) was used to measure brazzein and miraculin protein expression in *E. coli* and yeast, and α-miraculin antibody [18] (provided by Tadayoshi Hirai, Graduate School of Life and Environmental Sciences, University of Tsukuba, Japan) was used to detect levels of miraculin expression in Arabidopsis. Monoclonal Anti-β-Tubulin antibody (Sigma-Aldrich, St-Louis, MO) was used to detect tubulin in Arabidopsis.

Additional file

Additional file 1: Supplementary Data for A BioBrick Compatible Strategy for Genetic Modification of Plants. Contains tables of primer sequences describing primers used to modify pORE vectors and verify integration and RNA expression of transgenes.

Abbreviations

MCS: Multiple cloning site.

Competing interests

The authors declare they have no competing interests.

Authors' contributions

Cloning schemes were designed by PMB, DRB, MCI, CMA, AD, JGdW, MAG, JYQ, MLP, AMR, MRT, LW, JCW, and OM. KS provided technical assistance with Arabidopsis culture and *Agrobacterium*-mediated transformation. PMB, DRB, MCI, and CMA performed PCR, qPCR and western blots; all other cloning and experiments were performed by AD, JGdW, MAG, JYQ, MLP, AMR, MRT, LW, and JCW. KAH, AV, TJB, GMC, JVS, and PAS provided general advising throughout the project. The manuscript was drafted by PMB, DRB, MCI, and CMA. All authors read and approved the final manuscript.

Acknowledgements

We would like to thank the people at iGEM for supporting this project and allowing us the opportunity to present it at the 2010 IGEM competition. Further thanks are owed to Sarah Mathews of the Harvard Arnold Arboretum for providing advice, access to her lab, and reagents. PMB was supported by the Harvard University Center for the Environment Graduate Consortium. PMB and DRB were supported by the National Science Foundation (NSF) Synthetic Biology Engineering Research Center (SynBERC). MCI was supported by the Natural Science and Engineering Research Council of Canada. CMA was supported by a NSF Graduate Research Fellowship. AD, JGdW, MAG, JYQ, MLP, AMR, MRT, LW, JCW, and OM were generously supported by the Wyss Institute for Biologically Inspired Engineering, Harvard's Office of the Provost, and a grant from the Howard Hughes Medical Institute Undergraduate Education Program awarded to Robert A. Lue, Department of Molecular and Cellular Biology, Harvard University. KS was supported by the Arnold Arboretum.

Author details

[1]Department of Systems Biology, Harvard Medical School, Boston, MA02115USA. [2]Harvard College, Harvard University, Cambridge, MA 02138, USA. [3]Department of Molecular and Cellular Biology, Harvard University, Cambridge, MA 02138, USA. [4]The Arnold Arboretum of Harvard University, Boston, MA 02131, USA. [5]Wyss Institute for Biologically Inspired Engineering, Harvard University, Boston, MA 02115, USA. [6]Department of Genetics, Harvard Medical School, Boston, MA 02115, USA. [7]Current Address: Department of Chemical and Biomolecular Engineering, University of California, Los Angeles, CA 90095, USA. [8]Current Address: School of Biological and Health Systems Engineering, Arizona State University, Tempe, AZ 85287, USA.

Received: 6 February 2012 Accepted: 6 June 2012
Published: 20 June 2012

References

1. Kingsbury N: *Hybrid: the history and science of plant breeding - Noël Kingsbury - Google Books*.: University of Chicago Press; 2009.
2. Welling F: Historical study: Johann Gregor Mendel 1822–1884. 1991, 40:1–25.
3. Jackson DA, Symons RH, Berg P: Biochemical method for inserting new genetic information into DNA of Simian Virus 40: circular SV40 DNA molecules containing lambda phage genes and the galactose operon of Escherichia coli. *Proc Natl Acad Sci USA* 1972, 69:2904–2909.
4. Lobban PE, Kaiser AD: Enzymatic end-to end joining of DNA molecules. *J Mol Biol* 1973, 78:453–471.
5. Cohen SN, Chang AC, Boyer HW, Helling RB: Construction of biologically functional bacterial plasmids in vitro. *Proc Natl Acad Sci USA* 1973, 70:3240–3244.
6. Antunes MS, Ha S-B, Tewari-Singh N, Morey KJ, Trofka AM, Kugrens P, Deyholos M, Medford JI: A synthetic de-greening gene circuit provides a reporting system that is remotely detectable and has a re-set capacity. *Plant Biotechnol J* 2006, 4:605–622.
7. Herrera-Estrella L, Depicker A, Van Montagu M, Schell J: Expression of chimaeric genes transferred into plant cells using a Ti-plasmid-derived vector. *Nature* 1983, 303:209–213.
8. Bevan MW, Flavell RB, Chilton M-D: A chimaeric antibiotic resistance gene as a selectable marker for plant cell transformation. *Nature* 1983, 304:184–187.
9. Fraley RT, Rogers SG, Horsch RB, Sanders PR, Flick JS, Adams SP, Bittner ML, Brand LA, Fink CL, Fry JS, Galluppi GR, Goldberg SB, Hoffmann NL, Woo SC: Expression of bacterial genes in plant cells. *Proc Natl Acad Sci USA* 1983, 80:4803–4807.
10. Murai N, Kemp JD, Sutton DW, Murray MG, Slightom JL, Merlo DJ, Reichert NA, Sengupta-Gopalan C, Stock CA, Barker RF, Hall TC: Phaseolin gene from bean is expressed after transfer to sunflower via tumor-inducing plasmid vectors. *Science* 1983, 222:476–482.
11. Shewry PR, Jones HD, Halford NG: *Advances in Biochemical Engineering/Biotechnology*. Berlin, Heidelberg: Springer Berlin Heidelberg; 2008:149–186.
12. Kant R: Sweet proteins–potential replacement for artificial low calorie sweeteners. *Nutr J* 2005, 4:5.
13. Assadi-Porter F: Efficient Production of Recombinant Brazzein, a Small, Heat-Stable, Sweet-Tasting Protein of Plant Origin. *Arch Biochem Biophys* 2000, 376:252–258.
14. Lamphear BJ, Barker DK, Brooks CA, Delaney DE, Lane JR, Beifuss K, Love R, Thompson K, Mayor J, Clough R, Harkey R, Poage M, Drees C, Horn ME, Streatfield SJ, Nikolov Z, Woodard SL, Hood EE, Jilka JM, Howard JA: Expression of the sweet protein brazzein in maize for production of a new commercial sweetener. *Plant Biotechnol J* 2004, 3:103–114.
15. Berlec A, Jevnikar Z, Majhenič AČ, Rogelj I, Štrukelj B: Expression of the sweet-tasting plant protein brazzein in Escherichia coli and Lactococcus lactis: a path toward sweet lactic acid bacteria. *Appl Microbiol Biotechnol* 2006, 73:158–165.
16. Koizumi A, Tsuchiya A, Nakajima K-I, Ito K, Terada T, Shimizu-Ibuka A, Briand L, Asakura T, Misaka T, Abe K: Human sweet taste receptor mediates acid-induced sweetness of miraculin. *Proc Natl Acad Sci USA* 2011, 108:16819–16824.
17. Matsuyama T, Satoh M, Nakata R, Aoyama T, Inoue H: Functional Expression of Miraculin, a Taste-Modifying Protein in Escherichia Coli. *J Biochem* 2009, 145:445–450.
18. Sun H-J, Cui M-L, Ma B, Ezura H: Functional expression of the taste-modifying protein, miraculin, in transgenic lettuce. *FEBS Lett* 2006, 580:620–626.
19. Hirai T, Fukukawa G, Kakuta H, Fukuda N, Ezura H: Production of Recombinant Miraculin Using Transgenic Tomatoes in a Closed Cultivation System. *J Agric Food Chem* 2010, 58:6096–6101.
20. Coutu C, Brandle J, Brown D, Brown K, Miki B, Simmonds J, Hegedus DD: pORE: a modular binary vector series suited for both monocot and dicot plant transformation. *Transgenic Res* 2007, 16:771–781.

21. Schmidt TG, Koepke J, Frank R, Skerra A: **Molecular interaction between the Strep-tag affinity peptide and its cognate target, streptavidin.** *J Mol Biol* 1996, **255**:753–766.
22. Carlson A, Armentrout RW, Ellis TP: **Enhanced Production and Purification of a Natural High Intensity Sweetener.** 2010, 1–34.
23. Logemann E, Birkenbihl RP, Ulker B, Somssich IE: **An improved method for preparing Agrobacterium cells that simplifies the Arabidopsis transformation protocol.** *Plant Methods* 2006, **2**:16.
24. Ronald P: **Plant Genetics, Sustainable Agriculture and Global Food Security.** *Genetics* 2011, **188**:11–20.
25. Ye X, Al-Babili S, Klöti A, Zhang J, Lucca P, Beyer P, Potrykus I: **Engineering the provitamin A (beta-carotene) biosynthetic pathway into (carotenoid-free) rice endosperm.** *Science* 2000, **287**:303–305.
26. Phillips IE, Silver PA: **A New Biobrick Assembly Strategy Designed for Facile Protein Engineering.** 2006, 1–6.
27. Helliwell C, Waterhouse P: **Constructs and methods for high-throughput gene silencing in plants.** *Methods* 2003, **30**:289–295.
28. Ossowski S, Schwab R, Weigel D: **Gene silencing in plants using artificial microRNAs and other small RNAs.** *Plant J* 2008, **53**:674–690.
29. Singh MB, Bhalla PL: **Genetic engineering for removing food allergens from plants.** *Trends Plant Sci* 2008, **13**:257–260.
30. Kennedy CJ, Boyle PM, Waks Z, Silver PA: **Systems-level engineering of nonfermentative metabolism in yeast.** *Genetics* 2009, **183**:385–397.
31. Agapakis CM, Ducat DC, Boyle PM, Wintermute EH, Way JC, Silver PA: **Insulation of a synthetic hydrogen metabolism circuit in bacteria.** *J Biol Eng* 2010, **4**:3.

doi:10.1186/1754-1611-6-8
Cite this article as: Boyle *et al.*: A BioBrick compatible strategy for genetic modification of plants. *Journal of Biological Engineering* 2012 **6**:8.

Appendix F

Inniss MC, Silver PA. 2013. Building synthetic memory. Curr Biol 23:R812–6.*

*Reproduced with permission from Elsevier

Current Biology 23, R812–R816, September 9, 2013 ©2013 Elsevier Ltd All rights reserved http://dx.doi.org/10.1016/j.cub.2013.06.047

Building Synthetic Memory

Minireview

Mara C. Inniss[1] and Pamela A. Silver[1,2,*]

Cellular memory — conversion of a transient signal into a sustained response — is a common feature of biological systems. Synthetic biologists aim to understand and re-engineer such systems in a reliable and predictable manner. Synthetic memory circuits have been designed and built *in vitro* and *in vivo* based on diverse mechanisms, such as oligonucleotide hybridization, recombination, transcription, phosphorylation, and RNA editing. Thus far, building these circuits has helped us explore the basic principles required for stable memory and ask novel biological questions. Here we discuss strategies for building synthetic memory circuits, their use as research tools, and future applications of these devices in medicine and industry.

Introduction

Synthetic biology encompasses a vast range of pursuits, including building novel transcriptional circuits [1,2], engineering metabolism on a large scale [3], and creating a minimal cell [1,2,4]. Early projects were mostly limited to building small genetic circuits consisting of only a few parts [1–3,5]; however, current work has extended our range to large multi-gene devices [6] and even entire genomes [7].

While some of the first synthetic circuits were built from a small number of parts, they exhibited complex behavior, including oscillations and pattern formation [5]. Cellular memory circuits were also among these early synthetic devices [1]. Cellular memory refers to the cell's ability to convert a transient signal or stimulus into a sustained response (see Box 1 for a glossary of definition of terms used in this article). Biological phenomena that rely on natural memory circuits include the lambda phage switch, cellular differentiation, and cell division [8,9]. Synthetic memory circuits can either require active cellular processes to maintain their state (volatile memory) or not (non-volatile memory). Volatile memory circuits include transcription-based devices, while non-volatile memory circuits can be based on DNA recombination. An important feature of volatile memory circuits is that they are bistable — they tend to exist in one of two states. Also, stochastic switching between the stable states should be rare [10]. Additionally, the change in state of both volatile and non-volatile memory circuits can be reversible or irreversible (Figure 1A).

Synthetic memory circuits can be engineered using a variety of biological mechanisms, including nucleic acid hybridization, DNA recombination, chromatin modification, transcription, and post-transcriptional phenomena. Here we will explore the current state of engineered memory circuits and their applications. We will then discuss the future of these devices in medicine and industry.

In Vitro Memory Circuits

Synthetic genetic circuits can be constructed *in vitro*. These circuits consist either solely of DNA, capable of performing calculations or logic functions via hybridization [11], or of more complex mixtures of DNA and purified enzymes that can carry out transcription and translation [12,13]. The advantage of building synthetic circuits *in vitro* is the high level of control over the environment in which the device will function [14]. This control results in increased predictability and allows careful unpacking and analysis of the specific interactions between circuit components. This detailed understanding should allow better predictions and interpretations of the behavior of the device when it is introduced into the more complex worlds of the cell and multicellular organisms.

In particular, there have been several recent examples of *in vitro* toggle switches and memory devices based on hybridization of oligonucleotides. One such circuit was built by engineering two mutually repressive DNA-hybridization-based transcriptional switches [12]. This circuit consists of DNA oligonucleotides, and two enzymes: T7 RNA polymerase and RNase H. The presence of activating single-stranded (ss) DNA, complementary to each switch, allows T7 RNA polymerase to transcribe inhibitory RNAs to the opposing switches, while RNase H degrades the inhibitory RNAs. By carefully balancing production and degradation rates, bistable behavior is observed: depending on the initial amounts of the opposing activating ssDNAs, production of one inhibitory RNA will completely suppress production of the other. Importantly, these results agree very closely with model predictions. While this system is bistable, it is not switchable; the circuit output depends entirely on the initial state of the system [12].

While reversibility is not necessary for a synthetic memory device, it may prove a useful feature. Recently, an *in vitro* switchable memory circuit was engineered consisting of DNA oligonucleotides, DNA polymerase, an endonuclease, and an exonuclease [13]. The bistable core of the circuit consists of four templates: two positive feedback loops, and two mutually repressive feedback loops. There are two additional templates that produce two activating oligonucleotides in response to external signals. In this case, these signals are the addition of additional complementary oligonucleotides. Each of these oligonucleotides interacts with the templates in the bistable core to promote their own production and repress production of the other. Thus, by adding the appropriate external stimulus, the circuit can be switched from one state to the other (Figure 1B).

While, in principle, these *in vitro* memory circuits could be modified to function in cells, these strategies for engineering bistability remain unexplored *in vivo*. However, these studies have produced extremely detailed mechanistic understanding that will benefit future efforts to transfer these devices into the cellular environment.

Writing Cellular Memory into DNA

Heritable memory encoded at the DNA level has been used in biological studies for many years [15]. Developmental biologists use recombinase systems, such as Cre–*loxP* recombination, to permanently mark cells of a given lineage, and to knock-out genes in specific cell types or at desired times [16,17]. To accomplish this, transgenic animals are created carrying circuits in which a reporter gene is interrupted by a transcriptional terminator flanked by *loxP* sites

[1]Department of Systems Biology, Harvard Medical School, Boston, MA 02115, USA. [2]Wyss Institute of Biologically Inspired Engineering, Boston, MA 02115, USA.
*E-mail: Pamela_Silver@hms.harvard.edu

Box 1

Glossary.

Bistable: A system that returns to one of two stable states after perturbation.
Circuit: A group of interacting parts (e.g. promoters, genes, proteins, oligonucleotides) engineered to integrate one or more inputs to produce a desired output.
Logic gate: A device that performs logical operations such as AND, OR, NOT, NOR, NAND, XOR, XNOR.
Memory: A long-lasting and/or permanent change in state of a system in response to a transient signal.
Toggle switch: A genetic circuit that can be switched repeatedly between two states (e.g. ON/OFF).

[17], or by replacing a gene of interest with a *loxP*-flanked version [16]. Cre recombinase expression is then put under the control of a tissue-specific or inducible promoter. Differentiation into a specific tissue or addition of an exogenous inducer results in expression of Cre, which excises the DNA between the *loxP* sites, either creating a functional reporter gene or removing the gene of interest, respectively. As a recombination event results in a change at the DNA sequence level, the change is irreversible and transmits memory of the stimulus heritably and permanently (Figure 1C).

By using invertases instead of standard recombinases, more complex multi-state memory circuits can be designed [18–20] (Figure 1C). For instance, a double-inversion recombination switch was built in *Escherichia coli* by constructing a plasmid with two overlapping inversion modules [18]. A separate plasmid carried the two inducible invertase genes. The state of this device can be probed by using a carefully chosen set of primers. The presence or absence of certain amplicons not only indicates whether each inducer has been added, but also the order in which they were introduced. More recently, memory circuits have been integrated with logic gates by flanking combinations of terminators, promoters, or reporter genes by two different pairs of recombinase target sites [19,21]. Depending on the arrangement of these elements, all input logic gates (AND, OR, NOR, and NAND) can be created. Additionally, multiple inversion-based memory circuits can be linked to build a genetic counter capable of indicating the number of pulses of inducer experienced by the cell [22]. As with the systems used in lineage tracing experiments [16,17], activation of these devices is irreversible.

Recently a rewritable recombination-based memory device was demonstrated in *E. coli*. This recombinase addressable data (RAD) module consists of a promoter flanked by phage attachment sites, attB and attP, situated between two fluorescent protein genes [20]. The device is 'set' by expression of a phage integrase (Int), inverting the DNA between the attB and attP sites and converting these to attL and attR sites. The device is reset by coexpression of Int and the corresponding excisionase (Xis), flipping the DNA between attL and attR sites and restoring the attB and attP sites. Depending on the orientation of the promoter, one of the two fluorescent proteins is produced. The state of the device is stable over many generations and can be switched back and forth reliably many times. A reversible memory circuit enables the design of a combinatorial genetic counter [23]. In contrast to a counter built from irreversible memory circuits — using N modules for N counts — a combinatorial counter with N modules can count to 2^N [23].

Transmitting Memory through Transcriptional Networks

The vast majority of synthetic genetic circuits implemented *in vivo* rely on the successful engineering of transcriptional regulation. One of the best-understood transcriptional regulation systems, lambda phage, is an example of a natural memory circuit [8]. As such, several synthetic memory circuits are transcription based [1,2,24–27]. There are two main gene network topologies that can demonstrate sustained memory behavior; double-negative feedback loops, and a positive feedback loop [10] (Figure 1D). Both of these strategies have been explored in different contexts and each has advantages and disadvantages. While the latter is a much simpler circuit with fewer components to engineer, the former, by virtue of its increased complexity, provides more options for modification and tuning.

An early example of a synthetic genetic circuit was an engineered toggle switch in *E. coli* [1]. Inspired by the natural lambda phage immunity region [8], which had previously been shown to function in a novel context [28], a double-negative feedback circuit was constructed, consisting of two repressors driven by constitutive promoters. Each repressor can repress synthesis of the other; therefore, when one repressor is expressed, the other is repressed, thereby creating two stable states. Importantly, it is possible to selectively inactivate each repressor by the addition of a specific small molecule, permitting the device to switch states. Careful tuning of promoter strength based on the choice of repressor created toggle switches that demonstrated bistability and long-term memory. Later, similar synthetic toggle switches were shown to function in mammalian cells, demonstrating the modularity of the design [24,29]. Recently, a toggle switch was combined with genetic logic circuits to create a switch that can be switched on and off by repeated addition of a single trigger molecule [25].

While several autoregulatory circuits were built having some degree of bistability [30–32], the first positive feedback loop that predictably and reliably transmitted memory for many cell divisions was built in *Saccharomyces cerevisiae* [2]. To create this device, the activities of several transcription factors under the control of a galactose-inducible promoter were characterized and a computational model of the circuit was used to predict which of these would form a functional memory circuit. Indeed, the model correctly predicted which of the transcription factors would succeed and which would fail. This memory device was later shown to be modular; when the galactose-inducible promoter was replaced with the promoter for a gene encoding a protein involved in the DNA repair response, the circuit maintained its activity, albeit while responding to DNA damage instead of galactose [26]. This re-engineered circuit was able to identify a subpopulation of cells that maintained a differential response to DNA damage for many generations after exposure to damage. As with the toggle switch, the modularity of the positive-feedback-based memory device extends to its transferability to a different organism. A similar device designed to respond to either doxycycline, ultraviolet radiation, or hypoxia was built in human cells and was successfully used to isolate a subpopulation of cells that responded differentially to these stimuli [27].

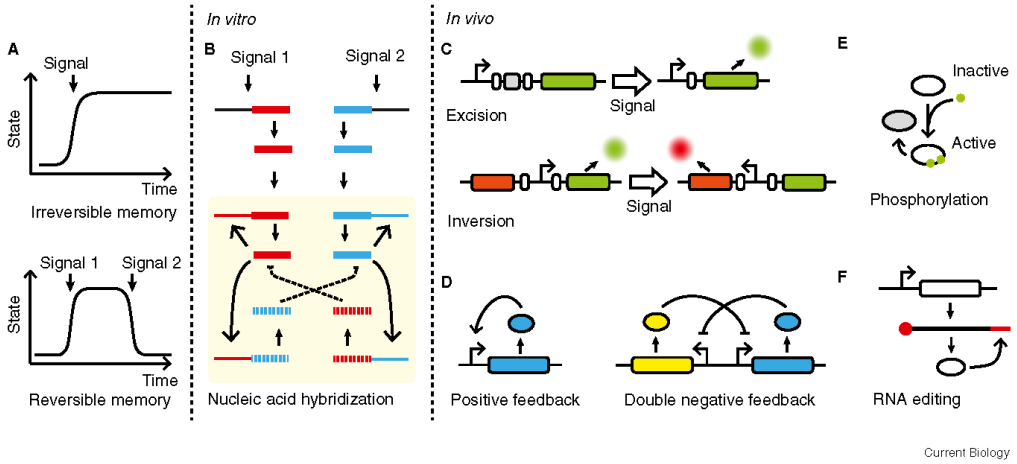

Figure 1. Cellular memory circuits can be built in many ways.

(A) The change in state of synthetic memory circuits can be either reversible or irreversible. (B) *In vitro* memory circuits rely on hybridization of nucleic acids. Interlocking negative and positive feedback loops form the bistable core (in box) of such devices. Once activated, each positive feedback loop produces an oligonucleotide that promotes its own production as well as an inhibitory oligonucleotide to the opposing positive feedback loop. (C–F) *In vivo* memory circuits are built using diverse strategies. (C) Recombination-based memory circuits can be based on excision or inversion of DNA sequences. (D) Both positive and double-negative transcriptional feedback loops can be used to engineer cellular memory. Novel memory circuits based on (E) protein phosphorylation and (F) RNA editing have also been proposed.

Memory after Transcription

While cellular memory circuits have been engineered that operate at the DNA sequence level as well as through regulation of transcription, post-transcriptional processes have yet to be explored. Natural systems exhibit bistability and even memory dependent on processes such as phosphorylation [33] and post-transcriptional modification of RNA [34]. Recent efforts to model these systems open the possibility of harnessing them in engineered circuits.

The phosphorylation state of proteins with multiple phosphorylation sites has been shown to be switch-like or bistable [33]. For example, multi-site phosphorylation is thought to contribute to the bistability of the MAP kinase cascade [35]. Other models predict that scaffolding is also a significant contributor to bistable phosphorylation cascades [36]. Now, synthetic phosphorylation-based circuits can be built to test these predictions, adding protein phosphorylation to the selection of tools available for engineering cellular memory (Figure 1E). This will allow synthetic biologists to build novel circuits that can respond on much quicker timescales than transcriptional or recombination-based circuits.

As another point of post-transcriptional regulation, translation level and thus protein level can be controlled through RNA modifications. Recently, construction of a positive feedback loop dependent on control of mRNA polyadenylation has been proposed [37] (Figure 1F). Transcripts with more polyadenylation are more likely to be translated compared to those without [38,39]. By expressing a polyadenylating enzyme from a transcript carrying its cognate polyadenylation signal, a positive feedback loop can be created [37]. This circuit has the potential to be bistable, making it a candidate for becoming the basis of a cellular memory device. These diverse methods of creating cellular memory will provide a powerful toolkit for building future synthetic circuits.

Learning through Building

Synthetic biologists have envisioned what may be possible once we can reliably and predictably re-engineer biology. While building novel genetic circuits both *in vitro* and *in vivo* has been a pursuit of synthetic biologists for several years, most of these have yet to find utility in real-world applications. Nevertheless, these early efforts have proven useful both as research tools and in gaining a better understanding of natural biological mechanisms (Figure 2A).

Synthetic memory circuits have been used to explore what is needed to engineer bistability. In particular, transcription-based circuits have been extensively modeled [40–43] and many examples have been built in diverse contexts [1,2,24–27]. The knowledge gained through these pursuits will allow synthetic biologists to better understand natural and novel transcriptional networks. In addition, memory circuits have been used to study biological questions that would otherwise be intractable. As described earlier, recombination-based memory circuits have been used extensively to trace developmental lineages of cells. These circuits also allow conditional gene knock-outs, making it possible to study the effects of gene loss in certain cell types and at specific times during development [16].

Synthetic memory circuits based on transcriptional positive feedback loops have been used to study the long-term effects of transient stimuli in *S. cerevisiae* and human cells [26,27]. *S. cerevisiae* cells carrying the DNA-damage-responsive memory circuit were exposed to genotoxic doses of the DNA-damaging agents EMS or hydroxyurea.

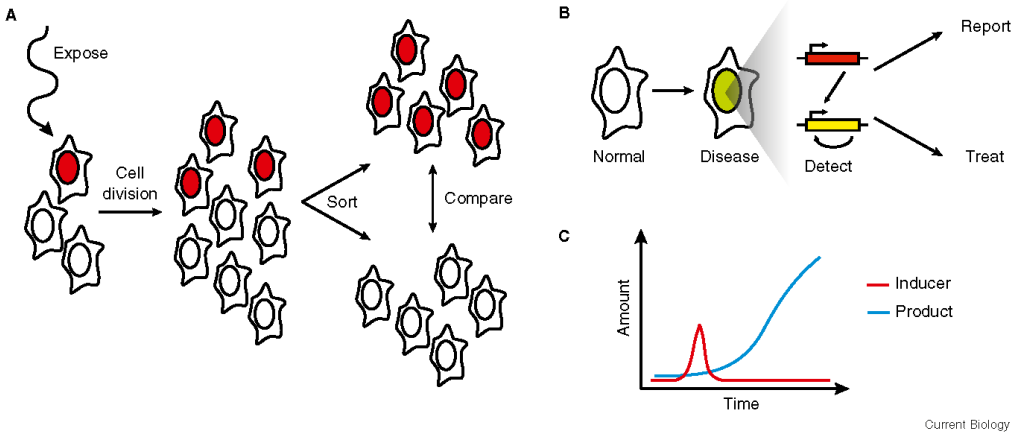

Figure 2. Engineered cellular memory circuits can be used to study biology and may be used to diagnose and treat disease, as well as solve unmet industrial needs.

(A) Memory circuits can be used to study heterogeneously responding cell populations. (B) When a cell changes from a healthy to a disease state, memory circuits can detect and report this change or treat the underlying condition. (C) Memory circuits will allow long-term expression by transient addition of inducer.

Due to the nature of the bistable circuit, cells only switch to the memory state if they respond above a certain threshold, allowing isolation of a more strongly responsive subpopulation. This subpopulation was shown to have a higher rate of mitochondrial activity and iron uptake and this phenotype persisted for many generations after exposure to the genotoxic agent [26]. Similarly, a DNA-damage-responsive memory device in human cells was also used to isolate a subpopulation of strongly responding cells. Gene expression in these memory cells differed from the non-memory population for many days after exposure to UV radiation [27]. Thus, using synthetic memory circuits, we can mark and influence biologically relevant subpopulations of cells.

The Future of Engineered Cellular Memory

While synthetic memory devices have been useful in learning more about biology and the function of genetic networks, we expect that, in the future, these circuits will find new applications in fields such as medicine or industrial biotechnology (Figure 2B,C). Other types of synthetic circuits and engineered cells are already being explored as potential next-generation therapies in the treatment of diseases such as diabetes, metabolic syndrome, and cancer [44–47]. The ability to induce a sustained response to a transient stimulus will enable new forms of treatment and diagnosis as well as meet unsolved industrial challenges [47].

Current medical treatment relies on diagnosis of a disease before an appropriate treatment can be administered, and a patient will often have to take repeated doses of a drug over the course of treatment [48,49]. A synthetic memory circuit could be engineered to detect a biological signal of disease and start producing either an easily detectable reporter or a therapeutic agent (Figure 2B). Transcriptional positive feedback loops have already been shown to be modular and thus can be coupled to different biological signaling pathways to detect transient changes in the biology of the cell [26]. Alternatively, the device can be engineered to respond to an extracellular stimulus, such as radiation or hypoxia. These devices will allow a physician to know whether a certain stimulus or condition has occurred, even if it is no longer present. While the output of the memory device can be an easily detectable reporter, such as a fluorophore, beta-galactosidase, or secreted alkaline phosphatase, in the future the output of these devices may be a therapeutic agent [50]. This will automate both the detection and treatment of disease, decreasing the time between the start of the condition and the first dose of therapy (Figure 2B).

Cellular memory devices will also be useful in an industrial setting. One barrier to cost-effective production of chemical products is the cost of constantly inducing the culture [19]. A synthetic memory device would convert transient induction of a large culture into permanent expression of the exogenous biosynthetic pathways of interest, significantly reducing the cost of production [19] (Figure 2C). In addition, one can imagine designing a synthetic memory circuit to be activated at a certain cell density or other internal condition, eliminating the need for an external inducer.

Conclusions

Engineering synthetic memory circuits has already taught us about designing bistability and building genetic circuits both *in vitro* and *in vivo*, and has helped answer diverse biological questions. However, there remain unmet needs that will enable new applications, namely, more diverse and well-characterized parts — e.g. transcription factors, recombinases, and inducible promoters — as well as more predictive models describing the interactions of these parts. As we apply this deepened understanding and incorporate new tools, such as phosphorylation and RNA modification, more complex systems will be designed and implemented, making these devices an important part of next-generation medical treatments and bioindustry.

Acknowledgments

Thanks to Tyler Ford and Cameron Myhrvold for critical reading of this manuscript. M.C.I. is supported by the National Sciences Foundation Synthetic Biology Engineering Research Center (NSF SynBERC) and the National Institutes of Health (NIH), and P.A.S. is supported by the NIH, the Wyss Institute for Biologically Inspired Engineering, and the Defense Advanced Research Projects Agency.

References

1. Gardner, T.S., Cantor, C.R., and Collins, J.J. (2000). Construction of a genetic toggle switch in Escherichia coli. Nature *403*, 339–342.
2. Ajo-Franklin, C.M., Drubin, D.A., Eskin, J.A., Gee, E.P.S., Landgraf, D., Phillips, I., and Silver, P.A. (2007). Rational design of memory in eukaryotic cells. Genes Dev. *21*, 2271–2276.
3. Wang, H.H., Isaacs, F.J., Carr, P.A., Sun, Z.Z., Xu, G., Forest, C.R., and Church, G.M. (2009). Programming cells by multiplex genome engineering and accelerated evolution. Nature *460*, 894–898.
4. Forster, A.C., and Church, G.M. (2006). Towards synthesis of a minimal cell. Mol. Syst. Biol. *2*, 45.
5. Basu, S., Gerchman, Y., Collins, C.H., Arnold, F.H., and Weiss, R. (2005). A synthetic multicellular system for programmed pattern formation. Nature *434*, 1130–1134.
6. Xie, Z., Wroblewska, L., Prochazka, L., Weiss, R., and Benenson, Y. (2011). Multi-input RNAi-based logic circuit for identification of specific cancer cells. Science *333*, 1307–1311.
7. Gibson, D.G., Glass, J.I., Lartigue, C., Noskov, V.N., Chuang, R.-Y., Algire, M.A., Benders, G.A., Montague, M.G., Ma, L., Moodie, M.M., *et al.* (2010). Creation of a bacterial cell controlled by a chemically synthesized genome. Science *329*, 52–56.
8. Ptashne, M. (2004). A Genetic Switch (Cold Spring Harbor, NY: Cold Spring Harbor Laboratory Press).
9. Burrill, D.R., and Silver, P.A. (2010). Making cellular memories. Cell *140*, 13–18.
10. Ferrell, J.E. (2002). Self-perpetuating states in signal transduction: positive feedback, double-negative feedback and bistability. Curr. Opin. Cell Biol. *14*, 140–148.
11. Qian, L., Winfree, E., and Bruck, J. (2011). Neural network computation with DNA strand displacement cascades. Nature *475*, 368–372.
12. Kim, J., White, K.S., and Winfree, E. (2006). Construction of an in vitro bistable circuit from synthetic transcriptional switches. Mol. Syst. Biol. *2*, 68.
13. Padirac, A., Fujii, T., and Rondelez, Y. (2012). Bottom-up construction of in vitro switchable memories. Proc. Natl. Acad. Sci. USA *109*, E3212–E2320.
14. Hockenberry, A.J., and Jewett, M.C. (2012). Synthetic in vitro circuits. Curr. Opin. Chem. Biol. *16*, 253–259.
15. Stern, C.D., and Fraser, S.E. (2001). Tracing the lineage of tracing cell lineages. Nat. Cell Biol. *3*, E216–E218.
16. Nagy, A. (2000). Cre recombinase: The universal reagent for genome tailoring. Genesis *26*, 99–109.
17. Srinivas, S., Watanabe, T., Lin, C.-S., William, C.M., Tanabe, Y., Jessell, T.M., and Costantini, F. (2001). Cre reporter strains produced by targeted insertion of EYFP and ECFP into the ROSA26 locus. BMC Dev. Biol. *1*, 4.
18. Ham, T.S., Lee, S.K., Keasling, J.D., and Arkin, A.P. (2008). Design and construction of a double inversion recombination switch for heritable sequential genetic memory. PLoS ONE *3*, e2815.
19. Siuti, P., Yazbek, J., and Lu, T.K. (2013). Synthetic circuits integrating logic and memory in living cells. Nat. Biotechnol. *31*, 448–452.
20. Bonnet, J., Subsoontorn, P., and Endy, D. (2012). Rewritable digital data storage in live cells via engineered control of recombination directionality. Proc. Natl. Acad. Sci. USA *109*, 8884–8889.
21. Bonnet, J., Yin, P., Ortiz, M.E., Subsoontorn, P., and Endy, D. (2013). Amplifying genetic logic gates. Science *340*, 599–603.
22. Friedland, A.E., Lu, T.K., Wang, X., Shi, D., Church, G., and Collins, J.J. (2009). Synthetic gene networks that count. Science *324*, 1199–1202.
23. Subsoontorn, P., and Endy, D. (2012). Design and analysis of genetically encoded counters. Procedia Comp. Sci. *11*, 43–54.
24. Kramer, B.P., Viretta, A.U., Daoud-El-Baba, M., Aubel, D., Weber, W., and Fussenegger, M. (2004). An engineered epigenetic transgene switch in mammalian cells. Nat. Biotechnol. *22*, 867–870.
25. Lou, C., Liu, X., Ni, M., Huang, Y., Huang, Q., Huang, L., Jiang, L., Lu, D., Wang, M., Liu, C., *et al.* (2010). Synthesizing a novel genetic sequential logic circuit: a push-on push-off switch. Mol. Syst. Biol. *6*, 350.
26. Burrill, D.R., and Silver, P.A. (2011). Synthetic circuit identifies subpopulations with sustained memory of DNA damage. Genes Dev. *25*, 434–439.
27. Burrill, D.R., Inniss, M.C., Boyle, P.M., and Silver, P.A. (2012). Synthetic memory circuits for tracking human cell fate. Genes Dev. *26*, 1486–1497.
28. Toman, Z., Dambly-Chaudière, C., Tenenbaum, L., and Radman, M. (1985). A system for detection of genetic and epigenetic alterations in Escherichia coli induced by DNA-damaging agents. J. Mol. Biol. *186*, 97–105.
29. Deans, T.L., Cantor, C.R., and Collins, J.J. (2007). A tunable genetic switch based on RNAi and repressor proteins for regulating gene expression in mammalian cells. Cell *130*, 363–372.
30. Becskei, A., Séraphin, B., and Serrano, L. (2001). Positive feedback in eukaryotic gene networks: cell differentiation by graded to binary response conversion. EMBO J. *20*, 2528–2535.
31. Isaacs, F.J., Hasty, J., Cantor, C.R., and Collins, J.J. (2003). Prediction and measurement of an autoregulatory genetic module. Proc. Natl. Acad. Sci. USA *100*, 7714–7719.
32. Kramer, B.P., and Fussenegger, M. (2005). Hysteresis in a synthetic mammalian gene network. Proc. Natl. Acad. Sci. USA *102*, 9517–9522.
33. Gunawardena, J. (2005). Multisite protein phosphorylation makes a good threshold but can be a poor switch. Proc. Natl. Acad. Sci. USA *102*, 14617–14622.
34. Salz, H.K., and Erickson, J.W. (2010). Sex determination in Drosophila: The view from the top. Fly *4*, 60–70.
35. Hadač, O., Schreiber, I., and Přibyl, M. (2013). On the origin of bistability in the Stage 2 of the Huang-Ferrell model of the MAPK signaling. J. Chem. Phys. *138*, 065102.
36. Chan, C., Liu, X., Wang, L., Bardwell, L., Nie, Q., and Enciso, G. (2012). Protein scaffolds can enhance the bistability of multisite phosphorylation systems. PLoS Comput. Biol. *8*, e1002551.
37. Aslam, N., and Shouval, H.Z. (2012). Regulation of cytoplasmic polyadenylation can generate a bistable switch. BMC Syst. Biol. *6*, 12.
38. Gallie, D.R. (1991). The cap and poly(A) tail function synergistically to regulate mRNA translational efficiency. Genes Dev. *5*, 2108–2116.
39. Wilusz, C.J., Wormington, M., and Peltz, S.W. (2001). The cap-to-tail guide to mRNA turnover. Nat. Rev. Mol. Cell Biol. *2*, 237–246.
40. Rodrigo, G., and Jaramillo, A. (2007). Computational design of digital and memory biological devices. Syst. Synth. Biol. *1*, 183–195.
41. Widder, S., Macía, J., and Solé, R. (2009). Monomeric bistability and the role of autoloops in gene regulation. PLoS ONE *4*, e5399.
42. Ghim, C.-M., and Almaas, E. (2009). Two-component genetic switch as a synthetic module with tunable stability. Phys. Rev. Lett. *103*, 028101.
43. Rodrigo, G., Carrera, J., Elena, S.F., and Jaramillo, A. (2010). Robust dynamical pattern formation from a multifunctional minimal genetic circuit. BMC Syst. Biol. *4*, 48.
44. Burrill, D.R., Boyle, P.M., and Silver, P.A. (2011). A new approach to an old problem: synthetic biology tools for human disease and metabolism. Cold Spring Harb. Symp. Quant. Biol. *76*, 145–154.
45. Weber, W., and Fussenegger, M. (2011). Emerging biomedical applications of synthetic biology. Nat. Rev. Genet. *13*, 21–35.
46. Ye, H., Charpin-El Hamri, G., Zwicky, K., Christen, M., Folcher, M., and Fussenegger, M. (2013). Pharmaceutically controlled designer circuit for the treatment of the metabolic syndrome. Proc. Natl. Acad. Sci. USA *110*, 141–146.
47. Ruder, W.C., Lu, T., and Collins, J.J. (2011). Synthetic biology moving into the clinic. Science *333*, 1248–1252.
48. Wieland, M., and Fussenegger, M. (2012). Engineering molecular circuits using synthetic biology in mammalian cells. Annu. Rev. Chem. Biomol. Eng. *3*, 209–234.
49. Folcher, M., and Fussenegger, M. (2012). Synthetic biology advancing clinical applications. Curr. Opin. Chem. Biol. *16*, 345–354.
50. Ausländer, S., and Fussenegger, M. (2012). From gene switches to mammalian designer cells: present and future prospects. Trends Biotechnol. *31*, 155–168.